Fundamentals of inductively coupled argon plasmas : a spectroscopic study

Fundamentals of inductively coupled argon plasmas

a spectroscopic study

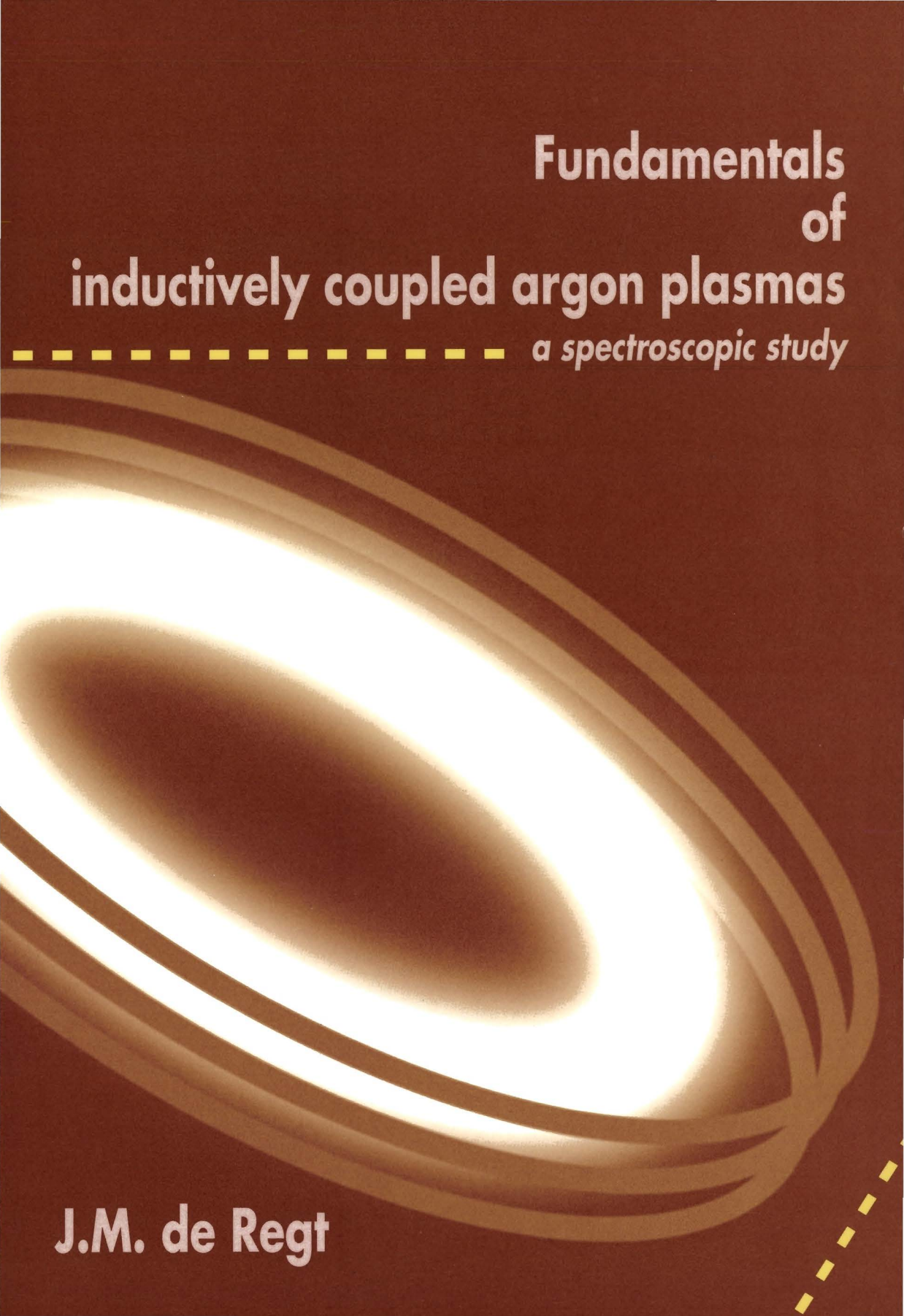

J.M. de Regt

Fundamentals of inductively coupled argon plasmas

a spectroscopic study

J.M. de Regt

Omslag: met dank aan C. van Buijten
Drukwerk: Ponsen & Looijen bv, Wageningen

CIP-DATA KONINKLIJKE BIBLIOTHEEK, DEN HAAG

Regt, Johannes Martinus de

Fundamentals of inductively coupled argon plasmas: a spectroscopic study / Johannes Martinus de Regt. - Eindhoven: Eindhoven University of Technology
Thesis Technische Universiteit Eindhoven. - With summary in Dutch.
ISBN 90-386-0237-5
Subject headings: inductively coupled plasmas / spectroscopy / laser diagnostics.

Fundamentals of inductively coupled argon plasmas

a spectroscopic study

PROEFSCHRIFT

ter verkrijging van de graad van doctor aan de Technische Universiteit Eindhoven, op gezag van de Rector Magnificus, prof.dr. J.H. van Lint, voor een commissie aangewezen door het College van Dekanen in het openbaar te verdedigen op woensdag 28 februari 1996 om 16.00 uur

door

Johannes Martinus de Regt

geboren te Oudenbosch

Dit proefschrift is goedgekeurd door de promotoren:

prof. dr. ir. D.C. Schram
en
prof. dr. W.R. Rutgers

Copromotor:
dr. J.A.M. van der Mullen

The work presented in this thesis was carried out at the Physics Department of the Eindhoven University of Technology and was supported by the fundamental research foundation FOM, the technology foundation STW and by Philips Forschungslaboratorien GmbH Aachen (Germany) and Philips Lighting Eindhoven (The Netherlands).

Contents

Dankwoord

Je eigen proefschrift vind je nooit toevallig in een hoekje, ook al neem je daar vier jaar voor. De wisselwerking met vele anderen is onmisbaar en maakte het voor mij juist extra interessant en aangenaam. Daarom wil ik hier iedereen bedanken die mij op welke wijze dan ook heeft geholpen en gestimuleerd. Zoals mijn enthousiaste en doortastende begeleider Joost van der Mullen, mijn eerste promotor Daan Schram en tweede promotor prof. Rutgers en de leden van de leescommissie prof. de Voigt en prof. Broeckaert. Daarnaast natuurlijk Dany Benoy, Richard Engeln, Bart van der Sijde, Jeroen Jonkers, Chris van Buijten, Annemeike Tan, Onno van Kessel, Ger Janssen en René Severens die direct betrokken waren bij het tot stand komen van dit proefschrift. Net als de studenten Robert Tas, Jeroen Damen, Jan van Dijk, Frank de Groote, Martijn Mulders en Anna Hansgard, die een grote bijdrage leverden aan dit onderzoek en de technici Ries van de Sande, Herman de Jong, Bertus Hüsken en Frans Overberg, zonder wie het leven als onderzoeker stilstaat. Voor het deelonderzoek in samenwerking met Philips zijn de discussies met Achim Körber, Pieter Postma en Johan van Vliet niet weg te denken. Natuurlijk zijn er nog veel meer mensen, zoals Jeanne Loonen, Richard van de Sanden, Seth Brussaard, Ruth Gruijters, John Gielen, Frank Fey, Roger Paffen, Ralph Meulenbroeks, Djoomart Otorbaev, Erik Timmermans, Mark de Graaf, Marcel Carrère, Gijs Meeusen, Sjaak Beulens, Zhou Qing, Bert van Lierop en Ad Buuron, die tot de wereld van dagelijkse collega's behoren samen met die van de zustergroep EPG. En tenslotte de andere dagelijkse wereld: mijn ouders, mijn zus en vooral ook Irma.

Chapter 1

General introduction

For the production of durable goods and for environmental protection, as is indispensable for the future society, plasmas will play a prominent role. One of the reasons is that due to its non-equilibrium nature, the plasma state offers a wide variety of conditions with a nearly unlimited chemical freedom. Several possibilities for further applications of plasmas can be found in light and laser sources, in particle and beam sources (plasma etching and deposition), in energy carriers (plasma welding and cutting), in excitation sources for chemical analysis, and in pollution control.

A special case of plasmas is formed by those created by inductive coupling. In these cases the plasma acts as a secondary coil of a transformer, in which electrons accelerated by the oscillating electro-magnetic field transfer their energy to the heavy particles, i.e. atoms, molecules and ions by means of collisions. Inductively coupled plasmas (ICPs) are produced in a wide power range varying from several watts for medical equipment to the 1 MW range used for material treatment.

In the present work we will confine ourselves to the smaller ICPs with power input in the 0.1 - 2 kW range, such as the open flowing ICPs used for spectrochemical analysis and the closed high pressure ICPs which might become light sources of the future.

In analytical laboratories worldwide, the open ICP[1] is very popular and powerful in the field of spectrochemistry for the analysis of aqueous solutions. Especially metals can be detected effectively by atomic emission spectroscopy (ICP-AES) down to the level of 1 atom per 10^9. The combination of the ICP with a mass spectrometer (ICP-MS) lowers the detection limits of metals down to the 1 atom per 10^{12} range.

The inductive energy coupling into a closed vessel can create a stable, stationary high pressure plasma useful for domestic and industrial lighting. The closed high pressure ICP is related to the low pressure QL-lamp,[2,3] recently introduced by Philips Lighting. The high pressure ICP might be a future light source with various promising aspects such as a very long lifetime, environmentally friendly fillings, and very high efficiencies. Note that even a small improvement in the efficacy of light sources will result in large energy savings as an appreciable part of the world energy-consumption is used for lighting.

Though the applications of the open and closed ICPs are quite different, the conditions of these (sub)atmospheric plasmas are rather similar. They also share various advantages with respect to their usage such as the inherent high purity of the plasma due to the absence of electrodes. This is required in order to obtain low detection limits for the open ICP as well as to reach long life times for the closed ICP. Therefore, both the open flowing ICP for spectrochemical purposes as well as the (sub)atmospheric pressure ICP for lighting is treated in this work and the presented fundamental insights can benefit the applicability of both plasmas.

Thesis objectives

The improvement of the applicability of both types of ICPs requires understanding of the behavior of the plasma which calls for fundamental research. At the same time, fundamental research can reveal unexpected insight into the processes and properties present on atomic scale. These two points are the motivation of the present research that is partially a continuation of earlier projects as we will see below.

Although especially the open spectrochemical ICP has already been introduced[4] in the early 1960s, its fundamentals are not yet well understood. This can be ascribed to the small dimensions of the plasma creating large gradients, so that transport effects are important and that deviations from equilibrium are substantial. Modeling the ICP finds problems in describing these large gradients, such as found at the edge were the entrainment of air and the role of molecules are important. Therefore, very accurate knowledge is required on the basic plasma parameters such as profiles of electron density and temperature, and heavy particle temperature.

In the early 1980s Van der Mullen[5] developed a classification theory of plasmas and studied non-thermodynamic equilibrium (non-LTE) aspects, which are among others applicable to open flowing argon ICPs. Late in the 1980s Nowak,[6] followed by Fey,[7] started working on emission experiments using a 100 MHz ICP. Comparative measurements of the electron density showed that deviations from equilibria could be determined. Later on emphasis was put on the power interruption technique by which the state of equilibrium departure was manipulated by the removal of the power during several tens of microseconds. Analyzing the plasma by means of the power interruption technique upon the introduction of nebulized water revealed new points of insight with respect to the evaporation of water droplets and excitation of metal atoms. At the same time, Benoy[8] worked on a numerical non-LTE model describing self-consistently the open ICP.

The aim of this thesis has three aspects. One is the fundamental research on the *open* ICP for spectrochemical analysis. A better understanding of the fundamentals of this ICP might lead to better detection limits or might widen the spectro-analytical applicability of this plasma, such as for the analysis of gases. Two, the fundamental research on the *closed* ICP for lighting, in cooperation with Philips,[i] can provide a basis for a better understanding of the reasons for the high efficacy of the inductively coupled plasma lamp. The observed mechanisms might also be useful for other types of light sources.

However, fundamental research requires accurate measurements of the plasma parameters. Therefore, the third and a vital aspect of the present work is the design, construction and optimization of a set of diagnostics for the determination of plasma parameters such as radial and axial density and temperature profiles. These diagnostics are all applied and tested on the open ICP and subsequently used for studying the closed ICP. By their extensive mutual comparison, the diagnostics provide a strong basis for the interpretation of plasma properties such as particle transport by ambipolar diffusion, recombination, and heat conduction.

[i] Philips Forschungslaboratorien Aachen (D) and Philips Lighting Eindhoven (NL).

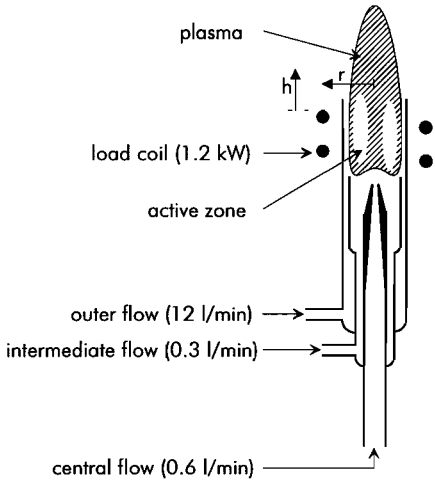

Figure 1. A schematic presentation of the open flowing ICP for spectrochemical purposes. The values of the argon flow are depicted. Note the effect of the asymmetrical coil on the shape of the plasma. All measurements are performed on the left wing, except the measurements presented in chapter 4.

Inductively coupled plasmas under study

The two studied types of ICPs, the open flowing and the closed ICP, will be described below.[i]

Open flowing ICP

The ICP is created by the inductive coupling of energy into an argon gas flow. The quartz torch, with an inner diameter of 18 mm, has three concentric tubes and is positioned in a coil of two windings having a diameter of 35 mm and a total height of 15 mm, see figure 1. The coil is fed by a 100 MHz RF-generator developed by Philips and operates at a power that is variable between 0.6 and 2.1 kW. The typical power is 1.2 kW. Note that these powers are delivered by the power supply and that the effective power dissipated in the plasma is considerably lower (about 50%). The three flows can be controlled separately. The outer flow (12 l/min at 1 atm. and 293 K) serves as the main gas supply and prevents the contact between plasma and quartz torch. The intermediate flow (0.3 l/min) lifts the plasma a few millimeters, whereas the central flow (0.6 l/min) can be used to introduce a nebulized aqueous solution into the plasma. Although we used this central flow, no nebulized water is introduced in the present work, and all the measurements are performed on a "dry" argon plasma. The standard position where the measurements are performed lies at 7 mm above the load coil (ALC), just above the hottest area in the plasma. Additionally, many experiments have been performed on the plasma between 7 mm and 22 mm ALC.

For the power interruption experiments the generator is provided with the additional feature to interrupt the power delivered to the plasma. It takes about 2 μs before the EM field has decreased to 5% of the stationary field value.

[i] Note that in the next chapters this part is left out from the original articles in order to avoid repetitions.

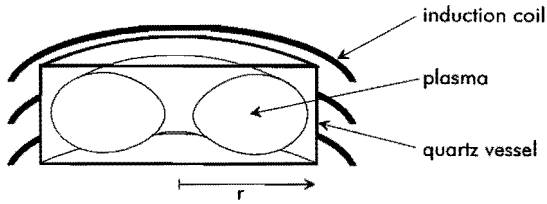

Figure 2. A schematic presentation of the closed ICP for lighting purposes. The shape of the plasma is typical for the 100 mbar argon filling. Note that the measurements are carried out on this cylinder-symmetrical plasma while the coil and vessel are positioned vertically.

Closed ICP

This plasma is created in a closed quartz vessel again by means of induction currents. The primary coil, consisting of three windings, is fed by a generator with a frequency of 13.56 MHz. The matching network with two capacitors, between the generator and the coil, is adjusted for each power setting and for every filling pressure of the vessel. The effective plasma powers are varied from 50 to 125 W. Effective powers above 125 W are avoided since the resulting high wall-temperatures would damage the quartz vessel.
The dimensions of the cylindrical vessel are an inner radius r of 9 mm and an inner height of 8 mm. To make any lateral observation possible, the cylindrical vessel is provided with optical windows on the top and the bottom. A cross section of the plasma is depicted in figure 2. The filling pressures are 10, 50 and 100 mbar of high purity argon. During operation the pressures are about a factor of ten higher due to the temperature increment. For further details we refer to chapter 10.

Thesis outline

Chapter 2 starts with the presentation of a method for unraveling the contribution of the different mechanisms responsible for continuum radiation. These are mechanisms related to electron-ion and electron-atom interactions. It is shown that in the open ICP both interactions are of equal importance at moderate power, whereas for higher powers the electron-ion interactions become dominant over the electron-atom interactions.
Chapter 3 introduces the Thomson scattering setup with the first results and discusses a new calibration method for Thomson scattering, namely Raman scattering. The next chapter (4) continues with the presentation of Thomson measurements performed during the power interruption of the generator, enabling a time-resolved study of electron density and temperature behavior. These measurements reveal properties of diffusion and recombination which are also present in the stationary plasma.
In chapter 5 the applicability and the results of the diode laser absorption method are discussed. Attention is paid to the shape of the line profiles of argon, especially to the behavior at the edge of the plasma where a large influence of the heavy particles is found.
In chapter 6 a new method for determining transition probabilities of the highly excited states in argon is presented and 15 new values with improved accuracy are given.
Chapter 7 gives a comparative study of all the applied diagnostics, resulting in a demarca-

diagnostics (abbreviation)	*parameters*	*chapters*
Thomson scattering (TS)	n_e, T_e	3, 4, 7, 10
Thomson scattering during power interruption (TSPI)	T_e^*, v_{n_e}, v_{T_e}	4, 7
Rayleigh scattering (RS)	n_h, T_h	7, 8
Raman scattering (RnS)	n_{N_2}	8
diode laser absorption (DLA)	T_h, n_{4s}, (n_e)	5, 7, 10
absolute line emission intensities (ALI)	n_e, T_e	6, 7, 10
line emission intensities during power interruption (LIPI)	T_e/T_e^*	7, 10
continuum emission intensities during power interruption	χ	2
H_β-broadening (HB)	n_e	7

Table 1. Overview of information about the diagnostics throughout the chapters.

tion of the validity region of each diagnostic tool as well as the discovery of difference in temperature between electrons and heavy particles during the power interruption period. Chapter 8 discusses the study for the entrainment of air into the open ICP.

In chapter 9 the results of chapter 3, 4, 7 and 8 are used to discuss the recombination and diffusion processes in the open ICP. A simulation of the electron density behavior during the power interruption shows partial agreement with established theories. For the edge of the plasma, the influence of molecules must be considered to explain the measured strong recombination rate. Chapter 10 discusses the results of measurements on the closed ICP. Though it is not the optimal filling, pure argon is used in this first approach in order to understand the basics of this type of plasma.

Finally, chapter 11 presents the general conclusions considering the whole thesis.

The chapters 2 - 10 contain articles which are published or submitted for publication. These chapters discuss the open flowing ICP (2 - 9) and the closed ICP (10). Notice that the open ICP is strongly associated with the closed ICP in both the physical properties as well as in the used diagnostics. The applied diagnostics are listed in table 1 together with reference to the chapters dealing with these diagnostics.

[1] P.W.J.M. Boumans, "Inductively coupled plasma emission spectroscopy", Wiley & Sons, New York, 1987.
[2] J. Jonkers, M. Bakker, J.A.M. van der Mullen, D.A. Benoy, K.T.A. Burm and D.C.Schram, "Measurements on the Philips QL-lamp for comparison with developed model", 7th International Symposium on the Science & Technology of Light Sources, Kyoto Japan, 1995.
[3] D.A. Benoy, K.T.A. Burm, J. Jonkers, J.A.M. van der Mullen and D.C. Schram, "Modeling of the Philips QL-lamp", 7th International Symposium on the Science & Technology of Light Sources, Kyoto Japan, 1995.
[4] T.B. Reed, J. of Appl. Phys. **32** (821), 1961.
[5] J.A.M. van der Mullen, "Excitation equilibria in plasmas; a classification", Physics Reports **191** (109), 1995.
[6] S. Nowak, J.A.M. van der Mullen and D.C. Schram, "Electron density and temperature determination in an ICP using a non-equilibrium concept", Spectrochim. Acta **43B** (1235), 1988.
[7] F.F. Fey, "Excitation balances and transport in an inductively coupled plasma", Ph.D. Thesis 1993.
[8] D.A. Benoy, "Modeling of thermal argon plasmas", Ph.D. Thesis 1993.

Chapter 2

Continuum radiation components*

* J.M. de Regt, J. van Dijk, J.A.M. van der Mullen, D.C. Schram, "Components of continuum radiation in an inductively coupled plasma", published in J. Phys. D: Appl. Phys. **28** (40), 1995.

Measurements of the continuum emission of an inductively coupled plasma in argon have been carried out. The mechanisms responsible for this radiation show different electron-density dependences. By interrupting the power that is followed by a decay of the electron density, it is possible to unravel these different mechanisms. From the measurements it is concluded that the electron-atom interactions are in general of equal importance to the electron-ion interactions in creating continuum radiation. The relative contribution of the electron-atom interactions depends on the conditions of the plasma. Furthermore, the measurements show that the cross section for electron-atom momentum transfer deduced from our experiment using the formula for electron-atom free-free continuum radiation is not in agreement with the literature.

1 Introduction

The inductively coupled plasma (ICP) is widely used as a spectrochemical analytical instrument. Knowledge of the fundamental processes can result in better understanding of the ICP and can help to improve its application. In this paper the origin of the continuum radiation in an argon ICP is studied. Three different processes and two different pairs of interacting particles, electron-ion (ei) and electron-atom (ea), are responsible. The three mechanisms are recombination or free-bound interactions (fb) by electron-ion interaction, free-free interactions (ff) between electrons and ions and free-free interactions between electrons and atoms. To estimate the contributions of these different mechanisms, a relatively old technique is used in an improved version.[1,2] This method is the interruption of the power to an ICP combined with registration of the emission. When the power of the ICP is switched off for about 70 μs, the continuum radiation changes in intensity. Two processes are relevant for these changes. First, the electrons will cool down to the heavy particle temperature within a few microseconds. Second, the electron density will decay due to recombination and diffusion. This happens with a time constant of about 200 μs. This change in the electron temperature (T_e) followed by that in electron density (n_e) can be used to distinguish between processes that differ in terms of dependency on electron density or electron temperature. In this paper we will discuss the difference in decay of the continuum contribution created by electron-atom interactions (n_e-dependency) on the one hand and that created by electron-ion interaction ($n_e n_i = n_e^2$) on the other. Therefore, we will rewrite the contributions to continuum radiation by introducing ξ-factors for each of the contributions and measure their relative contribution to the total continuum radiation.

2 Origins of continuum radiation

Continuum radiation originates from interaction of free electrons with atoms and ions. If a free electron is captured by an ion then we speak about free-bound radiation or recombination radiation. If only the momentum of the electron is changed by the interaction with an atom or ion then the radiation is called free-free radiation. Depending on the pairs of interacting particles, we distinguish between free-free of ei and free-free of ea type. Therefore, the emission coefficient ε of continuum radiation in a singly ionized gas is given by,

$$\varepsilon_{cont} = \varepsilon_{fb}^{ei} + \varepsilon_{ff}^{ei} + \varepsilon_{ff}^{ea}. \tag{1}$$

Here ε is the power emitted per unit of volume, solid angle and wavelength interval, ε_{fb}^{ei} is the continuum emission coefficient due to two particle recombination, ε_{ff}^{ei} the emission coefficient related to free-free interaction between an electron and an ion and ε_{ff}^{ea} is related to the electron-atom interaction. The essence of the experimental technique as presented in this study is that the emission created by ei interaction depends on the product of $n_e n_i$, whereas ε_{ff}^{ea} scales with $n_e n_a$. In an n_e-decaying plasma it is possible to unravel the ei and ea contributions from each other. Since $n_e = n_i$ in a singly ionized, quasi-neutral plasma the total continuum emission can be written as,

$$\varepsilon_{cont} = n_e^2 f(\lambda, T_e) + n_e n_a g(\lambda, T_e), \tag{2}$$

where $f(\lambda, T_e) = \left(\varepsilon_{ff}^{ei} + \varepsilon_{fb}^{ei}\right) n_e^{-2}$ and $g(\lambda, T_e) = \varepsilon_{ff}^{ea} / n_e n_a$ are functions of T_e and the wavelength of emission, λ.

For quantitative approximation of ε_{fb}^{ei}, ε_{ff}^{ei} and ε_{ff}^{ea}, we can use the expressions given by Cabannes[3] *et al.*,

$$\varepsilon_{fb}^{ei} = C_1 \frac{n_e n_i}{\lambda^2 \sqrt{T_e}} \left(1 - e^{\frac{-hc}{\lambda k_B T_e}}\right) \xi_{fb}^{ei}(\lambda, T_e), \tag{3}$$

$$\varepsilon_{ff}^{ei} = C_1 \frac{n_e n_i}{\lambda^2 \sqrt{T_e}} e^{\frac{-hc}{\lambda k_B T_e}} \xi_{ff}^{ei}(\lambda, T_e), \tag{4}$$

$$\varepsilon_{ff}^{ea} = C_2 \frac{n_e n_a}{\lambda^2} T_e^{\frac{3}{2}} Q(T_e) \left(\left(1 + \frac{hc}{\lambda k_B T_e}\right)^2 + 1\right) e^{\frac{-hc}{\lambda k_B T_e}}, \tag{5}$$

in which C_1 and C_2 are constants respectively equal to 1.632×10^{-43} $\mathrm{Jm^4K^{1/2}s^{-1}sr^{-1}}$ and 1.026×10^{-34} $\mathrm{Jm^2K^{3/2}s^{-1}sr^{-1}}$, ξ_{fb}^{ei} and ξ_{ff}^{ei} the free-bound and free-free Biberman factors for argon and $Q(T_e)$ the cross section for momentum transfer in electron-neutral species interaction.[4] The constants h, c and k_B are respectively Planck's constant, the velocity of light and Boltzmann's constant. It should be noted that ei free-free interactions described by equation (4) are only valid in the short-wavelength limit,[3] that is for $\lambda << hc/k_B T_e$. Our plasma parameters do not completely fulfill this wavelength restriction, but inaccuracies

can be neglected since this type of ei interaction makes only a minor contribution to continuum radiation of the studied plasma.
In order to compare the ei and ea continuum contributions we normalize the ε values with respect to $n_e n_i / \lambda^2 \sqrt{T_e}$ by introducing the generalized ξ^{ei} factor for electron-ion interactions and ξ^{ea}-factor for electron-atom interactions:

$$\xi^{ei}(\lambda, T_e) = \xi^{ei}_{ff} e^{-u} + \xi^{ei}_{fb}\left(1 - e^{-u}\right), \tag{6}$$

$$\xi^{ea}(\lambda, T_e, \alpha) = \frac{C_2}{\alpha C_1} T_e^2 Q(T_e)\left((1+u)^2 + 1\right)e^{-u}, \tag{7}$$

with $u = \dfrac{hc}{\lambda k_b T_e}$ and $\alpha = n_e/n_a$, the degree of ionization just after the cooling jump for $n_a >> n_e$.
Now the total continuum radiation can be described by,

$$\varepsilon_{cont} = \xi^{total} \frac{C_1}{\lambda^2} \frac{n_e^2}{\sqrt{T_e}}, \tag{8}$$

with

$$\xi^{total} = \xi^{ei}(\lambda, T_e) + \xi^{ea}(\lambda, T_e, \alpha). \tag{9}$$

In figure 1 the ξ-factors as functions of wavelength are depicted for an electron temperature of 12 000 K and a degree of ionization of 0.25%. For $Q(T_e)$ in ξ^{ea} the value calculated at 12 000 K by Devoto[4] is taken. The experimental values for the Biberman factors ξ_{fb}^{ei} and ξ_{ff}^{ei} are taken from Wilbers[5] *et al.* The influence on the results of the inaccuracy (<10%) in these data is negligible relative to the data obtained in our experiment.
To estimate the importance of the free-free ea interaction the parameter $\chi(\lambda, T_e, \alpha)$ is introduced, which is the relative contribution of this n_e dependent process to the total continuum radiation:

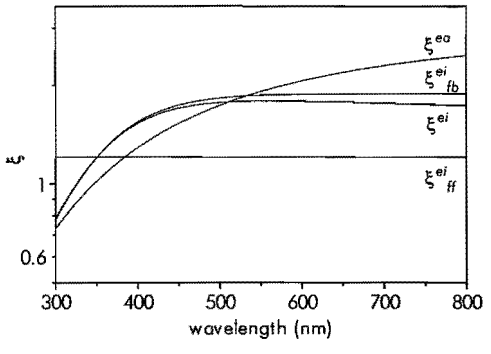

Figure 1. Continuum Biberman factors for T_e = 12000 K and α = 0.25%, separately and combined.

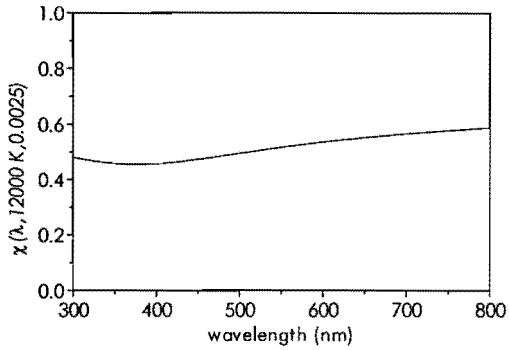

Figure 2. The χ-factor as a function of wavelength for T_e = 12 000 K and α = 0.25%.

$$\chi(\lambda,T_e,\alpha)=\frac{g(\lambda,T_e)}{g(\lambda,T_e)+\alpha\, f(\lambda,T_e)}=\frac{\xi^{ea}(\lambda,T_e,\alpha)}{\xi^{ea}(\lambda,T_e,\alpha)+\xi^{ei}(\lambda,T_e)}. \tag{10}$$

As an example the χ-factor versus wavelength is given in figure 2 for the conditions of figure 1. Note the relatively weak dependence on wavelength. The χ-factor at 550 nm is shown in figure 3 as a function of electron temperature and degree of ionization. These were calculated by using equations (6), (7) and (10). Again, for the electron-atom momentum-transfer cross section the electron temperature dependent value of Devoto[4] is used. Note the strong dependence of χ on the degree of ionization and electron temperature. Except for very small values, χ depends relatively weakly on the exact value of the Biberman factors ξ_{ff}^{ei} and ξ_{fb}^{ei}.

3 Experiments

3.1 Description of the setup

The basic experimental setup of the power interruption technique is shown in figure 4. Switching off the generator is performed by a pulse circuit inside the generator, which is controlled by block pulses at TTL level. The off period is chosen to be about 70 μs. There

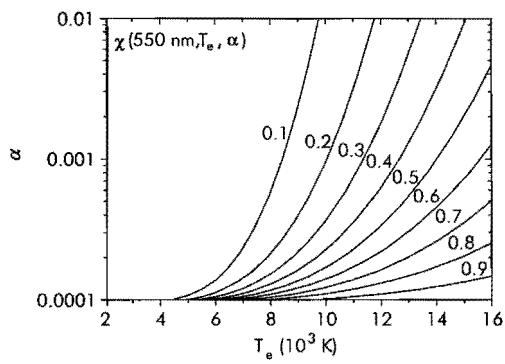

Figure 3. The χ-factors for different degrees of ionization and electron temperatures at 550 nm.

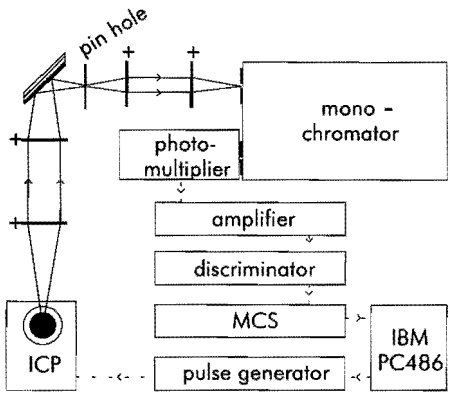

Figure 4. The basic experimental setup for the emission experiments.

is a limitation on this off-period since the plasma will extinguish and will not be restarted for long off periods. The plasma is focused on the entrance slit of a 1 m B&M BM100 monochromator with a 1200 lines per millimeter grating. The light is detected by a Hamamatsu R376 photomultiplier tube (PMT) operating at a voltage of 1100 V. The pulses from the PMT are amplified and analyzed by a pulse-height discriminator. Then the signal is recorded as a function of time by a multi channel scaler (MCS). This MCS has 4096 24-bit counters with a minimum integration time of 2 μs each. By using this MCS about 8 ms can be recorded continuously with a resolution of 2 μs. To obtain a good signal-to-noise ratio from the measurements, the results are the averaged signal over 50 000 repetitions.

3.2 Determining $\chi(\lambda, T_e, \alpha)$

To obtain information on the interactions in the plasma, the power interruption (PI) technique is used. For extensive description of the PI technique we refer to Fey[2] *et al.*, here we will give only a global explanation.

The technique is based on the fact that, under standard conditions, energy from the RF coil is transferred via the electrons to the heavy particles and that, therefore, the electron temperature is higher than the heavy particle temperature ($T_e > T_h$). Schematically the energy balance is presented by:

$$RF \rightarrow \{e\} \rightarrow \{h\} \rightarrow surroundings.$$

A sudden interruption of the power creates a decay in T_e towards T_h with a typical time scale of 1 μs, followed by a decay in n_e with a time scale of 100 μs.

The measured argon levels (Ar_p) are close to the ion ground state (Ar_1^+). This makes it true that the populations of these levels are ruled by the Saha balance

$$Ar_p + e + (I_p) \leftrightarrow Ar_1^+ + e + e, \tag{11}$$

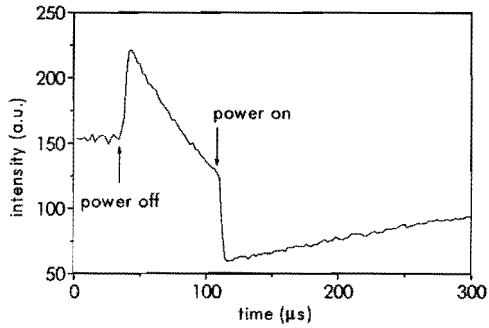

Figure 5. A typical argon line response induced by power interruption.

of ionization (to the right) and recombination (to the left). The energy I_p between the brackets is the ionization energy needed for electrons to execute the ionization process. Switching off the power supply means that the electrons will cool down to the heavy particle temperature. This implies that the group of electrons with sufficient translation energy will decrease in number. Owing to the fact that recombination is going on, the balance (11) will shift towards the left. This implies that the density of Ar_p will increase suddenly. After this so-called cooling jump the density of the argon level will decay due to decay of the electron and ion density ($n_e = n_i$). It is assumed that the density of Ar_p obeys the Saha balance at any time, which predicts that Ar_p scales with n_e^2. It is this decay that will be used to unravel the continuum radiation due to ei interactions (n_e^2) from that of the ea type (n_e). An example of the response of the 6d argon line to power interruption is shown in figure 5. Measurements of an argon line during interruption provide the time constant related to the decay[2] of n_e^2. This time constant largely depends on the position and plasma power, so it is necessary to measure it for each condition. If we assume that the electron density as a function of time decays exponentially, then the time dependent continuum emission at a certain wavelength can be described as,

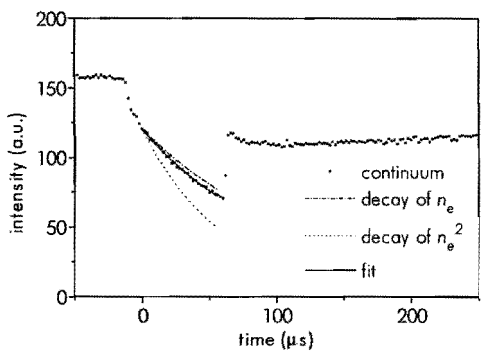

Figure 6. A typical continuum measurement during power interruption at 525 nm.

$$\varepsilon_{cont} = \varepsilon_0 \left(\chi(\lambda, T_e, \alpha) e^{\frac{-t}{\tau}} + (1 - \chi(\lambda, T_e, \alpha)) e^{\frac{-2t}{\tau}} \right). \quad (12)$$

The first term describes the contribution to the continuum of electron-atom interactions (n_e dependency) and the second term that of electron-ion interactions (n_e^2 dependency). A typical value of τ is found to be $\tau = 200\ \mu s$ (for $P = 1.5$ kW), deduced from the measured decay in intensity of line radiation at the same lateral position. ε_0 is the emission coefficient of the continuum radiation at $t = 0$ s. After switching off the power the electrons cool down to the heavy particle temperature within 1 μs and start to recombine. Since we are only interested in the last process, the fit has to start when the electron temperature becomes more or less stable. This is defined to be $t = 0\ s$, which is usually 12 μs after the start of the power interruption.

The response of the continuum to power interruption, induced by decreasing electron density, can be seen in figure 6. The lower and upper lines are respectively the decay described by only the n_e dependent processes or only the n_e^2 dependent processes. The line in between is the measured and fitted decay (using equation (11)), a combination of n_e and n_e^2 dependent processes. In this way a value of χ, the relative contribution of the n_e dependent part of the continuum, is obtained for each measured wavelength.

4 Results and discussion

The initial response to power interruption of the argon line intensity is the opposite to that of the continuum radiation, compare figures 5 and 6. On switching off the power supply, the line intensity increases whereas the continuum intensity decreases. Therefore, studying the time resolved emission during interruption of the plasma power gives unequivocal information about the detected radiation, whether it is line or continuum radiation. Hence, this method can be used for tracing continuum radiation.

Now the results of the measured χ-factors, that is, the importance of electron-atom interactions for the continuum radiation, will be discussed. All the presented measurements were performed 7 mm above the load coil (ALC) and 4.5 mm from the plasma center. Using the measured decay time of an argon line as a response to the power interruption, the χ-factor is measured as explained in section about the calibration procedure. In figure 7 the experimentally obtained χ-factors are given for two different input powers, as a function of three different wavelengths. The weak dependence on wavelength of the χ-factor was predicted by the theory. The difference in χ, that is, the relative contribution of electron-atom interactions to the continuum, for the two plasma powers is large. This large power dependence is shown more explicitly in figure 8, which gives the χ-factor measured at wavelength 526 nm for different plasma powers.

The inaccuracies in measured χ-factors are dominated by the uncertainty in the decay time τ. This inaccuracy in τ causes an average uncertainty in the χ-factor of about 13%. The reproducibility in measured continuum emission during power interruption is so good that it causes only a slight additional inaccuracy of 2%. Note that the first inaccuracy of 13% in χ-factor is independent of wavelength. This means that the relative values in figure 7 for a

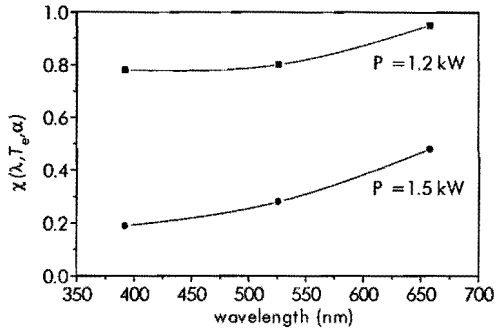

Figure 7. Measured χ-factors as a function of wavelength for two different input powers. The position is 7 mm ALC and 4.5 mm from the center of the plasma torch.

certain power have an inaccuracy of only 2%.

As can be seen from figure 8, the χ-factor is large for low powers. This implies that electron-atom interactions are of major importance at low powers. As the plasma power is increased, the contribution of electron-ion interactions becomes increasingly important. This is just as expected because higher power will create more electrons and ions. At a power of 2.1 kW, nearly the highest attainable power in the used setup, the continuum radiation is almost entirely created by electron-ion interactions and electron-atom interactions can be neglected. From these measurements it is very clear that for a plasma like the atmospheric ICP, driven at powers of order 1 kW, the contributions of electron-atom interactions to continuum radiation can certainly not be neglected in further calculations.

From the measured χ-factors it can be concluded that the trend in their behavior agrees with the theory. The absolute value of χ can be compared with the calculated values depicted in figure 3. Here, the value of χ was displayed in a contour plot as a function of electron temperature and the degree of ionization. If these parameters are known from other diagnostics like Thomson scattering,[6] then the corresponding χ can be estimated.

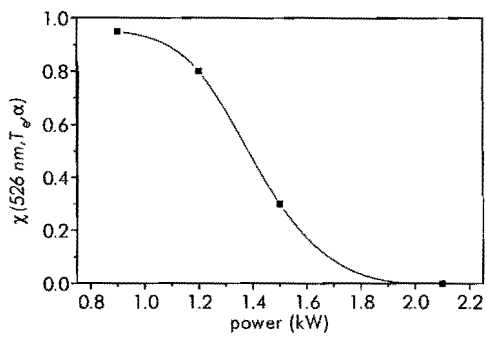

Figure 8. The measured χ-factor as a function of input power at 526 nm. The position is 7 mm ALC and at a radius of 4.5 mm.

This comparison shows a discrepancy in χ. It turns out that the calculated χ value is much lower than the value obtained from the measurements. This discrepancy cannot be explained by inaccuracies in the measured parameters. As can be seen from formulas (7) and (10), the influence on the χ-factor of the electron-atom cross section is significant. The calculations can be made to agree with the theory by taking a larger value of this momentum transfer cross section. This leads to the conclusion that the value for the electron-atom cross section used in equation (5) is about 2.5 times larger than predicted. The reason for the discrepancy is not clear, but might be due to the used approximation for the ε-values which could lose validity under these plasma conditions, or to differences between the definitions of $Q(T_e)$ by Devoto and by Cabannes *et al.*

5 Conclusions

This paper gives a new procedure for measuring the relative contributions to the continuum of electron-ion and electron-atom interactions. From these measurements it can be concluded that it is certainly not acceptable to neglect the contributions of electron-atom interactions to the continuum under widely used ICP conditions. Furthermore, the discrepancy between measurements and theory of the mechanisms contributing to the continuum is about a factor of 2.5. The experiments show a larger experimental cross section for electron-atom interactions than predicted by theories taken from the literature. Finally, the technique can be used for tracing the continuum, because the initial response to power interruption of the continuum is opposite to that of a line emission.

[1] D.B. Gurevich, I.V. Podmoshenskii, "The relationship between the excitation temperature and the gas temperature in the positive column of an arc discharge", Opt. Spectroscopy **15** (319), 1963.
[2] F.H.A.G. Fey, W.W. Stoffels, J.A.M. van der Mullen, B. van der Sijde and D.C. Schram, "Instantaneous and delayed responses of line intensities to interruption of the RF power in an argon inductively coupled plasma", Spectrochimica Acta **46B** (885), 1991.
[3] F. Cabannes, J.C. Chapelle and M. Venugopalan (Editor), "Reactions under plasma conditions", Wiley Interscience, John Wiley & Sons New York, 1971.
[4] R.S. Devoto, "Transport coefficients of ionized argon", Phys. Fluids **16** (616), 1973.
[5] A.T.M. Wilbers, G.M.W. Kroesen, C.J. Timmermans and D.C. Schram, "The continuum emission of an arc plasma", J. of Quant. Spectr. and Rad. Transfer **45** (1), 1991.
[6] J.M. de Regt, R.A.H. Engeln, F.P.J. de Groote, J.A.M. van der Mullen, D.C. Schram, "Thomson scattering experiments on a Inductively Coupled Plasma calibrated by Raman scattering", Rev. Sci. Instrum. **66** (3228), 1995. (Chapter 3)

Chapter 3

Thomson scattering with Raman scattering calibration*

* J.M. de Regt, R.A.H. Engeln, F.P.J. de Groote, J.A.M. van der Mullen and D.C. Schram, "Thomson scattering experiments on a 100 MHz inductively coupled plasma calibrated by Raman scattering", published in Rev. Sci. Instrum. **66** (3228), 1995.

A new calibration method to obtain the electron density from Thomson scattering on an inductively coupled plasma is discussed. Raman scattering of nitrogen is used for recovering the Rayleigh scattering signal. This has the advantage that no corrections are necessary for stray light, like with other calibration methods, using the direct measured Rayleigh scattering signal on a well-known gas. It is shown that electron densities and electron temperatures can be measured with an accuracy of about 15% in density and of about 150 K in temperature.

1 Introduction

Fundamental studies of inductively coupled plasmas (ICP) are necessary to improve their applications in spectrochemical analysis and in the use for light sources. Since the electron temperature and electron density are central plasma parameters, a Thomson scattering setup is designed for these parameters on a 100 MHz argon ICP. The construction of the diagnostic is similar to the one realized by Van de Sanden[1] *et al.* One of the features of this diagnostic is a detector, consisting of a photodiode array, in combination with a holographic grating with 2000 lines/mm. This results in a high spectral resolution in combination with a small apparatus profile.

Since the ICP is an atmospheric plasma of small dimensions, it is necessary to pay more attention to the method of measuring Thomson profiles and performing the calibration. The presence of atmospheric conditions causes an extremely intense Rayleigh scattering signal compared to the Thomson scattering signal. This large number of Rayleigh photons, together with stray light, will cause blooming on the photodiode array, which disturbs the spectrally broader Thomson signal. To eliminate the large number of disturbing photons on our detector, the detector is physically darkened for the channels that would otherwise cause blooming. By blocking these channels, it is possible to measure an undisturbed Thomson scattering profile, from which only a limited central part is missing.

The small dimensions of the plasma and its surroundings are the origin of the laser stray light that can enter the detector and looks similar to the Rayleigh scattering profile, with the shape of the apparatus profile. Therefore, the Rayleigh scattering signal cannot be measured separately. In order to unravel Rayleigh scattering from the stray light component one has to measure Rayleigh scattering on two different gases with different cross-sections. The difference between the ratio of the measured intensities and the ratio of the known scattering cross sections can be used to estimate the amount of stray light. This method of calibrating the setup takes a long time. Moreover, since we darkened the detector for this signal, it is not possible to use this calibration method as performed by Hieftje[2] *et al.*, that is, measuring the Rayleigh signal. Their apparatus[3] has less spectral resolution, but has the advantage that blooming is absent.

In the past it was suggested by Röhr,[4] that a Raman spectrum can be used for calibration. This calibration method[5] for Thomson scattering experiments on a tokamak uses Raman scattering on hydrogen. In our case, a procedure was developed to recover the Rayleigh intensity from the Raman spectrum of nitrogen. The advantages of this calibration method

are that stray light no longer plays any role and that the procedure can be applied easily and quickly.
This new method of calibrating the Thomson measurements on an atmospheric plasma is described in this paper.
Further, the results of experiments on a 100 MHz ICP are presented, where a large skin effect might be responsible for the difference with Thomson experiments on a 27 MHz ICP as previously published by Huang[6] *et al.*

2 Rayleigh and Raman scattering of nitrogen

To use the Raman spectrum for calibration, the intensity ratio of a specific Raman transition to the Rayleigh signal has to be presented as a conversion factor. It has to be noticed that the calibration will be done on nitrogen at room temperature, while the Thomson measurements to obtain electron density (n_e) and electron temperature (T_e) are carried out on free electrons in the plasma. Since the cross sections for the different Raman transitions depend on more parameters than the Rayleigh transitions, we choose for recovering the Rayleigh scattering signal of nitrogen instead of the direct approach which does not discern the Rayleigh signal and converts the Raman scattering intensity directly into the sensitivity of the setup. Ultimately, the discussed procedure leads to a conversion factor between the several Raman transitions in nitrogen and the Thomson scattering signal. In the derivation given below no explicit formulas are used to avoid large expressions which contain parameters of little interest for the final explicit expressions (see section 2.3).
In general, both the Rayleigh and the Raman scattering intensity I^J are proportional to

$$I^J \propto N_J \left(\frac{d\sigma}{d\Omega}\right)^J, \tag{1}$$

with J the rotational quantum number and N_J the number density of particles in the states with rotational quantum number J. This density is predicted by the Boltzmann relation, given by,

$$N_J \propto N g_J (2J+1) e^{-E(J)/k_B T}. \tag{2}$$

where N is the total number density of particles, g_J the nuclear degeneracy (for nitrogen $g_J = 2$ (J even) and $g_J = 1$ (J odd)), k_B the Boltzmann constant, T the temperature and $E(J) = B\,J(J+1)$, the energy of the rotational level J in the vibrational ground state with for nitrogen $B = 2.0$ cm^{-1}. We neglect any vibrational dependent part, since more than 99.9 % of the nitrogen molecules are in the vibrational ground state at $T = 300$ K.
The scattered light has two polarization dependent contributions, one parallel and one perpendicular to the polarization of the incoming beam. Since the efficiency of the diagnostic is less for the perpendicular part than for the parallel part, an instrumental correction factor C_0 is introduced. The difference is caused by the difference in efficiency of the grating for the two polarizations (for the used grating $C_0 = 2.21$ at 532 nm).

2.1 Rayleigh scattering

The Rayleigh signal arises from the rovibrational transitions for which $\Delta v = 0$ and $\Delta J = 0$. Using the Rayleigh formulas for diatomic molecules,[7] the differential Rayleigh cross section is calculated to be

$$\left(\frac{d\sigma}{d\Omega}\right)^{J}_{Rayl} \propto \frac{1}{45}\left(\frac{3}{\rho_{N_2}} + 3C_0\right) b_{J,J}\gamma^2, \tag{3}$$

where γ is the anisotropic part of the polarizability tensor. The often used averaged dipole polarizability, α, is here expressed in $b_{J,J}$, γ and ρ_{N_2}. ρ_{N_2} is the depolarization ratio (2.7×10^{-3} for nitrogen[8]). The factor $b_{J,J}$ is given by

$$b_{J,J} = \frac{J(J+1)}{(2J-1)(2J+3)}.$$

The total Rayleigh signal is given by a summation over all states J, and is found by combining equations (1) and (3),

$$I^{tot}_{Rayl} \propto \left(\frac{3}{45\rho_{N_2}} + \frac{3C_0}{45}\right)\gamma^2 N \sum_{J=0}^{\infty} b_{J,J}(2J+1) g_J e^{\frac{-E(J)}{k_B T}}. \tag{4}$$

Introducing the parameters A_{Rayl} and S, equation (4) can be rewritten as,

$$I^{tot}_{Rayl} \propto A_{Rayl}\gamma^2 N S, \tag{5}$$

with A_{Rayl} the term within the brackets (r.h.s. of equation (4)) and S the summation for $J = 0$ to, in principle, infinity. At a temperature of 300 K and a summation up to $J = 15$ we get a value of $S = 38.43$ (for nitrogen).

2.2 Raman scattering

Analogue to Rayleigh scattering, the Raman scattering intensity I^{J}_{Raman} can be calculated with equation (1), where the Raman scattering contains the parallel and perpendicular polarized parts with respect to the incoming beam. The perpendicular part can easily be found in the equations because it is accompanied by the instrumental factor C_0.

During the measurements the S-branch as well as the O-branch pure rotational Raman spectrum is detected. The Raman cross section for the S-branch ($\Delta J = +2$), is given by[7]

$$\left(\frac{d\sigma}{d\Omega}\right)^{J+2,J}_{Raman} \propto \frac{1}{45}(4+3C_0) b_{J+2,J}\gamma^2 = A_{Raman} b_{J+2,J}\gamma^2, \tag{6}$$

with $A_{raman} = (4 + 3C_0)/45$ and

$$b_{J+2,J} = \frac{3(J+1)(J+2)}{2(2J+1)(2J+3)}.$$

For the O-branch ($\Delta J = -2$):

$$\left(\frac{d\sigma}{d\Omega}\right)_{Raman}^{J-2,J} \propto \frac{1}{45}(4+3C_0)b_{J-2,J}\gamma^2 = A_{Raman}b_{J-2,J}\gamma^2, \tag{7}$$

with

$$b_{J-2,J} = \frac{3J(J-1)}{2(2J+1)(2J-1)}.$$

These equations describe the Raman intensity for the different transitions that can be measured with the experimental setup. Finally, a combination of the above-mentioned formulas will give a conversion factor that transfers the measured Raman intensities to the Rayleigh intensity.

2.3 The conversion factors from Raman to Rayleigh scattering intensity

Dividing the total Rayleigh intensity by the single peak Raman intensity, the two separate conversion factors for $\Delta J = +2$ and $\Delta J = -2$, which depend only on the temperature and on J, are given by,*

$$\Delta J = +2: \qquad \frac{I_{Rayl}^{tot}}{I_{Raman}^{J+2,J}} = \frac{A_{Rayl}}{A_{Raman}} S \frac{2(2J+3)}{(J+1)(J+2)} g_J^{-1} e^{\frac{E(J)}{k_B T}}, \tag{8}$$

$$\Delta J = -2: \qquad \frac{I_{Rayl}^{tot}}{I_{Raman}^{J-2,J}} = \frac{A_{Rayl}}{A_{Raman}} S \frac{2(2J-1)}{J(J-1)} g_J^{-1} e^{\frac{E(J)}{k_B T}}. \tag{9}$$

Note that in the case of measuring free electrons in the plasma, the difference in the differential scattering cross section for nitrogen and for free electrons has to be taken into account ($d\sigma_{Thomson}/d\Omega = 7.95 \times 10^{-30}$ m^2 and $d\sigma_{nitrogen}/d\Omega = 6.90 \times 10^{-32}$ m^2 at a wavelength of 532 nm).[9] Further, the Raman spectrum consists out of several peaks corresponding to specific transitions from J to $J \pm 2$, so for each of these transitions the formulas can be applied (see section 3.2). In this way for several of the peaks (six in total), a corresponding Rayleigh scattering intensity can be calculated. Averaging gives the final value of the Rayleigh scattering intensity.

3 Experimental

3.1 Thomson scattering diagnostic

The experimental setup is depicted in figure 1. A frequency doubled Nd:YAG-laser (GCR 3 Quanta Ray, $E_{pulse} = 0.45$ J, $\tau_{pulse} = 7$ ns, $f_{rep} = 10$ Hz) at 532 nm is used. Two prisms lead the beam into the detection volume. The beam is focused by a lens L_1 ($f = 1000$ mm). Finally, the laser beam is absorbed in a laser dump. The detection branch starts with two lenses L_2 and L_3 ($f = 600$ mm) that image the detection volume onto the entrance slit (300 mm) of the monochromator. Behind the slit a half-lambda mica retarder R is placed, since the grating efficiency is higher for a normally polarized beam. The dispersive element is the

* See remark at the end of this chapter.

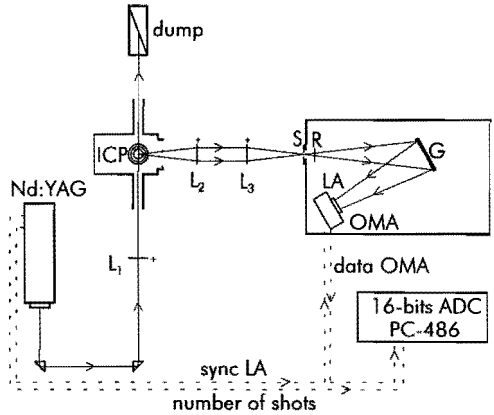

Figure 1. The Thomson scattering setup, viewed from the top. With L_1, L_2 and L_3 the focusing and detection lenses, S the entrance slit, M the mica retarder, G the 2000 lines/mm grating, LA the image intensifier and OMA the optical multichannel analyzer.

concave holographic grating G (Jobin Yvon, 2000 lines/mm, (100 × 100) mm and f = 1 m). To reject the stray light, the prisms are positioned at about 3 m from the detection volume and the focusing lens L_1 has an anti-reflection coating for 532 nm. Anyhow, in the case of measuring close to the torch, the most interesting area, the largest source of scattering is the quartz ICP torch itself, which, of course, can not be eliminated.

The detector consists of three parts: a gated image intensifier LA (10^4 times amplification, τ_{gate} = 100 ns, imposed by laser synchronization problems), a cooled (–20 °C) optical multichannel analyzer OMA (photodiode array of 1024 pixels, 25 mm × 2.5 mm each, total length 25.6 mm) and an IBM 486 PC with a 16-bits AD converter. The full spectral range of the detector is 13 nm, the apparatus profile has a *1/e* width of 0.14 nm. To prevent the array from blooming during the measurements due to the intense Rayleigh and stray light, the OMA is physically darkened for about 50 pixels in the center, which eliminates the core of the Rayleigh scattering profile. However, it should be noticed that apart from the core, there is also a contribution of Rayleigh and stray light photons in the wings of the profile. This originates from the finite contrast of the monochromator. For the plasma-on Rayleigh scattering this wing contributions turns out to be negligible. This is due to the high gas temperature and consequently low density.

In figure 2 a measured Thomson scattering profile (squares) and the fitted Gaussian profile (dashed line) are depicted. The perfect fit of the Gaussian profile shows that the Doppler broadened profile is indeed not disturbed by Rayleigh scattering or stray light. From the width of this Doppler broadened profile the electron temperature can be calculated.[1,*] The surface of the profile is used for calculating the electron density. Therefore, the sensitivity of the setup has to be calibrated.

[*] See remark at the end of chapter 4.

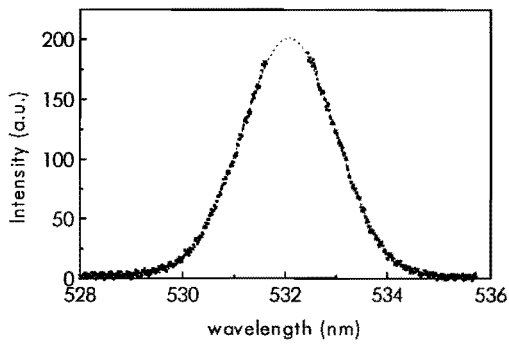

Figure 2. A typical Thomson profile with a fitted Gauss corresponding to $n_e = (2.7 \pm 0.4) \times 10^{21}$ m^3 and $T_e = 8925 \pm 150$ K. Notice the absence of signal in the central channel, which is caused by blocking these pixels, in order to avoid blooming.

3.2 Calibration procedure

To get absolute results on the electron density by the Thomson scattering signal, the sensitivity of the setup has to be calibrated absolutely. Van de Sanden[1] *et al.* used the Rayleigh scattering signal for this purpose. Therefore, measurements on an argon gas sample of well-known pressure were performed under equal conditions as during the plasma measurements. Knowing the ratio between the Rayleigh (at 532 nm) and the Thomson cross section (equal to 1/143) and measuring the pressure and gas temperature of the sample, using the ideal gas law, a relation was derived between the absolute density and the number of ADC counts.

In the case of measuring on an atmospheric plasma, that shows a strong Rayleigh signal, and moreover measuring on a geometrically small plasma, causing stray light, the Rayleigh signal can not be measured properly together with the Thomson signal using the detector mentioned above. Therefore, as already mentioned, the detector is blocked for Rayleigh

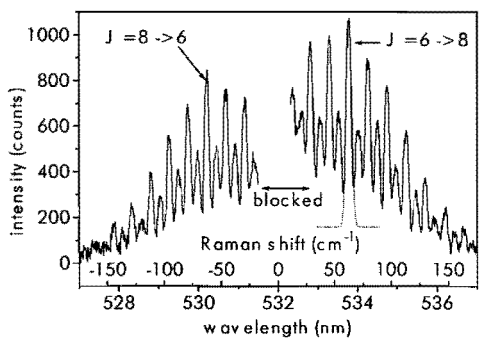

Figure 3. A measured Raman spectrum of nitrogen at room temperature. As an example the fitting of a Raman transition is depicted. This fitting is based on the known apparatus profile and shows that the Raman peaks are superimposed on a Rayleigh and stray light background. Present at room temperature calibration conditions, this background will disappear under plasma conditions.

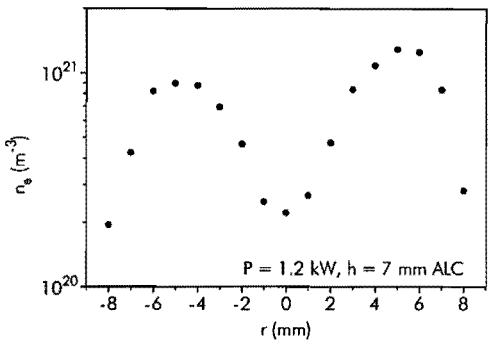

Figure 4. The measured n_e as a function of radial position at 7 mm ALC.

and stray light photons.

If the calibration on gas (plasma off) would be performed on a nonblocked detector, Rayleigh scattering would be measured together with stray light and separating them needs additional effort. Moreover, removing the strip, that is used to cover the detector for measuring the Rayleigh signal, would increase the inaccuracy of the calibration and takes a lot of time. This is not done in our study, so the only signal that can be measured with this setup at atmospheric conditions is Raman scattering (see figure 3), with peaks at wavelengths which are different from that of the laser and stray light peak. Fitting the surface under a Raman peak for a value of the rotational quantum number J with an apparatus profile, a corresponding Rayleigh intensity can be recovered using the conversion factors of equations (8) and (9). The fits are performed with a fixed width, the width of the apparatus profile, and using only the upper-half of the profile. This has the advantage that a small overlap of the Raman peaks and a background by, for example, Rayleigh scattering does not influence the results. As an example, the fit of one Raman peak is depicted in figure 3. The origin of the "background" lies in a small overlap of the Raman peaks and in a flank of the Rayleigh and stray light profile. Under plasma conditions, this flank of Rayleigh scattering and stray light can be neglected because the intensity of Rayleigh scattering decreases by at least a factor

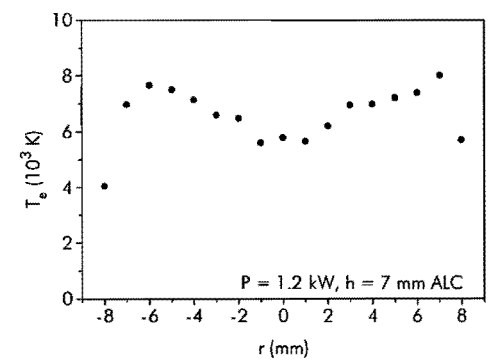

Figure 5. The measured T_e as a function of radial position at 7 mm ALC.

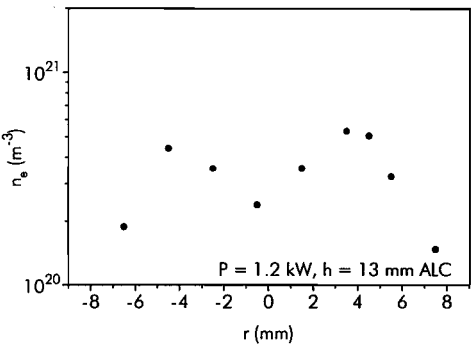

Figure 6. The measured n_e as a function of radial position at 13 mm ALC.

of 10 as a result of the higher temperature and therefore lower density of heavy particles. During the calibration, when the plasma is not lit, the amount of stray light is small compared to the Rayleigh scattering signal. This can be concluded from the Thomson measurements. The perfect Gaussian fit through the Thomson measurements shows that stray light has a negligible influence, so that it appears to be small compared to the Thomson profile as well as the Raman scattering measurement. To increase the accuracy of calibration, six Raman peaks are treated and the recovered Rayleigh signals are after this conversion averaged. In this way it is possible to recover the eliminated Rayleigh signal from the Raman measurements with an accuracy better than 9% (see section 2.3) and to calibrate the setup without inaccuracies caused by stray light.

4 Results

In figures 4 and 5 sets of measurements for different radial positions at 7 mm above the coil (ALC) are presented. The plasma power settings are 1.2 kW. The asymmetry of the radial dependent electron density and electron temperature profiles are due to the asymmetry of the coil. Further, the lower density and lower temperature in the center of the plasma are well-known features of the ICP. Here, the advantage of Thomson scattering is

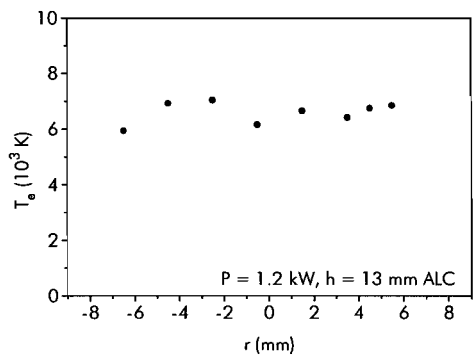

Figure 7. The measured T_e as a function of radial position at 13 mm ALC.

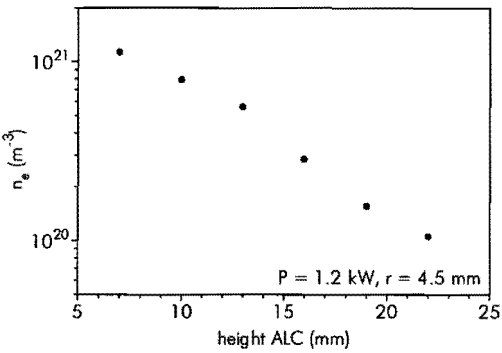

Figure 8. The measured n_e as a function of height at a radial position of 4.5 mm.

directly shown by the spatially resolved information. There is no need for mathematical routines to reconstruct local information out of line-of-sight measurements (Abel-Inversion). Comparing these results with measurements performed by Huang[6] *et al.* we see a much larger difference in density and temperature between the center and the hottest area of the plasma. In general this difference is due to the skin effect. So we conclude that in our plasma a larger skin effect is present. This might be explained by our high frequency generator of 100 MHz instead of the normally used frequency of 27 MHz.

In figures 6 and 7 the electron temperatures and electron densities are shown at a height of 13 mm ALC. Since this region is farther away from the ionizing part of the plasma, we see lower values. Moreover, the skin effect is decreased as well. The radial profiles are much smoother. The measurements of figures 8 and 9 show also the change in electron density and electron temperature by increasing the height above the load coil at a radial position of 4.5 mm. Finally, the dependence of the power input on the density and temperature is presented in figures 10 and 11.

The highly dispersive grating in combination with the gated image intensifier and the 1024 channel photodiode array is responsible for a very accurately measured Thomson profile (within 1%), see also figure 2. But still the accuracy of these measurements is about 15% in

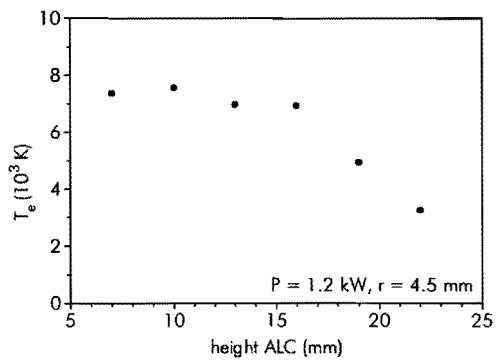

Figure 9. The measured T_e as a function of height at a radial position of 4.5 mm.

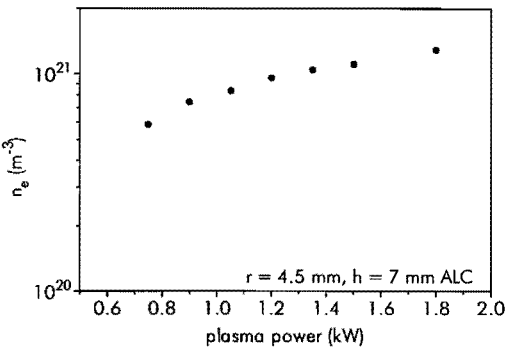

Figure 10. The measured n_e as a function of power at a radial position of 4.5 mm and 7 mm ALC.

the electron density and about 150 K in the electron temperature. The inaccuracies in electron temperature do not include reproducibility, which is an important source of inaccuracies in the electron temperature since the power settings can only be reproduced by about 0.1 kW. The inaccuracy imposed by this problem is about 500 K. For the influence of the power on the electron temperature see figure 11.

The main inaccuracy in the electron density is caused by the calibration of each Thomson measurement. Beside minor inaccuracies in the conversion of the Raman to the Rayleigh intensity, the most important sources are the instabilities in the setup and the measured Raman spectrum itself. The Nd:YAG-laser has a power stability within 3%. Other origins of variations in the intensity of the detected signal can be found in a slight drifting of the optical components, for example, by heating. These variations are directly responsible for the inaccuracies since the electron density depends on the surface under the Thomson profile. To avoid these instability effects, a rather long period of about 1 hour waiting time is necessary to get the whole setup stable. Further, the more often a calibration on nitrogen is carried out, the more accurate the electron density will be. In practice calibrating each hour will do. Inaccuracies in the Raman measurements will in future be lowered by a better conditioned nitrogen gas sample above the torch instead of flowing nitrogen through the torch.

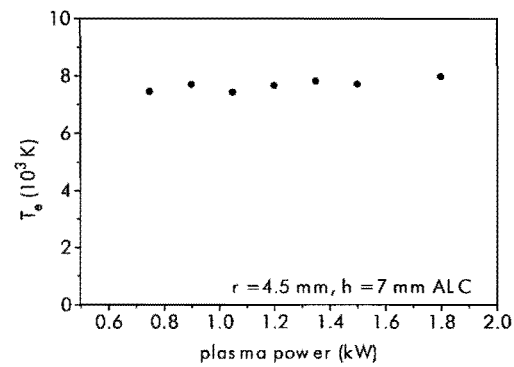

Figure 11. The measured T_e as a function of power at a radial position of 4.5 mm and 7 mm ALC.

[1] M.C.M. van de Sanden, G.M. Janssen, J.M. de Regt, D.C. Schram, J.A.M. van der Mullen, and B. van der Sijde, "A combined Thomson-Rayleigh scattering diagnostic using an intensified photodiode array", Rev. Sci. Instrum. **63** (3369), 1992.
[2] M. Huang and G.M. Hieftje , "Thomson scattering from an ICP", Spectrochimica Acta **40B** (1387), 1985.
[3] K.A. Marchall and G.M. Hieftje, "Thomson scattering for determining electron concentrations and temperatures in an inductively coupled plasma- II. Description and evaluation of a multi channel instrument", Spectrochemica Acta **43B** (851), 1988.
[4] H. Röhr, "Rotational Raman scattering of hydrogen and deuterium for calibrating Thomson scattering devices", Physics Letters A, **81A** (451), 1981.
[5] H. Röhr, K.-H. Steuer, G. Schramm, K. Hirsch, H. Salzmann, "First high-repetition-rate Thomson scattering for fusion plasmas", Nuclear Fusion **22** (1099), 1982.
[6] M. Huang, D.S. Hanselman, P. Yang and G.M. Hieftje, "Isocontour maps of electron temperature, electron number density and gas kinetic temperature in the Ar inductively coupled plasma obtained by laser-light Thomson and Rayleigh scattering", Spectrochemica Acta **47B** (765), 1992.
[7] D.A. Long, "Raman Spectroscopy", McGraw-Hill, Inc., 1977.
[8] R.F.G. Meulenbroeks, D.C. Schram, L.J.M. Jeagers, and M.C.M. van de Sanden, "Depolarization Rayleigh Scattering as a Means of Molecular Concentration Determination in Plasmas", Phys. Rev. Letters **69** (2796), 1992.
[9] J. Trapy, J.C. Lelievre and J. Picard, "Mesure des sections efficaces de diffusion de la lumiere a l'aide d'un laser He/Ne de faible puissance", Physics Letters **47A** (85), 1974.
[10] F.H.A.G. Fey, W.W. Stoffels, J.A.M. van der Mullen, B. van der Sijde and D.C. Schram, "Instantaneous and delayed reponses of line intensities to interruption of the RF power in an argon inductively coupled plasma", Spectrochemica Acta **46B** (885), 1991.

Raman scattering calibration in retrospective

The use of Thomson scattering for the n_e determination requires an absolute calibration. In section 2 of this chapter a Raman scattering procedure is presented to enable quick and stray light independent calibrations.
Recently, this Raman calibration method is compared to the commonly used Rayleigh scattering calibration procedure as is also discussed briefly in section 3.2 Unfortunately, using the same setup, the Raman method proves to give a factor of 3 too high electron densities compared to the results of the straightforward method of Rayleigh scattering.
In the original article, equations (8) and (9) and the obtained n_e-values are erroneously missing a factor 3. However, in this chapter both the equations (8) and (9) and the vertical axis of the n_e-figures 4, 6, 8 and 10 are corrected and represent the correct values of n_e.

Chapter 4

Electron density and temperature response to power interruption*

* J.M. de Regt, J.A.M. van der Mullen and D.C. Schram, "The response of the electron density and temperature to the power interruption measured by Thomson scattering in an inductively coupled plasma", published in Phys. Rev. E **52** (2982), 1995.

Electron density and temperature measurements during a power interruption of the generator are performed on a 100 MHz flowing argon inductively coupled plasma. The Thomson scattering setup for measuring the density and temperature is triggered in such a way that temperatures and densities are obtained as a function of time while the power is interrupted. The response of the electron temperature to the power interruption shows a jump downwards within 5 μs, presumably towards the heavy particle temperature. Therefore, the method can be used to determine the heavy particle temperature. Furthermore, insight is obtained as to the behavior of the electron density in the center of the plasma; it increases rather than decreases after the power interruption.

1 Introduction

In this paper we present the results of Thomson scattering experiments while the power of an atmospheric 100 MHz inductively coupled plasma (ICP) is interrupted. This type of ICP is widely used as a spectrochemical analytical instrument. In the future, a closed version might be used for lighting applications. Research on this type of plasma can improve their application and performance. Since the plasma is created by an EM field in an argon flow, we will find ionizing and recombining parts in the plasma. Using the technique of power interruption, the plasma can be studied while every part is recombining. This technique was developed by Gurevich[1] *et al.* and improved by Fey[2] *et al.* The essence of this technique is that instantaneously the EM field is dropped to zero by switching off the generator for a period of typically 100 μs, resulting in an absence of energy input for that period. The technique of power interruption can be used for studying plasma processes such as recombination rates, heat transfer, transport and deviations from equilibrium. In past years, a lot of measurements were performed using passive emission spectroscopy.[2,3] This paper presents a new method: a combination of the power interruption technique and the Thomson scattering measurements. Thomson scattering has proved to be a valuable technique for measuring local electron densities and temperatures.[4,5,6] The opportunity to combine these two methods gives a lot of additional information such as the spatially resolved decay of the electron density and temperature as a function of time. Moreover, in contrast to line emission spectroscopy, it is a direct and spatially resolved observation of the electron gas during the power interruption. The results show that after switching off the generator the electron temperature decreases instantaneously (within 5 μs) to a lower level, presumably the temperature of the heavy particles. This is followed by a decrease of the electron density in the active plasma parts with a typical time scale of 100 μs. More remarkable, it is found that the electron density in the center of the plasma increases during the power interruption.

2 The power interruption technique

Since a plasma can exist by the grace of the production of electrons, information on the properties of this plasma component can help us to understand and model the ICP. Especially the processes of ionization, recombination, and diffusion are very closely connected to the kinetics of the electrons. Therefore, a sudden change in the kinetics of the electrons can provide a lot of information about these processes. This is the main goal of the power interruption technique.

For the stationary plasma, where the electron temperature (T_e) is higher than the heavy particle temperature (T_h), there is a stepwise energy balance that schematically can be presented by

$$EM\ field \rightarrow \{e\} \rightarrow \{h\} \rightarrow surroundings. \qquad (1)$$

The field heats the electrons $\{e\}$ which are cooled by the heavy particles $\{h\}$. These, on their turn, give their energy to the environment. The transfer from electrons to heavy particles is only possible if $T_e > T_h$.

Since the presence of local thermodynamic equilibrium (LTE) implies that

A) the temperature of the species is equal, thus $T_e = T_h$, and

B) the internal state distribution of the particles obeys the Saha-Boltzmann relation,

we should realize that due to the energy balance given above (1), the plasma can, strictly speaking, not be in LTE. Interrupting the power of the generator gives insight in the degree of equilibrium departure. To that account we study the following sequence of events:

1) Cooling: Immediately after the sudden power interruption the first step of the balance disappears, the EM field is removed, so the electrons are not heated anymore. This induces the decay in T_e towards T_h with a typical time scale of a few microseconds.[1,7,8] After this time scale, the first aspect of LTE (A) is reached. The change in T_e can be measured indirectly by following the line radiation in the cooling mechanism.[1,2] The technique as presented in this paper follows T_e directly.

2) Decay: While the plasma as a whole cools down very slowly due to energy transfer to the surroundings, the electrons recombine and diffuse away. By studying these processes, insight is obtained in the Saha-equilibrium disturbing mechanisms that violate aspect (B) of LTE. This violation is expected to be generated by diffusion and recombination. It is also expected that diffusion is dominant over recombination and that the electron density (n_e) decreases with a typical time scale of 100 μs.[7] This time scale τ can easily be estimated with the ratio of the square of the gradient length (Λ^2) and the diffusion rate (D_a),

$$\tau = \frac{\Lambda^2}{D_a}. \qquad (2)$$

For the ICP one can use 10^{-2} m^2s^{-1} for D_a and 10^{-3} m for Λ, finding indeed the typical time

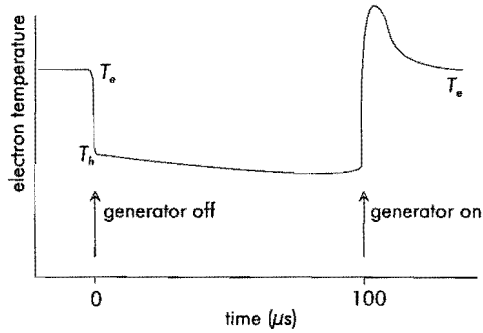

Figure 1. The expected effect of the power interruption on the electron temperature. At the time of switching on the generator, a peak above the stationary T_e value is expected (this is subject for future research).

scale of 100 μs. This is confirmed in previous spectroscopic studies. However, with the present technique we follow the electron density locally, directly, and more precisely. In this way it is found that the decay time is lower in the presence of large gradients. In the center of the plasma an increase rather than decay is found in n_e.

3) Heating: Immediately after the power is switched on again, the opposite of cooling takes place, restoring $T_e > T_h$.

4) Ionization: The interruption cycle is finished by a rather slow increase of the n_e back to the steady state value.

In this paper we present the measurements on the first two stages, the cooling and decay stages. By applying a trigger circuit, we are able to use Thomson scattering to measure n_e and T_e as a function of time while the power is interrupted. In this way, we are able to get direct and spatially resolved insight in the properties of the electron gas.
Figure 1 shows, as an example, how the electron temperature is expected to change during the interruption of the power from $t = 0$ to 100 μs. Since after interruption of the generator, the decay of the electron temperature presumably towards the heavy particle temperature (T_h) takes place within a few microseconds, whereas there are no other mechanisms which drive T_e and T_h apart from each other, we expect that during the power interruption T_e remains equal to T_h. This implies that measuring the electron temperature just after switching off the generator can be used as a method to obtain the heavy particle temperature for the steady state condition.

3 Experimental setup

3.1 The description of the plasma

The power interruption is carried out on a pure argon plasma. This plasma is created in a RF coil, fed by a 100 MHz generator developed by Philips with the additional feature of the capability to switch the generator on and off by a TTL-signal. It takes about 2 μs

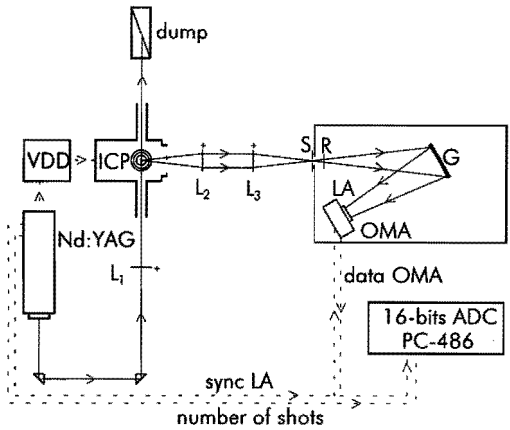

Figure 2. The Thomson scattering setup, viewed from the top. L_1, L_2 and L_3 are focusing and detection lenses, S is the entrance slit, R is the mica retarder, G 2000 lines/mm grating, LA is the image intensifier, OMA is the photodiode array, and VDD is the variable delay device.

before the EM field is decreased down to 5% of the stationary field. The power supply is kept on to make a fast restore of the EM field possible. The RF coil has two windings with a diameter of 35 mm and a total height of 15 mm. The plasma torch is placed in the center of the coil.

3.2 The Thomson scattering diagnostics

Thomson scattering in the ICP originates from the scattering of incident light by the free electrons present in the plasma. Since this process has a very low efficiency, an intense light source and a very sensitive detector have to be used. The experimental setup is depicted in figure 2. The light source is a frequency doubled pulsed Nd:YAG laser at 532 nm (GCR 3 Quanta Ray, E_{pulse} = 0.45 J, τ_{pulse} = 7 ns, f_{rep} = 10 Hz). Two prisms and a lens L_1 focuses the laser light into the detection volume. With the lenses L_2 and L_3 the plasma and detection volume are imaged on the entrance slit of the monochromator. The detector is an intensified photodiode array with 1024 pixels and is cooled down to –20° C. The full spectral range of the system is 13 nm with a resolution of 0.14 nm. The intensifier is gated, which allows us to measure during the short laser pulse only. In this way the plasma light is reduced by a factor of about 10^6 and can be neglected compared to the Thomson scattering signal. The Thomson scattering signal is broadened by the Doppler effect of the thermal electron motion. Therefore, the temperature of the electrons can be taken from the width of the Thomson scattering profile.* After an absolute calibration of the setup using Raman scattering on nitrogen, the total scattering signal can be used for obtaining the n_e. For more details about the used Thomson scattering diagnostic and calibration technique we refer to [6].

Since the laser pulse is relatively short, it determines the point in time of the actual meas-

* See remark at the end of this chapter.

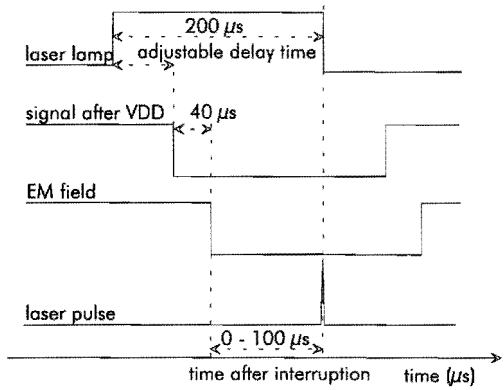

Figure 3. The signals dealing with the triggering of the measurements.

urement of the density and temperature of the electrons. Therefore, a variable trigger circuit is necessary to choose the delay between switching off the generator and pulsing the laser. In figure 3 the signals dealing with the triggering are depicted. The trigger output of the flash lamps of the laser is used to trigger the generator. This signal precedes the actual laser light pulse by about 200 μs, taking into account that the generator itself has an internal delay of 40 μs. A variable delay device (VDD) is designed, with 0.1 μs resolution, to choose the time of interruption. In this way, the trigger circuit can be used to perform measurements conveniently at several points in time after the switching off of the generator. This happens with a repetition frequency of 10 Hz, the repetition frequency of the Nd:YAG laser. The final results are obtained by the integration of 1000 laser shots, which means 100 s to measure one position in the plasma for a certain moment after the switching off of the generator.

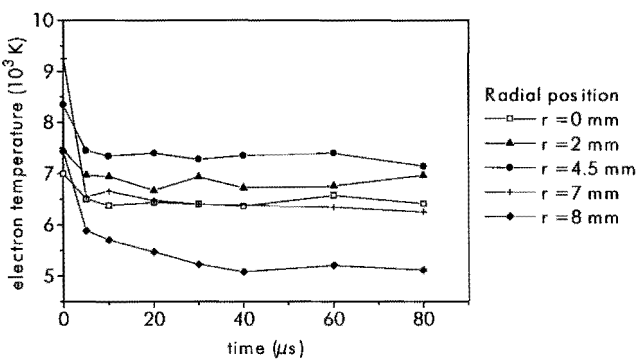

Figure 4. The electron temperature as a function of time after switching off the generator for several radial positions at 7 mm ALC and with an input power of 1.2 kW.

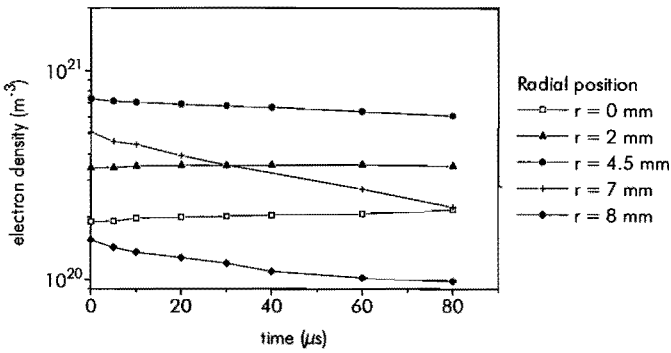

Figure 5. The electron density as a function of time after switching off the generator for several radial positions at 7 mm ALC and with an input power of 1.2 kW.

4 Results and discussion

The measurements were performed at 7 mm and 13 mm ALC with an input power of 1.2 kW, for ten different radial positions. A second series was performed at 7 mm ALC and 4.5 mm from the center of the plasma with different power inputs, namely, 0.6, 0.9, 1.2, 1.5, and 1.8 kW. All the series of measurements start with a measurement without interrupting the generator. Immediately after this, Thomson measurements are carried out 5, 10, 20, 30, 40, 60, and 80 μs after switching off the generator. In this way, a set of measurements is obtained for several radial positions as a function of the time.

In figure 4 the electron temperatures and in figure 5 the electron densities are depicted for five of the ten radial positions as a function of time for a power of 1.2 kW. Note that at 7 mm ALC and for 1.2 kW input power the center of the active area lies about 4.5 mm from the center. Here we will find the highest n_e and also the highest heavy particle temperatures, as we will see in section 4.1. The edge of the plasma lies at about 8 mm from the center, as can be seen in figures 4 and 5, where it is shown that the lowest values for n_e and

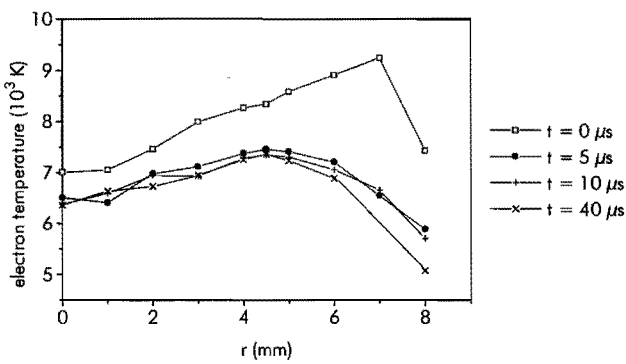

Figure 6. Radial profiles of the electron temperature at 0, 5, 10, and 40 μs after switching off the generator, measured at 7 mm ALC, the input power equals 1.2 kW.

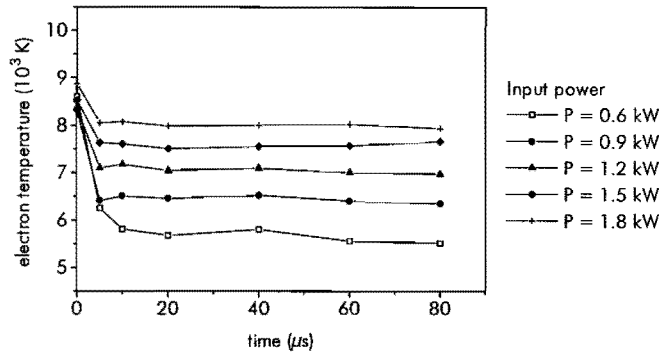

Figure 7. The electron temperature as a function of time during the power interruption for five different power values. The measurements are performed at r = 4.5 mm and at 7 mm ALC.

T_e are found for $r = 8$ mm. Efforts to measure even further at the edge of the plasma failed due to the presence of nitrogen at that position. Here, the measured signal shows a weak Thomson profile, because of the low densities, with a superposition of a strong Raman scattering spectrum, because the presence of some nitrogen.
The center of the plasma also has lower densities and temperatures compared to the skin, a well-known ICP feature originating from the limited skin-depth of the plasma for the EM field, the source of the ionization energy.
The further discussion of the results will consider first the behavior of the electron temperature and is continued by the response of the electron density to the power interruption. However, note that n_e and T_e are obtained from the same Thomson scattering profile.

4.1 The electron temperature during the power interruption

Looking at the behavior of the electron temperature as a function of time (cf. figure 4), we find large differences for the different radial positions. In the skin center, at $r = 4.5$ mm, the response to the power interruption is as expected, namely, a sudden decrease of T_e

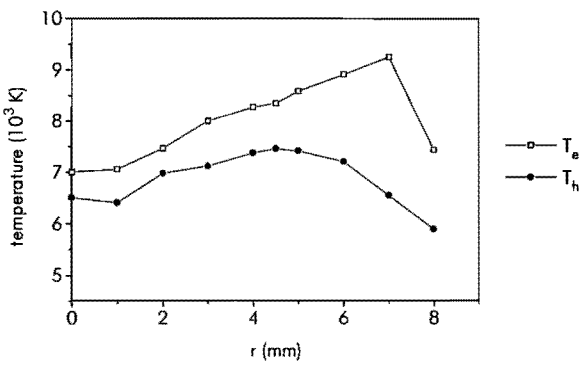

Figure 8. The electron and heavy particle temperature as a function of radius obtained by combining the Thomson scattering diagnostic with the power interruption technique; the axial position was 7 mm ALC, the input power equals 1.2 kW.

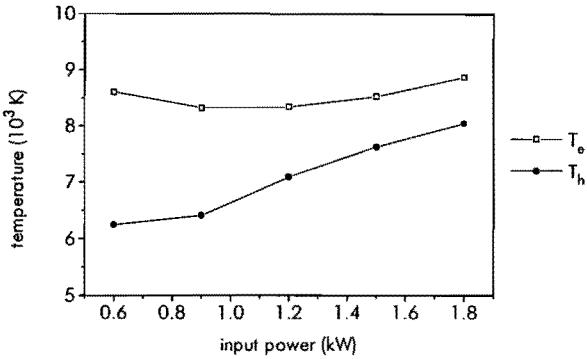

Figure 9. The electron and heavy particle temperature for five different input powers obtained by combining the Thomson scattering diagnostic with the power interruption technique. The axial and radial positions are 7 mm ALC and 4.5 mm, respectively.

towards a lower level, assumed to be the heavy particle temperature, and afterwards a slow decrease due to the cooling of the plasma by heat transfer to the surroundings. We will refer to this behavior with "typical response." The time scale of the jump of T_e to T_h is indeed within a few microseconds, as predicted by theory. Remarkable is the behavior as a function of time at the edges of the ionizing area, at $r = 2$ and $r = 7$ mm. Here we find from 0 – 5 μs a decrease followed by an increase of T_e in the next five microseconds. Since these jumps up in temperature are in the order of 100 K whereas the accuracy[6] in T_e is about 150 K, the behavior can be due to inaccuracies of the diagnostics.

The temperature responses to the power interruption at the center ($r = 0$ mm) and outer side ($r = 8$ mm) of the plasma are comparable to that of the skin center ($r = 4.5$ mm). Figure 6 shows how the radial T_e profile evaluates as a function of time. After the jump downwards, we see globally a slow decrease of the temperature. Note that at the center of the plasma ($r = 0$ mm), T_e remains constant after the small jump downwards immediately after the power switch off.

The measurements at $r = 4.5$ mm and $h = 7$ mm ALC for different powers (cf. figure 7) show a similar response to the power interruption as the one given in figure 4. For five powers the response is measured. The measurement with 1.2 kW input power corresponds just to the measurement at $r = 4.5$ mm in figure 4 if the mentioned accuracies are taken into account, but is measured one day later. Nevertheless, the reproducibility after having restarted the plasma is dominated by the accuracy of the power settings, which results in an estimated accuracy[6] of about 500 K. As a function of increasing input power, figure 7 shows that the size of the jump downwards decreases. This implies that the higher the input power the smaller the temperature difference is between the electrons and heavy particles, or in other words, the plasma will be more in thermal equilibrium for higher input powers. Assuming that the temperature of the electrons drops down to the heavy particle temperature within 5 μs after switching off the generator, the heavy particle temperature T_h for the steady state condition can be determined. In figure 8 the steady state values of T_e and T_h are given as a function of the radial position. In figure 9 T_e and T_h are shown as a function

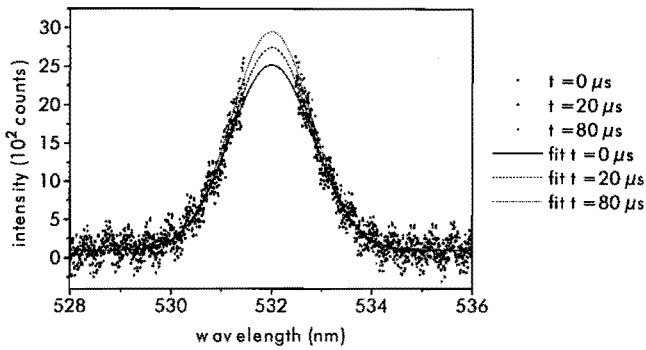

Figure 10. Three Thomson scattering profiles obtained at 7 mm ALC and in the center of the plasma (r = 0 mm). The lines in the figure are the corresponding fits, representing an accuracy better than 2% in width and surface. Note the increasing surface (density) as a function of time after switching off the generator. Note that the central part of the Thomson profile is absent, because this part is blocked on the detector to prevent it for blooming by the intense Rayleigh scattering signal.

of input power at $h = 7$ mm ALC and at $r = 4.5$ mm.

We can conclude that this technique offers a good method to obtain heavy particle temperatures in an ICP. The more often used method uses Rayleigh scattering.[9, 10] Rayleigh scattering can be used to measure the heavy particle density and combining this with the known pressure (1 atm) the heavy particle temperature can easily be calculated using the ideal gas law. The temperatures measured by Marshall[9] *et al.* show comparable results, but for a detailed comparison a further study is required.

4.2 The electron density during the power interruption

In figure 5 can be seen that n_e decays slowly which can be interpreted as a result of recombination and diffusion processes. The time scale in the hottest area ($r = 4.5$ mm) is about 100 μs. The decay of n_e is larger at the outer side of the plasma, at $r = 7$ and 8 mm, as can be deduced from the measurements. Surprisingly, the center of the plasma ($r = 0$ mm) is

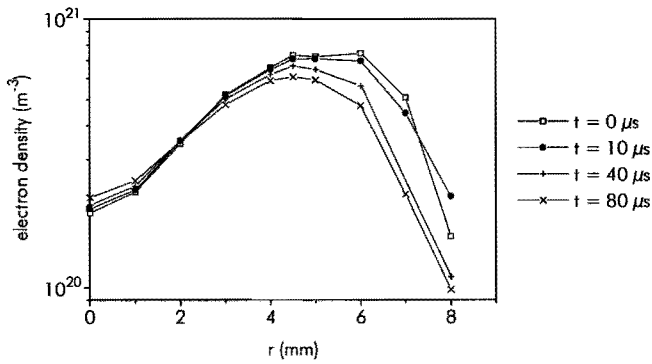

Figure 11. Radial profiles of the electron density at 0, 10, 40, 80 μs after switching off the generator, measured at 7 mm ALC and with an input power of 1.2 kW.

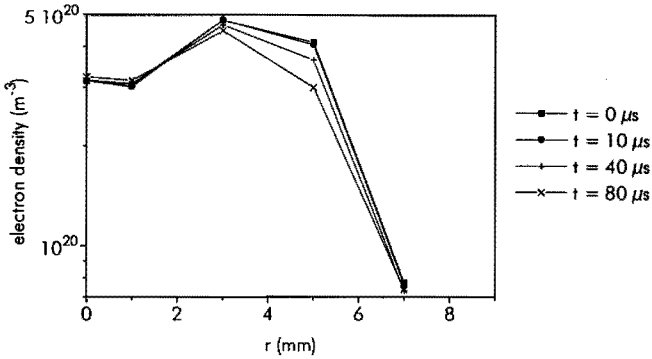

Figure 12. Radial profiles of the electron density at 0, 10, 40, 80 μs after switching off the generator, measured at 13 mm ALC and with an input power of 1.2 kW.

an exception. Here, we find an increasing electron density as can be concluded from the fitted raw data depicted in figure 10 as well. The Thomson scattering profiles are obtained at 7 mm ALC for 0, 20, and 80 μs after the generator is switched off. The rather low values of the electron densities cause profiles with noise. Nevertheless, the large number of measured points make the fits accurate within 2% for both width and total surface.
The increasing density indicates that there must be a large transport of electrons inwards. This could be driven and controlled by the large spatial n_e gradient present at stationary conditions. Before the plasma would be extinguished, there is a force that tries to smooth the electron density profile. This behavior can also be seen very clearly in figure 11, which shows that the density decreases everywhere but in the center, where it increases. Also at higher positions, at $h = 13$ mm ALC, a slowly increasing n_e is observed in the center of the plasma, see figure 12. Since the accuracy[6] of the density measurements is within 15%, the response must be a physical effect.

5 Conclusions

The combination of the Thomson scattering diagnostics and power interruption enables us to study the response of the electron density and temperature to the power interruption of the EM field. The typical response is a sudden decrease of the electron temperature to the temperature of the heavy particles, followed by a slow decay due to cooling of the plasma as a whole. This typical response is predicted by theory. Furthermore, after the power of the generator is switched off, the electron density is expected to decay slowly, due to recombination and diffusion. This decrease is measured everywhere, except along the plasma axis, where an increase in electron density is observed, probably due to transport of electrons towards the center by the large spatial electron density gradient present at stationary conditions.

[1] D.B. Gurevich and I.V. Podmoshenskii, "The relationship between the excitation temperature and the gas temperature in the positive column of an arc discharge", Opt Spectroscopy **15** (319), 1963.
[2] F.H.A.G. Fey, W.W. Stoffels, J.A.M. van der Mullen, B. van der Sijde, and D.C. Schram, "Instantaneous and delayed responses of line intensities to interruption of the RF power in an argon inductively coupled plasma", Spectrochimica Acta **46B** (885), 1991.
[3] F.H.A.G. Fey, J.M. de Regt, J.A.M. van der Mullen, and D.C. Schram, "The effect of evaporation on the analyte emission intensities during power interruption in an argon inductively coupled plasma", Spectrochimica Acta **47B** (1447), 1992.
[4] M.C.M. van de Sanden, G.M. Janssen, J.M. de Regt, and D.C. Schram, J.A.M. van der Mullen, and B. van der Sijde, "A combined Thomson-Rayleigh scattering diagnostic using an intensified photodiode array", Rev. Sci. Instrum. **63** (3369), 1992.
[5] M. Huang, D.S. Hanselman, P.Yang, and G.M. Hieftje, "Isocontour maps of electron temperature, electron number density and gas kinetic temperature in the Ar inductively coupled plasma obtained by laser-light Thomson and Rayleigh scattering", Spectrochimica Acta **47B** (765), 1992.
[6] J.M. de Regt, R.A.H. Engeln, F.P.J. de Groote, J.A.M. van der Mullen, and D.C. Schram, "Thomson scattering experiments on a 100 MHz inductively coupled plasma calibrated by Raman scattering", Rev. Sci. Instum. **66** (3228), 1995. (Chapter 3)
[7] E.L. Bydder and G.P. Miller, "A relaxation method for determining state of equilibrium and temperature ratio T_e/T_g in an argon ICPT", Spectrochimica Acta **43B** (819), 1988.
[8] G.P. Miller, "A theoretical evaluation of the relaxation method in determining the temperature ratio T_e/T_g in an inductively coupled plasma", Spectrochimica Acta **45B** (329), 1990.
[9] K.A. Marshall and G.M. Hieftje, "Measurement of true gas kinetic temperatures in an inductively coupled plasma by laser-light scattering", J. Anal. At. Spectrom. **2** (567), 1987.
[10] A.B. Murphy and A.J.D. Farmer, "Temperature measurement in thermal plasmas by Rayleigh scattering", J. Phys. D: Appl. Phys. **25** (634), 1992.

Thomson profile analysis in retrospective

The thermal broadened spectrum obtained by Thomson scattering can be used for the determination of T_e. If the scattering is incoherent, i.e. the photons are scattered by single electrons, this profile represents the velocity distribution of the electrons. Since the electron-electron collision frequency (in our ICP typical 10^{10} s^{-1}) is much larger than the frequency of the generator (10^8 s^{-1}) this velocity distribution will be Maxwellian which results in a Gaussian profile.

However, when the wavelength of the incident laser beam (λ_0) becomes large compared to the Debeye length (λ_D), the scattering will be on shielded charges. The scattered spectrum depends on the collective behavior of groups of charges. This scattering process is named coherent scattering.

The nature of the Thomson scattering signal is determined by the scattering parameter α, given by

$$\alpha = \frac{1}{k\lambda_D} = \frac{\lambda_0}{4\pi \sin(\theta/2)} \sqrt{\frac{n_e e^2}{\varepsilon_0 k_B T_e}}, \tag{3}$$

where $1/k = \lambda_0/4\pi\sin(\theta/2)$, the laser wave number minus the scattered wave number, and θ the scattering angle, the angle between laser beam and detection branch. e, ε_0 and k_B have their usual meaning. For $\alpha << 1$ the collective effects can be neglected, the scattering is said to be incoherent and the Thomson profile directly reflects the velocity distribution. We have coherent scattering if $\alpha \geq 1$ and the collective behavior will affect the shape of the scattered spectrum.

For the chapters 3 and 4 the scattering is assumed to be incoherent, and so all the Thomson profiles are fitted with Gaussian profiles. However, determining the scattering parameter α for our ICP we find that at all measured positions $\alpha < 0.4$, but certainly not $\alpha << 1$. Therefore, we can state that for the conditions present in the ICP Thomson scattering with a primary wavelength of 532 nm will be in between coherent and incoherent and so neglecting the collective effects is not permitted for all plasma conditions and positions.

The largest influence can be found on T_e. Obtained from a Gaussian fit, T_e is in general overestimated for conditions where $0.2 < \alpha < 0.4$ with about 500 to 1500 K. In the next chapters the Thomson data is fitted with an explicit expression containing the collective scattering effects,

$$P_S d\omega = C n_e \left(1+\alpha^2\right) \left| \frac{1}{1+\alpha^2 W(x)} \right|^2 \frac{e^{-x^2}}{\sqrt{\pi}} dx, \tag{4}$$

with P_S the scattered intensity, ω the frequency of the scattered light and C the calibration constant obtained from either Raman or Rayleigh scattering including the difference in cross section of Ar and Thomson scattering. x is defined by,

$$x = \frac{\omega}{k} \sqrt{\frac{m_e}{2k_B T_e}}. \tag{5}$$

Finally, the plasma dispersion function $W(x)$ is given by:

$$W(x) = 1 - xe^{-x^2}\left(2\int_0^x e^{p^2}dp - i\sqrt{\pi}\right). \qquad (6)$$

The original publications of chapter 3 and 4 contain the results obtained by fitting with a Gaussian profile. However, in the chapters 3 and 4 of this dissertation all the measured profiles have been fitted with the expression corrected for collective scattering, where T_e and n_e are the only free parameters after determining C, the sensivity of the setup. For more information on the collective scattering effects and the Thomson profile analysis we refer to the literature.[i,ii,iii,iv]

[i] M.C.M. van de Sanden, "The expanding plasma jet: Experiments and model", Ph.D. thesis, Eindhoven University of Technology (NL), 1991.
[ii] M. Huang, P.Y. Yuang, D.S. Hanselman, C.A. Monnig and G.M. Hieftje, Spectrochemica Acta **45B** (511), 1990.
[iii] D.E. Evans and J. Katzenstein, Rep. Prog. Phys. **32** (207), 1969.
[iv] M. Huang and G.M. Hieftje, Spectrochimica Acta **44B** (291),1989.

Chapter 5

Diode laser absorption spectroscopy*

* J.M. de Regt, R.D. Tas and J.A.M. van der Mullen, "A diode laser absorption study on a 100 MHz argon inductively coupled plasma", submitted for publication to J. Phys. D: Appl. Phys.

Diode laser absorption on the 4s $^3P_2$ - 4p $^3D_3$ argon transition is used to measure heavy particle temperatures in a 100 MHz argon inductively coupled plasma. Radial profiles of this temperature are obtained from the Gaussian part of the absorption profile with an accuracy of about 500 K, for four different input powers and at two different heights. The integrated profile is used to calculate the 4s-level density and to trace the ionizing and recombining plasma parts. The measurements also show that the method of attributing the Lorentzian width only to Stark broadening for calculating electron densities is not correct for this argon transition in atmospheric plasmas. A second broadening process with Lorentzian shape, van der Waals broadening, has to be taken into account. Under the measured conditions at the hottest positions in the plasma about 50% of the Lorentzian component is due to van der Waals broadening and this increases to almost 100% at the edges of the plasma.

1 Introduction

In the past, various diagnostic methods were designed to obtain plasma parameters from atmospheric plasmas like the inductively coupled plasma (ICP). The reason is that knowledge on values for electron and heavy particle densities and temperatures can improve the quality of models that describe the behavior of the plasma and help to enhance the applicability of ICPs for spectrochemical analysis and lighting. Among the various techniques such as Thomson and Rayleigh scattering[1] and H_β-broadening[2], we focus ourselves in this article to the method of diode laser absorption. Also Baer[3] *et al.* applied a semi-conductor diode laser as a source for line-of-sight absorption experiments on a 4s - 4p transition in an argon inductively coupled plasma.

This technique can in principle be used to obtain the heavy particle temperature and electron density as well as the density of the 4s-level group. This latter quantity cannot be obtained by simple optical emission spectroscopy since the wavelength corresponding to the 4s - 3p transition lies around 100 nm. The advantage of the diode laser is that it has a narrow bandwidth which makes a deconvolution unnecessary, and that the wavelength can be scanned easily by changing the current through or the temperature of the diode laser, allowing a quick measurement of the absorption profile. This profile has the shape of a Voigt, a convolution of a Doppler broadened Gaussian profile and a pressure broadened Lorentzian profile. Fitting the measurements gives the Doppler width, which can be used for calculating the heavy particle temperature (T_h). The pressure broadened Lorentzian part originates in general from Stark, resonance and van der Waals broadening mechanisms. Assuming that all other broadening processes can be neglected, which is not allowed under atmospheric conditions, the Lorentzian width can be employed for calculating the electron density (n_e) using the Stark broadening theory of Griem.[4]

To obtain local information on the plasma parameters, it is necessary to apply Abel-inversion, which is based on the assumption that the plasma is cylinder symmetric. Note that the absorption measurement is a line-of-sight measurement and that Abel inversion has to be

applied for each wavelength separately. In this way, a line profile can be constructed for each position, from which, after fitting this profile, the local value of the relevant parameters can be obtained.

This work presents the results of diode laser absorption measurements on a 100 MHz argon ICP in order to obtain the density (n_{4s}) of the 4s-level group and the heavy particle temperature. A discussion will be devoted to the correctness of the method for obtaining electron densities. The 4s-level group, consisting out of two resonant and two metastable levels, is important since it is the first excited group of levels in the path to ionization of argon. This makes that the 4s-group acts like a "second" ground level and although there are two resonant levels, they all act as metastable levels since the resonant radiation will be trapped almost completely. Therefore, it is expected that there is not much variation in the density per statistical weight (η_{4s}) of the four levels. Since the used absorption wavelength is 811.531 nm, which corresponds to the transition 4s $^3P_2$ - 4p $^3D_3$, the measurements are performed on the metastable 4s $^3P_2$ level, so the measured densities correspond to this level. As stated before, the other 4s-levels are supposed to have approximately the same density per statistical weight.

A combination of the earlier performed Thomson scattering measurements[5] with the measured 4s-level density gives more insight in the overpopulation of the 4s-level with respect to Saha.[6] This departure of the 4s-level density from equilibrium indicates which plasma part is ionizing or recombining.

In this paper we will, after a brief theoretical overview given in section 2, explain more about the experimental setup and the diode laser diagnostics (section 3) in combination with a discussion on the Abel inversion technique, to continue with the presentation and conclude with a discussion of the results (section 4).

2 Level population in an ICP

It is known from earlier research[6] that plasmas like the atmospheric ICP are not in thermodynamic equilibrium and that even departures from local thermal equilibrium (LTE) are present. In the ICP this is caused by the fact that the energy is transferred from the coil to the free electrons, which on their turn transfer the energy to the heavy particles. Since this energy coupling between electrons and heavy particles is, due to the large mass ratio, not very effective, whereas the heavy particles are heavily cooled by the environment, the heavy particles will not reach the temperature of the electrons. This will result in a departure from LTE: a two temperature plasma in which the electron temperature (T_e) is a factor of about 1.4 higher than the heavy particle temperature (T_h).[7]

A second departure from LTE stems from the fact that the Saha balance of ionization and recombination is out of equilibrium. To quantify this departure the dimensionless quantity $b(p)$ is introduced, describing the deviation from Saha of a certain level p and defined as,

$$b(p) = \frac{n(p)}{n^S(p)}, \tag{1}$$

with $n(p)$ the actual density and $n^S(p)$ the Saha density of level p. The Saha density in a pure argon plasma, assuming that the presence of multiple ionized atoms can be ignored, reads[6]

$$\eta^S(p) = \frac{n^S(p)}{g(p)} = \frac{1}{2g_+} n_e^2 \frac{h^3}{(2\pi m_e k_B T_e)^{3/2}} e^{\frac{I_p}{k_B T_e}}, \qquad (2)$$

where $\eta^S(p)$ is the Saha density per statistical weight in level p. Whereas $g(p)$ and g_+ are the degeneracies of level p and the ion ground state. Further, h and k_B are respectively Planck's and Boltzmann's constant and I_p is the ionization potential of level p. If the electron density n_e and temperature T_e are known, e.g. by Thomson scattering experiments, formula (2) can be applied to calculate the Saha density for all relevant levels. By means of absolute measurements (emission or absorption) the actual density $n(p)$ can be determined and $b(p)$ can be obtained. A level with $b(p) > 1$ will be denoted as overpopulated with respect to Saha. If $b(p) < 1$ the level is so-called underpopulated.
Since the 4s-group is the first station in the stepwise ionization flow, it is important to know its $b(p)$ value as a function of position. With this information insight can be obtained into ionizing and recombining zones of the plasma. Due to the laser absorption technique we can determine the density of the first excited level in the 4s-group accurately. Together with values for the electron density and temperature, the $b(4s)$ factor can be determined, showing the deviation of the 4s-group population from Saha. In this way the ionizing and recombining plasma parts can be distinguished from each other.

3 Experimental

3.1 The diode laser absorption setup

The diagnostic method is designed to measure a set of absorption profiles as a function of wavelength for several lateral positions. To perform these measurements the setup of figure 1 is constructed. The source is the IR-diode laser of the type Sharp LT016MD0, which has a maximum output power of 30 mW at a maximum operation current of 85.8 mA. The bandwidth $\Delta\lambda_w < 0.1$ pm is small compared to absorption profile (typical about 25 pm), so that there is no need for a deconvolution of the absorption profile. The diode laser, mounted in a box, is temperature controlled by a Peltier element within a precision of 1 mK stability. Both the temperature and the diode laser current are adjustable by the diode laser control unit, which can be controlled manually or by a PC. The selection of the laser mode in the neighborhood of 811.531 nm is done by adjusting the temperature. Fine adjustments to the absorption wavelength, including the scanning of the absorption profile, are performed by changing the laser current step by step. One step is equal to $\Delta I = 0.05$ mA and corresponds with $\Delta\lambda = 0.3$ pm. Note that apart from the wavelength also the laser power changes as a function of current. The relative change in wavelength induced by a change in the diode laser current is measured using a Fabry-Pérot interferometer. The absolute calibration of the wavelength is obtained from an absorption measurement on an argon low pressure discharge lamp.

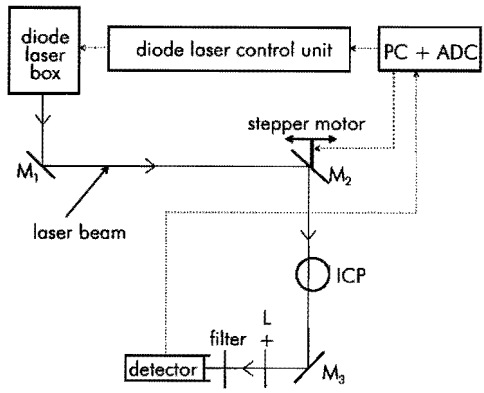

Figure 1. The experimental setup of the diode laser absorption diagnostics. The diode laser beam is led by the mirrors M_1, M_2 and M_3 through the plasma and to the detector. Lens L focuses the beam for all lateral positions onto the detector. The PC with the ADC controls both the laser wavelength and the position of mirror M_2 to select the lateral position.

A lens positioned in the laser box focuses the laser beam into the plasma. The two mirrors M_1 and M_2 are used to point the laser into the plasma. The mirror M_2 can be moved by a stepper motor in such a way that wavelength profiles at different lateral positions can be measured. The plasma with a radius of 9 mm is measured with steps of 0.5 mm, so that 19 lateral positions are measured. After the plasma the mirror M_3 reflects the laser beam onto the detector. Just before the detector the lens L is mounted to focus the beam for all lateral positions on the photodiode detector and a red filter is applied to eliminate the main part of the plasma light, increasing the signal to noise ratio of the measurements. To eliminate the remaining part of the light, an additional measurement with the detector is performed without laser light. This emission has to be subtracted from the measured absorption profile to get a zero intensity at the edges of the absorption profile, which is important for a successful Abel-inversion and Voigt fitting-procedure. The reading of the detector is synchronized to the 50 Hz of the mains in order to reduce the noise on the measured profiles. This is advisable since the plasma generator has a ripple in its power, so that the power varies about 10% with 100 Hz. To correct for the laser power dependence of the wavelength, a wavelength scan is performed when the plasma is not lit ("background" scan). The measured absorption profile divided by this "background" scan gives the absolute, line-of-sight integrated absorption profile. An example of such an absorption profile at $r = 5$ mm (after Abel-inversion) can be found in figure 2, together with a Voigt fit and residue. The fitting routine is applied to the complete range presented, so till far in the wings of the profile. This allows an accurate determination of the offset and the Gaussian and Lorentzian profiles, especially the determination of the latter is, due its nature, very sensitive for information far from the center.

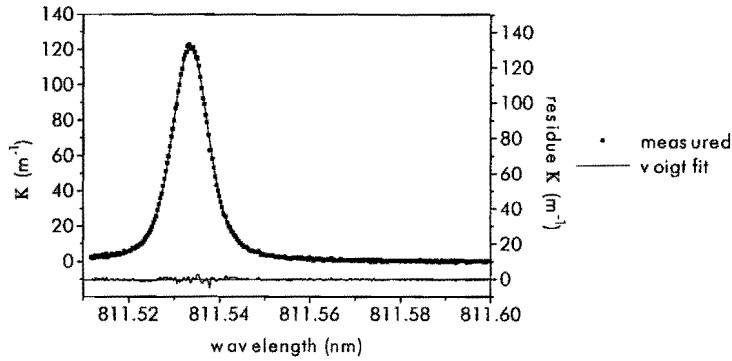

Figure 2. An example of an absorption profile with the absorption coefficient κ as a function of wavelength at one radial position at 7 mm ALC (after Abel-inversion) and the corresponding Voigt fit with residue.

3.2 The local heavy particle temperature, electron density and 4s-level group density

This section gives a brief overview on the used absorption method and the Abel-inversion procedure.

First consider the general situation for a laser beam with initial intensity $I_\lambda(0)$ passing through a plasma slab with thickness d. The intensity $I_\lambda(d)$ for a certain wavelength λ after transmission can be described by

$$I_\lambda(d) = I_\lambda(0)\exp(-\tau(\lambda)) + S_\lambda(1-\exp(-\tau(\lambda))), \tag{3}$$

in which S is the source function of the measured transition and

$$\tau(\lambda) = \int_0^d \kappa(\lambda)dx, \tag{4}$$

the optical depth which equals to the integral of the absorption coefficient $\kappa(\lambda)$ over the line of sight. The equation (3) shows that $I_\lambda(d)$ consists of two contributions, the first term represents the intensity that remains from the laser beam after being partially absorbed and second term is the contribution of spontaneous emission reduced by self-absorption. The basis of the absorption technique lies in finding the absorption coefficient, which for a certain wavelength can be described by

$$\kappa(\lambda) = \frac{\lambda_{4p4s}^2}{8\pi} A_{4p4s} n_{4s} \frac{g_{4p}}{g_{4s}} \left[1 - \frac{g_{4s} n_{4p}}{g_{4p} n_{4s}}\right] \phi(\lambda), \tag{5}$$

where λ_{4p4s} is the central wavelength for the measured 4p - 4s transition, A_{4p4s} the probability of spontaneous emission from state 4p to 4s taken from Wiese[8] *et al.* and g_{4p} and g_{4s} the degeneracy's of the levels in question and c the speed of light. The absorption profile $\phi(\lambda)$ is normalized to 1. The integration of $\kappa(\lambda)$ over the wavelength profile gives the density of the lower state η_{4s}, provided that η_{4p} is negligible, i.e. stimulated emission is negligible, that is omitting the fraction between the brackets. This assumption is reasonable for the ICP

with electron temperatures lower than 9000 K. The line profile $\phi(\lambda)$ provides inside into the broadening mechanisms. The following procedure will be applied to the measurements.

1) We have to convince ourselves that κ is not changed by the presence of the laser. This can be checked by changing the incident laser power and being sure that the absorption coefficient is not influenced.

2) We subtract the spontaneous emission reduced by self absorption (second term of equation (3)), which can easily be obtained measuring the intensity of the plasma without laser beam.

3) From the remaining part, being the first term in (3), the logarithm is taken. This gives,

$$\ln\left(\frac{I_\lambda}{I_\lambda(0)}\right) = \tau = \int_o^d \kappa(\lambda)\, dx. \tag{6}$$

4) Since the logarithm leads to τ that, according to equation (4) and (5), equals to a line integral (an additive quantity), Abel-inversion can be used to retrieve a local absorption coefficient. This is justified if the Abel-inversion routines are applied for each wavelength separately. With this procedure the absorption coefficient can be constructed for each radial position in wavelength dependent profiles $\kappa(r,\lambda)$. Now we will discuss the procedure of Abel-inversion and the fitting procedure of the wavelength dependent absorption coefficient.

The Abel-inversion technique starts with the assumption that at maximum radius, in our case at about 9 mm from the center, the measured value of the optical depth at the *lateral* position divided by the corresponding segment of the line of sight is equal to the value $\kappa(\lambda)$ for the maximum *radial* position. This value at the edge is used to construct the radial value of $\kappa(\lambda)$ for one step in position towards the center. This stepwise process goes on till the center is reached. Note that for this procedure the plasma has to be assumed to have a cylinder symmetry and that the more lateral positions are available, i.e. the smaller the steps are, the better the result of Abel-inversion will be. Moreover, as a consequence of the process, the inaccuracies will increase towards the center. In fact, the inaccuracies are added when we follow the Abel-inversion process towards the center. This is the reason why due to the hollow structures of the 100 MHz ICP it is difficult to recover the radial profile for the central region. For a description of the Abel-inversion routines using the method of filtered back projection we refer to [9 ,10 ,11].

To get an idea on the behavior of the inaccuracies after Abel-inversion, a simulation is carried out for the central wavelength on a fictitious plasma with torrodial shape, for which the absorption coefficient at central wavelength for $r = 0$ and $r = r_{max}$ is zero. Figure 3 shows the fictitious radial distribution of the center line absorption coefficient, which is used to calculate the corresponding lateral scan as it would result from line-of-sight measurements. Next we add 10% noise to this lateral scan, simulating a physical measurement with inaccuracies of 10%. Then this scan is used as input for our Abel-inversion routines. The result of applying Abel-inversion is also depicted in figure 3. The reconstruction of the radial dependency has the largest inaccuracies in the center, as predicted. Nevertheless,

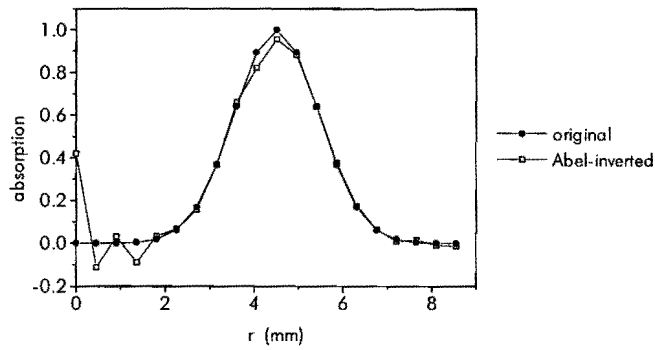

Figure 3. An assumed fictitious radial absorption scan with a reconstructed radial scan using the Abel-inversion procedure. Before the Abel-inversion routine is applied, 10% noise is added to the lateral data. Note that the radial shape is retrieved well, except for the central part of the plasma where the inaccuracies become very large.

the hollow structure is retrieved reasonably by the Abel-inversion routines. This information on the increasing inaccuracies towards the center of the plasma is helpful for the interpretation of our measurements.

After the wavelength profiles are obtained from the Abel-inversion, a least-mean-squares fitting program is used to adjust the measurements to a Voigt profile, the convolution of a Gaussian and a Lorentzian profile. The results from the fit give the width of the Gaussian and Lorentzian parts of the profile and the surface of the total profile. The width of the Gaussian profile $\Delta\lambda_D$, which is caused by Doppler broadening, is used to calculate the temperature of the argon atoms in the 4s-level group (T_{4s}), which is supposed to be equal to the heavy particle temperature T_h. This temperature can be obtained using the equation,[12]

$$T_h = \frac{mc^2}{8k_b}\left(\frac{\Delta\lambda_D}{\lambda_0}\right)^2, \tag{7}$$

in which m is the mass of the argon atom, λ_0 the linecenter wavelength and $\Delta\lambda_D$ is the measured full *1/e* width of Gaussian part of the absorption profile.

Using the theory of Griem,[4,13] like Baer[3,14] *et al.* did, the full width at half maximum of the Lorentzian profile ($\Delta\lambda_L$) gives n_e, assuming that all other broadening processes can be neglected. The Stark width ($\Delta\lambda_S$) is given by

$$\Delta\lambda_S = 2\,10^{-22} n_e w\left[1+5.5\,10^{-6} n_e^{\frac{1}{4}}\alpha\left(1-0.0068 n_e^{\frac{1}{4}} T_e^{-\frac{1}{2}}\right)\right], \tag{8}$$

where α is the ion broadening parameter and w is the electron impact parameter. Note that the width depends very weakly on T_e. The assumption that no other pressure broadening effects than Stark are present for the measured transition in an atmospheric plasma is doubtfully, as we will see in section 4.

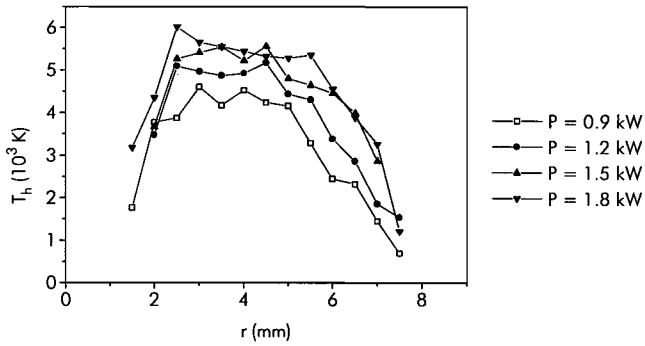

Figure 4. Heavy particle temperatures for different input powers as a function of radius at 7 mm ALC. In the high temperature region of the profiles the inaccuracies are about 10%.

4 Results and discussion

The results derived from the Gaussian part of the absorption profiles are depicted in figure 4. This figure shows T_h for several input powers of the plasma as a function of radius at 7 mm ALC. The estimated inaccuracies are 500 K in the high temperature region of the profile, but as mentioned in section 3.2, the inaccuracies increase towards the center of the plasma due to the Abel-inversion. For the standard power of 1.2 kW, T_h is slightly above 5000 K at the maximum value. Furthermore, for all the powers a good radial profile is obtained, showing the typical shape of the inductively coupled plasma, a hollow structure with a relatively cold center. Only in the center of the plasma the results from Abel-inversion can not be trusted, therefore, these values for T_h are not depicted.

The measurement of the 4s-level group density is considerable more accurate than that of the heavy particle temperature, since η_{4s} is obtained from the integrated absorption profile. The inaccuracy for η_{4s} is 2×10^{15} m^{-3}. The estimated inaccuracies for both T_h and η_{4s} are based on the uncertainty in the fitted width of the profile and on the reproducibility of the setup. In figure 5 the density per state $\eta_{4s} = n(4s)/g(4s)$ is given as a function of the radius

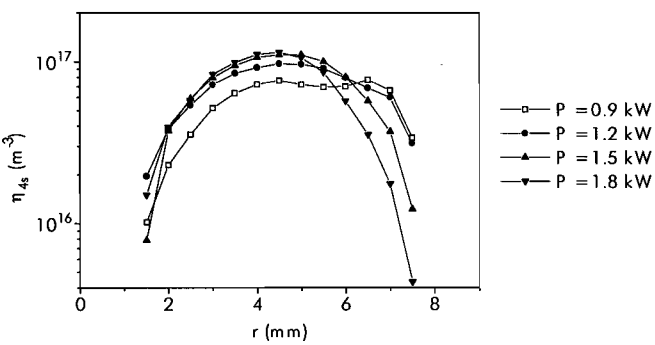

Figure 5. The 4s-level density per statistical weight as a function of radius for four different input powers at 7 mm ALC.

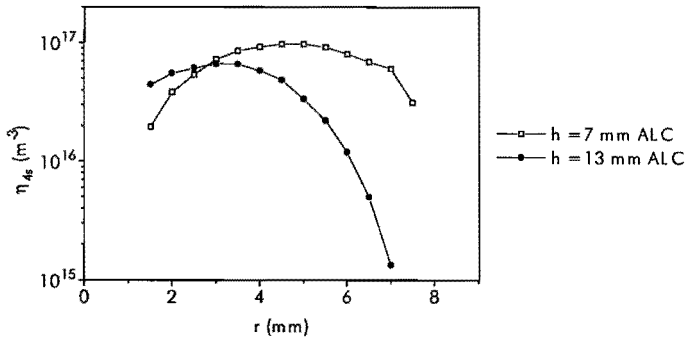

Figure 6. The 4s-level density per statistical weight as a function of radius at 7 and 13 mm ALC, for 1.2 kW.

for several input powers at 7 mm ALC. The good retrieved hollow structure of the ICP is here even more striking, so it indicates that the Abel-inversion routines perform accurate values for radii larger than $r = 1.5$ mm. Note that for the lower powers, $P = 0.9$ and 1.2 kW there is a kind of wing in η_{4s} at the outer side, at $r = 6.5$ mm.

In figure 6 the 4s-level density is depicted as a function of radius at 7 and 13 mm ALC for an input power of 1.2 kW. Apart from the fact that the maximum density at $h = 13$ mm is lower than that at $h = 7$ mm, the profile as a whole is shifted towards the center. Using the electron density and temperature obtained by the Thomson experiments,[5] the 4s-level group density predicted by Saha can be calculated, using equation (2). The corresponding b_{4s} factor is calculated using equation (1) and shown in figure 7. From this figure we can deduce that the plasma is ionizing at intermediate radii ($3 < r < 7$ mm), since there the b_{4s} factor is larger than unity. The b_{4s}-values are smaller than one at larger and smaller radii, so the plasma is recombining in these regions. Remarkable is the fact that the maximum of the radial profile at 7 mm and at 13 mm has the same value for b_{4s}. The difference is that the top position at 13 mm ALC lies more towards the center.

In figure 8 a fictitious electron density is depicted as a function of radius, which is obtained

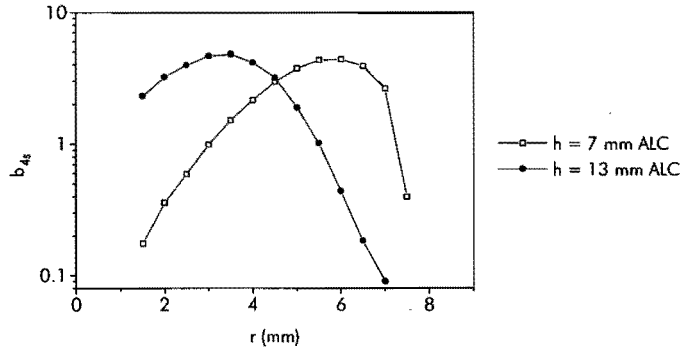

Figure 7. The 4s population factor b_{4s} as a function of radius at 7 and 13 mm ALC with an input power of 1.2 kW.

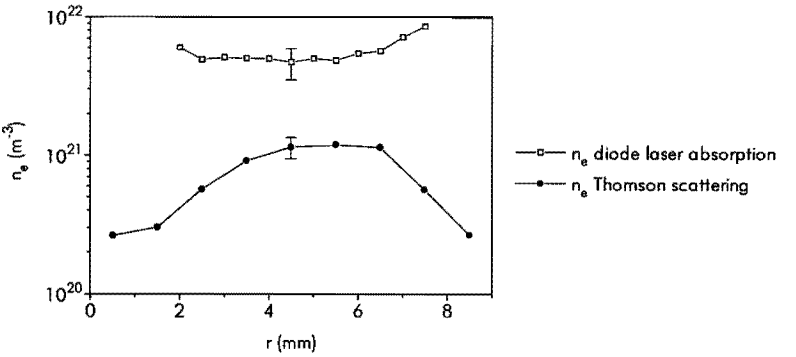

Figure 8. The electron density as a function of radius using the whole Lorentzian part of the absorption profile (open squares) and measured by Thomson scattering experiments (dots) at 7 mm ALC, the input power equals 1.2 kW.

using the assumption that the Lorentzian width of the absorption profile is a result of Stark broadening solely. The input power equals 1.2 kW. In this figure the measured electron density using the Thomson scattering technique[5] is shown as well. The accuracy of the Thomson measurements[5] is about 15% and is mainly due to inaccuracies in calibration and stability of the setup. The Lorentzian width of the absorption profile is certainly better than 20%. The results differ by a factor of about 3 and, therefore, there must be an other mechanism that apparently causes a systematic error. An indication can be found in the shape of the radial dependency. While n_e measured by the Thomson experiments behaves as expected, a decreasing density at the center and at the edge of the plasma, the n_e obtained from the absorption profiles shows the strange behavior of an increasing density at the center and the edge of the plasma. This points towards the conclusion that there might be an other broadening mechanism having a Lorentzian shape as well, which is more present at the center and edges. Resonance broadening can be assumed to be negligible since we are measuring on a metastable level. The van der Waals broadening, caused by the interaction of atoms and molecules, could be a good candidate. As measured by Moussounda and

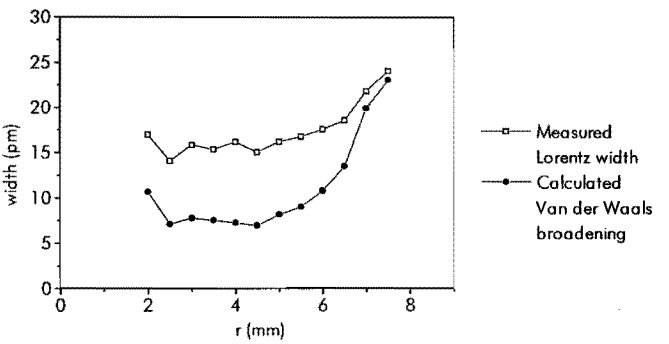

Figure 9. The measured Lorentzian width and the calculated width by Van der Waals broadening as a function of radius, at 7 mm ALC and with 1.2 kW input power. The value of γ is set to 5×10^{-27} nm/m^{-3}.

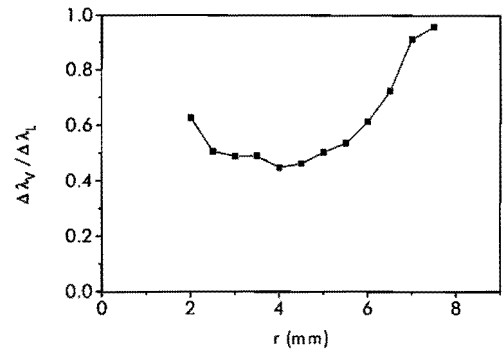

Figure 10. The ratio of the calculated width due to Van der Waals broadening to the measured Lorentzian width as a function of the radius at standard conditions and locations.

Ranson[15] and Tachibana[16] *et al.* this mechanism leads to broad line profiles in atmospheric plasmas. Because the densities of the neutral particles are larger at the center and the edges of the plasma, due to lower heavy particle temperatures, the van der Waals broadening is at its largest in these areas. For a numerical estimation of the broadening by the van der Waals effect, a broadening coefficient γ can be introduced with the following expression:[17]

$$\gamma = \frac{\Delta\lambda_V}{n_a}, \tag{9}$$

with $\Delta\lambda_V$ the broadening by the van der Waals effect (full width at half maximum). n_a is the neutral particle density which can be obtained by using T_h in combination with the ideal gas law and the fact that the pressure is 1 bar. Due to the low degree of ionization the partial pressures of the ions and electrons can be neglected. The characteristic value for γ by the van der Waals effect is estimated by Sobelman[18] and Chen[19,20] *et al.* to be in the order of 10^{-27} nm/m^{-3}. If we calculate the broadening by the van der Waals assuming γ equal to 5×10^{-27} nm/m^{-3} and using n_a based on the T_h measurements, figure 9 is obtained. The broadening by the van der Waals effect contributes roughly half of the measured broadening in the hottest part of the plasma, but it almost completely determines the measured broadening at the edges of the plasma. In figure 10 it is shown how the fraction of the van der Waals broadening behaves as a function of the radius. It shows that in the hottest part the Stark effect is comparable to the van der Waals broadening and that at the edges the only present broadening mechanism is van der Waals broadening. The presence of a significant contribution of van der Waals broadening compared to Stark broadening at all radial positions, explains the discrepancy as depicted in figure 8. Therefore, we must conclude that the method of diode laser absorption on this specific argon transition is not useful to obtain the electron density in an atmospheric argon ICP as long as the van der Waals broadening is not accurately known as a function of radius. To include van der Waals broadening accurate values for the neutral particle density are required. Furthermore, the estimation of γ equal to 5×10^{-27} nm/m^{-3} fits the measurements assuming that at the edges of the plasma there is only van der Waals and no Stark broadening, which is quite reasonable

since at the edges the neutral particle densities are high (van der Waals) and the electron densities low (Stark).

A comparison of these results with the results of Baer *et al.* shows large differences in both T_h and n_e. The ICP studied by Baer *et al.* has the same dimensions, but has a lower generator frequency (27.12 MHz, present work: 100 MHz), a lower argon gas flow (8 l/min, present work: 13 l/min) and a higher power (effective power 1 kW, present work: input power 1.2 kW, estimated effective power 0.6 kW). The effect of the difference in generator frequency might result is a different radial profile of the parameters, but does hardly influence the top values. The differences in power and gas flow might explain the roughly 2000 K higher T_h-values of the plasma of Baer *et al.* However, the factor of three higher electron densities they found, is most probably due to the fact that Baer *et al.* did not take the van der Waals broadening into account, especially since we get the same densities (see figure 8) if we also subscribe the total Lorentzian part to the Stark effect. In that case, the assumption of the presence of a suprathermal electron number density distribution, as is given by Baer *et al.* to the explain the high measured electron density, is not required.

5 Conclusions

From the Gaussian part of the diode laser absorption profile heavy particle temperatures in an inductively coupled plasma can be obtained. The accuracy in this determination is about 500 K, except in the center where Abel-inversion is hard to apply because of the hollow structure of the ICP. Outside this central region, the radial shape is good measurable. The integrated surface of the total profile can be used for the calculation of the 4s-level group densities The Lorentzian part of absorption profile, which in a study of Baer[3] *et al.* is completely attributed to the Stark effect, is found to originate not only from the Stark effect, but also from the van der Waals effect. The latter effect has a considerable contribution, roughly 50% in the hottest part of the plasma, increasing to 100% at the edges of the plasma. Therefore, the diode laser absorption profile can only be used to obtain electron densities in an atmospheric plasma like an ICP, if the van der Waals effect is properly estimated.

[1] M. Huang, D.S. Hanselman, Pengyuan Yang and G.M. Hieftje, "Isocontour maps of electron temperature, electron number density and gas kinetic temperature in an Ar inductively coupled plasma obtained by laser-light Thomson and Rayleigh scattering", Spectrochim. Acta **47B** (765), 1992.

[2] B.L. Caughlin and M.W. Blades, "An evaluation of ion-atom emission intensity ratios and local thermodynamic equilibrium in an argon inductively coupled plasma", Spectrochim. Acta **39B** (1583), 1984.

[3] D.S. Baer and R.K. Hanson, "Tunable diode laser absorption diagnostics for atmospheric pressure plasmas", J. Quant. Spectrosc. Radiat. Transfer **47** (455), 1991.

[4] H. Griem, "Spectral Line Broadening by plasmas", Academic Press, New York, 1974.

[5] J.M. de Regt, R.A.H. Engeln, F.P.J. de Groote, J.A.M. van der Mullen and D.C. Schram, "Thomson scattering experiments on a 100 MHz inductively coupled plasma calibrated by Raman scattering", Rev. of Sci. Instrum. **66**, 1995. (Chapter 3)

[6] J.A.M. van der Mullen, "Excitation equilibria in plasmas: a classification", Physics Reports **191** (109), 1990.

[7] F.H.A.G. Fey, W.W. Stoffels, J.A.M. van der Mullen, B. van der Sijde and D.C. Schram, "Instantaneous and delayed responses of line intensities to interruption of the RF power in an argon ICP", Spectochim. Acta **46 B** (885), 1991.
[8] W.L. Wiese, J.W. Brault, K. Danzmann, V. Helbig, M. Kock, "Unified set of atomic transition probabilities for neutral argon", Phys. Rev. A **39** (2461), 1989.
[9] M.C.M. van de Sanden, "The expanding plasma jet: experiments and model", Ph.D. Thesis Eindhoven University of Technology, 1991.
[10] V. Bangert, "Nuclear magnetic response tomography, NMR scanner techniques and the theory of image reconstruction", Berlin VDI Verlag, Berlin, 1982.
[11] C.A. Kak and M. Slaney, "Principles of computerized tomographic imaging", IEEE Press, New York, 1988.
[12] M. Mitchner and C.H. Kruger, "Partially Ionized Gases", Wiley Interscience, New York, 1973.
[13] H.R. Griem, "Plasma Spectroscopy", McGraw-Hill Book Company New York, 1964.
[14] D.S. Baer, H.A. Chang and R.K. Hanson, "Fluorescence diagnostics for atmospheric-pressure plasmas using semiconductor lasers", J. Opt. Soc. Am B **9** (1968), 1992.
[15] P.S. Moussounda, P. Ranson, "Pressure broadening of argon lines emitted by a high-pressure microwave discharge (Surfatron)", J. Phys. B: At. Mol. Phys. **20** (949), 1987.
[16] K. Tachibana, H. Harima and Y. Urano, "Measurements of collisional broadening and the shift of argon spectral lines using a tunable diode laser", J. Phys. B: At. Mol. Phys. **15** (3169), 1982.
[17] V.W. Lelevkin, D.K. Otorbaev and D.C. Schram, "Physics of non-equilibrium plasmas", North-Holland Amsterdam, 1992.
[18] I.I. Sobelman, "Introduction to the Theory of Atomic Spectra", Physmatgis, Moscow, 1963
[19] S. Chen and M. Takeo, Sov. Phys. Uspechi, **66** (301), 1958.
[20] S. Chen and M. Takeo, "Broadening and shift of spectral lines due to the presence of foreign gases", Rev. Mod. Phys. **29** (20), 1957.

Chapter 6

Transition probability determination*

* J.M. de Regt, R.D. Tas, J.A.M. van der Mullen, B. van der Sijde and D.C. Schram, "Determination of transition probabilities for argon using Thomson scattering on an inductively coupled plasma", submitted for publication to J. Quant. Radiat. Transf.

The inductively coupled plasma is used as an emission source for determining transition probabilities of highly excited argon states. The population densities of these higher levels in are assumed to be populated according to the Saha formula. To establish the Saha line we used the electron temperature from Thomson scattering together with the densities of three well-known levels by absolute line emission intensity measurements. In order to determine the transition probabilities the corresponding absolute line emission of 15 levels is measured using a two dimensional optical multichannel analyzer and is subsequently compared to the Saha line. The obtained transition probabilities have estimated maximum errors of less than 20% whereas the original specified inaccuracies are in most cases larger than 50%.

1 Introduction

While there are several advanced and accurate techniques to obtain information on plasma parameters, the simple method of measuring the intensity of emission lines[1,2] is still widely applied. The most simple method is the 2λ method which uses the relative intensity of two levels from which electron temperature T_e can be deduced. With absolute measurements of the intensities the value of the electron density n_e can be obtained as well.

These techniques are only successful if the levels in question are populated according to the Saha-Boltzmann law and if accurate values of the transition probability A are available. In most cases the transitions low in the atomic system are measured because of their high intensities and well-known A-values. However, especially the lower levels are very sensitive for deviation from equilibrium. Therefore, to determine the essential plasma parameters one should measure transitions high in the atomic system. Unfortunately, these higher levels have large inaccuracies in their A-value, often in the range of 25 – 50% or even higher. Moreover, since the A-values of higher states are generally low, the detection of radiation from the highly excited states is difficult.

In the past years, several efforts[3,4,5,6] have been made to measure and calculate transition probabilities with higher accuracies, often in order to obtain fundamental information on the atomic structure. Unfortunately, the most often treated transitions are situated in the lower part of the electronic system in which, as stated before, deviations from Saha equilibrium easily occur.

In this paper we present a method to obtain more accurate A-values for 15 highly excited levels in the argon system with an ionization potential (I_p) smaller than 0.7 eV. The basis of the technique is to use the absolute densities of three relatively well-known highly excited states together with T_e obtained by Thomson scattering to construct the upper part of the atomic state distribution function (ASDF). With the assumption that these reference lines are in partial local Saha equilibrium (pLSE), we can predict the poorly known densities of other levels. Due to the advent of the two dimensional CCD-array which can be placed in the focal plane of a spectrograph, we are able to measure with high accuracy simultaneously the emission of these lines and their background for various lateral positions. After

Abel-inversion the local value of these emission coefficients can be obtained making a determination of the corresponding A-values possible.

2 Experimental setup

The experiments are performed on an atmospheric 100 MHz inductively coupled argon plasma. The power of 1.2 kW input is coupled into the plasma with a coil of two windings. The argon flow through the quartz torch is about 13 l/min; the plasma radius is 9 mm. The measurements are obtained at 7 mm above the coil.

The two methods of measuring the plasma parameters are Thomson scattering (TS) and absolute line emission intensity (ALI) measurements. The first technique provides accurate electron temperatures and densities. It is based on the scattering of light from a pulsed Nd:YAG laser by the free electrons in the plasma, which is collected by a monochromator in combination with an intensified multichannel photodiode array. In this article we only use the T_e-values obtained with this method. For more information on the setup we refer to [1].

The absolute line emissions are measured using a 1 m monochromator with a two dimensional CCD-array placed in the focal plane. The two dimensions of this optical multichannel analyzer (OMA) offer the possibility to obtain in one single measurement spatially resolved information at 25 radial positions of an emission line with the adjacent continuum. The system is absolutely calibrated by a tungsten ribbon lamp. The data is Abel-inverted[8] to obtain local values of the emission coefficient. Note that Abel-inversion is required, but that it also introduces additional inaccuracy. Especially local information in the center of the plasma ($r = 0$ mm) is difficult to determine due to the presence of the hollow structure in the densities and temperatures. Therefore, we will use only the information obtained for $r > 3.5$ mm. For a detailed description of the setup of measuring absolute line emission intensities (ALI) we refer to [2].

3 Method of determining transition probabilities

The transition probability A of a certain transition is an atomic constant, depending on the specific atomic structure only. Therefore, it is independent on the plasma conditions as long as fields in the plasma are not so high that the atomic structure is distorted. In the presented method, partial Local Saha Equilibrium (pLSE) is assumed for the levels with ionization energy $I_p < 0.7$ eV. In this case, the density n_p of state p per statistical weight g_p ($\eta_p = n_p/g_p$) is predicted by Saha's law:

$$\eta_p = \frac{n_i n_e}{2g_+} \frac{h^3}{(2\pi m_e k_B T_e)^{3/2}} e^{\left(\frac{I_p}{k_B T_e}\right)}, \tag{1}$$

where n_i and g_+ are the density and statistical weight of the argon ion ground state and h, m_e and k_B have their usual meaning. So with this equation the level density per statistical weight η_p can be calculated easily for known plasma conditions, i.e. T_e and n_e under the assumption that $n_e = n_i$.

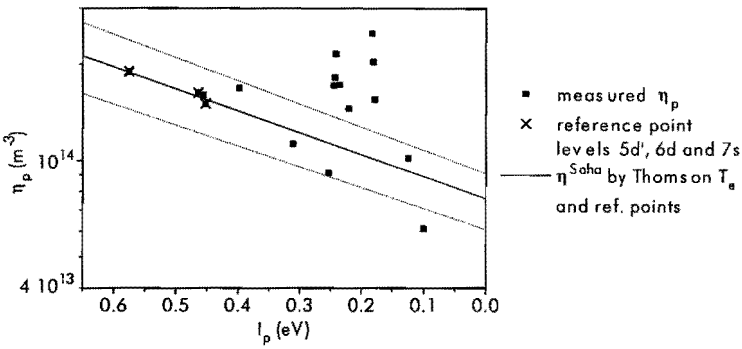

Figure 1. State population density as a function of the ionization energy I_p of level p. The full line is the level population predicted by Saha based on T_e by Thomson scattering and η_∞ by three level densities as obtained by emission experiments, indicated by crosses. The outer dotted lines indicate the inaccuracy interval. The measurements are carried out on an inductively coupled plasma with an input power of 1.2 kW at a radius of 6 mm from the center and at 7 mm above the load coil.

On the other hand, the density of a state p can be obtained by measuring the emission coefficient j_{pq}:

$$j_{pq} = \frac{n(p)A_{pq}h\nu}{4\pi}, \tag{2}$$

of a transition from level p to level q emitting a photon $h\nu$. For an optically open transition this emission coefficient can be obtained with ALI after Abel-inversion. Since the error margins in A as given in literature[3] are much larger than those in the measured intensity j_{pq}, a more accurate value for the transition probability can be obtained if an independent determination of the relevant level densities is available.

The method we follow is to construct the atomic state distribution function (ASDF) of highly excited states using a T_e-value from Thomson scattering experiments[9] together with a set of level densities obtained by ALI. Three emission lines are selected for this purpose as reference lines. These have a relatively low uncertainty in the transition probabilities of 25% and are situated high in the electronic system where the presence of pLSE may be assumed. The reference transitions are 7s - 4p, 6d - 4p and 5d' - 4p with corresponding wavelengths of 588.9 nm, 516.2 nm and 518.8 nm. To illustrate the method we present in figure 1 the upper part of the ASDF ($\ln\eta$ as a function of I_p) for r = 6 mm as obtained by ALI measurements of 15 levels. In the ASDF construction the A-values of Wiese[10] *et al.* are used. The reference emission lines are indicated by crosses.

With the T_e-value from Thomson scattering and the level densities η_p per statistical weight of the reference lines we determine the level density η_∞ at $I_p = 0$ using

$$\ln\left(\frac{\eta_p}{\eta_\infty}\right) = \frac{1}{k_B T_e} I_p. \tag{3}$$

Now η_∞ and the slope are known we have the Saha line as indicated by the full line in the figure. Note that the inaccuracy in the slope of this line is due to both the uncertainty of 5% in T_e from Thomson scattering and the combined effect of the errors in the absolute density based on the three reference lines. As indicated by the dotted lines, this leads to an uncertainty in Saha predicted density for η_∞ of 17% which is still mainly due to the inaccuracies in A, but lower than 25% because of the use of *three* reference lines.
The absolute emission intensities j_{pq} of transitions can now be used to determine the corresponding A-values by combining equation (2) and (3):

$$A_{pq} = \frac{4\pi\, j_{pq}}{h\nu g_p \eta_\infty} e^{\frac{I_p}{k_B T_e}}. \qquad (4)$$

This formula can be applied with T_e, η_∞ and j_{pq} from experiments for all the different transitions. As can be seen from equation (4), the errors in A-values originate mainly from inaccuracies in η_∞ and j_{pq}. This will be discussed in the next section.

4 Results and discussion

The method of determining transition probabilities as presented in the previous section is applied on 15 transitions in the argon system close to the ionization limit. The procedure is repeated for nine different radial positions between 3.8 and 6.7 mm resulting in nine A-values for each transition. By averaging these values systematic deviations due to errors in the shape of the radial profile are removed. The results with estimated inaccuracies of 20% are presented in table 1 and are compared with the original values for the transition probabilities taken from Wiese[10] *et al.* Most of these values have inaccuracies of 50% or even larger, so that a significant improvement of the A-values is achieved. Note that all the obtained A-values are within the uncertainties of those given in [10].

λ (nm)	I_p (eV)	E_p (cm^{-1})	A^{old} (10^5 s^{-1})	$(\Delta A/A)^{old}$	A^{new} (10^5 s^{-1})
474.7	0.242	125163	3.70	> 50 %	7.44
475.3	0.245	125136	4.70	> 50 %	7.53
476.9	0.254	125067	9.00	50 %	7.40
487.6	0.311	124603	8.10	50 %	7.46
495.7	0.183	125631	1.90	> 50 %	4.83
499.0	0.181	125651	1.10	> 50 %	2.33
503.2	0.221	125329	0.85	> 50 %	1.17
506.0	0.234	125220	3.90	> 50 %	6.29
510.5	0.179	125671	0.91	> 50 %	1.51
511.8	0.243	125149	2.80	> 50 %	4.67
516.2 *	0.452	123467	20.00	25 %	19.40
518.8 *	0.464	123373	13.80	25 %	14.00
531.8	0.127	126090	2.70	> 50 %	3.11
542.1	0.398	123902	6.20	50 %	7.33
588.9 *	0.580	122440	13.40	25 %	13.30

*Table 1. Transition probabilities for 15 transitions high in the argon system with an uncertainty of 20%. The emission lines marked with * are used as reference lines.*

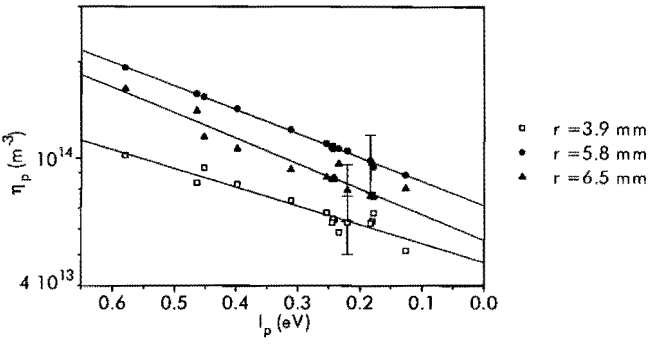

Figure 2. Level densities of corresponding emission lines obtained using the new derived transition probabilities for three different radial positions. The error bars are related to the uncertainty in the transition probability solely. The lines are fits through the measured points.

The origins of the inaccuracies can be divided in two parts: First, those related to the determination of the Saha line which predicts the density of the levels and second the inaccuracies associated with the measurement of the various j_{pq}-values. Note that the instability of the plasma can also be a source of error, however, these are taken into account in the measured parameters j_{pq} and T_e.

Concerning the Saha line, we have the errors in the Thomson scattering[7] determined T_e-value which is 5%. More important is the inaccuracy induced by the uncertainty of the A-values of the three reference lines (25%) which together give rise to an uncertainty of 14% in the η_∞ determination. The error of 9% in the j_{pq}-value required for the three reference points is also present, but will be reduced to 3% by the treatment of nine radial positions. The Saha line together with the uncertainty margin is depicted in figure 1 by respectively the full and dotted lines. Concluding we may state that an inaccuracy of the three reference lines is the most important error source in the determination of the Saha line.

In principle, the n_e from Thomson scattering experiments could be used for calculating η_∞. However, since the inaccuracy in n_e is 15%, this will cause an uncertainty in the density η_∞ of about 30% due to the n_e^2-dependency. Nevertheless, Thomson scattering and the reference points by ALI are in agreement for the value of η_∞ within 10%. Lowering the inaccuracy in the Saha line can be best achieved by determining more accurate values of n_e with Thomson scattering ($< 6\%$) to obtain an accurate value of η_∞ or improving the used method by reducing the errors in the intensity measurements by treating more than three levels to increase the accuracy of η_p. The last option is difficult to implement since most of the A-values high in the electron system have large inaccuracies.

In the second class we have the inaccuracies associated with the emission coefficient j_{pq}. As stated before this is better than 9%. This inaccuracy has several contributions. The use of the CCD array as a detector enables measurements with a small inaccuracy of less than 1%, including dark current and read-out noise. The absolute calibration of the setup using a tungsten ribbon lamp together with the variations in plasma intensities introduces an error

of 4%. Finally, Abel inversion can influence the radial profile. However, for positions larger than $r = 3.5$ mm this inaccuracy is less than 5%. All these inaccuracies together make the emission intensity measurements of j_{pq} accurate within 9%. Combining the errors in the Saha line construction (17%) and the j_{pq} determination (9%) and averaging the nine, for the different radial positions obtained, A-values lead to a total inaccuracy in the transition probabilities of less than 20%.

Figure 2 shows the result of the ASDF construction using the new A-values for three different plasma positions. It is found that the corrected transition probabilities are indeed independent from plasma conditions. Comparing these results with the uncorrected level densities of figure 1, shows that the decrease in scatter is striking. For the different positions the obtained level densities are, within the accuracy, on one line. In general, all the scatter is created by the inaccuracies in the determination of the j_{pq} for the radial position in question (CCD-read out and Abel-inversion).

5 Conclusions

The inductively coupled plasma can be used as a source for determining transition probabilities for transitions high in the argon system, because of the presence of partial local Saha equilibrium for highly excited states in parts of this plasma. A combination of absolute line emission measurements with Thomson scattering experiments allows improving the accuracy in the transition probability of often about 50% down to 20%.

[1] J.A.M. van der Mullen, S. Nowak, A.C.A.P. van Lammeren, D.C. Schram and B. van der Sijde, "Non equilibrium characterization and spectroscopic analysis of an inductively coupled plasma", Spectrochimica Acta **43B** (317), 1988.

[2] J.M. de Regt, F.P.J. de Groote, J.A.M. van der Mullen and D.C. Schram, "Comparison of active and passive methods to investigate atmospheric plasmas", to be published, 1995. (Chapter 7)

[3] W.L. Wiese, "Spectroscopic diagnostics of low temperature plasmas: techniques and required data", Spectochimica Acta **46B** (831), 1991.

[4] W.L. Wiese, J.W. Brault, K. Danzmann, V. Helbig and M. Kock, "Unified set of atomic transition probabilities for neutral argon", Physical review A **39** (2461), 1989.

[5] W.L. Wiese, "The atomic transition probabilities of argon - a continuing challenge to plasma spectroscopy", Journal of Quantitative Radiative Transfer **40** (421), 1988.

[6] K. Katsonis and H.W. Drawin, "Transition probabilities for argon(I)", Journal of Quantitative Radiative Transfer **23** (1), 1980.

[7] J.M. de Regt, R.A.H. Engeln, F.P.J. de Groote, J.A.M. van der Mullen and D.C. Schram, "Thomson scattering experiments on a 100 MHz inductively coupled plasma calibrated by Raman scattering", Review of Scienitfic Instruments **66** (3228), 1995. (Chapter 3)

[8] M.C.M. van de Sanden, "The expanding plasma jet: experiments and model", Ph.D. Thesis Eindhoven University of Technology, 1991.

[9] J.M. de Regt, J.A.M. van der Mullen and D.C. Schram, "The response of the electron density and temperature to the power interruption measured by Thomson scattering in an inductively coupled plasma", Physical Review E **52** (2982), 1995. (Chapter 4)

[10] W.L.Wiese, M.W.Smith, B.M.Miles, "Atomic Transition Probabilities Volume II. Institute for Basic Standards", National Bureau of Standards, Washington D.C. USA,1969.

Chapter 7

Active and passive spectroscopic methods compared*

* J.M. de Regt, F.P.J. de Groote, J.A.M. van der Mullen and D.C. Schram, "Comparison of active and passive spectroscopic methods to investigate atmospheric ICPs", submitted for publication to Spectrochimica Acta B.

A comparison of Thomson and Rayleigh scattering, diode laser absorption and line emission measurements is performed on a 100 MHz atmospheric argon-flowing inductively-coupled plasma. The parameters, which are measured in two or more ways, are the electron density, the electron temperature and the heavy particle temperature. The optimized diagnostics show the same behavior for the electron density and temperature. Nevertheless, the Thomson scattering diagnostics is the best in retrieving the radial profile. The heavy particle temperature as measured by using both Rayleigh scattering and diode laser absorption is identical within the estimated errors. The technique of measuring the temperature during power interruption, with both Thomson scattering and emission spectroscopy, shows that the electron and heavy particle temperatures are not equal during the period of power interruption.

1 Introduction

Inductively coupled plasmas are widely used for spectrochemical analysis and material treatment and might be used in future as light sources. Since the knowledge on the fundamental behavior of the inductively coupled plasma (ICP) will improve its applicability, information on the temperatures and particle densities in the plasma is indispensable. In this article we present the study on a 100 MHz argon-flowing atmospheric ICP. The main three parameters, the electron density (n_e), electron temperature (T_e) and heavy particle temperature (T_h) are measured using several techniques. Such a comparative study allows estimating the quality of the used techniques and gives more insight in the plasma itself. Moreover, once the validity region of the various techniques is known, they can be used for other plasmas with comparable plasma conditions.

Recently, a new set of diagnostic methods is developed and implemented in our laboratory. The techniques can be divided in active techniques, Thomson and Rayleigh scattering (TS and RS) and diode laser absorption (DLA), and in passive techniques, H_β-line broadening (HB) and absolute line emission intensity (ALI) measurements. TS and RS make it possible to measure T_e, n_e and T_h locally.[1] A second way to determine T_h is the method of Thomson scattering in combination with the power interruption of the generator (TSPI).[2] The DLA diagnostic[3] is built to measure n_e and T_h. Beside these active methods, earlier implemented passive techniques like ALI and HB are expected to be useful as well. Absolute line emission spectroscopy[4] is used to calculate n_e and T_e. A combination of this method with the power interruption[5] (LIPI) can be used to estimate T_h. Finally, the HB method[6] is applied for measuring n_e. In this article, we will first briefly explain the used diagnostics and then continue with a comparison and discussion of the results. The results of the power interruption experiment makes a discussion on the behavior of T_e during the switch off period necessary. This can be found at the end of the chapter with the results.

2 Applied diagnostics

The laboratory is equipped with several techniques which can be applied to various kinds of small plasmas. These plasmas are placed on a table which can be moved horizontally and vertically. The main advantage of moving the plasma is that the diagnostics have a fixed detection volume and re-alignment is not required. An exception is the diode laser absorption diagnostic, for which a stepper motor controlled moving mirror is used to measure at each lateral position. The different diagnostics can be controlled using one single PC486 computer and no changes in the experimental setup are necessary when switching to an other experimental technique. This makes a fast data acquisition possible and implies that all techniques can be used within one day which is desirable in order to reduce errors due to the non-reproducibility and instability of the plasma itself. In figure 1 the experimental setup is depicted, showing all the used diagnostics. The detection volume and the relative position of the instruments can be recognized easily.

An overview on the used experimental methods with their measured parameters is given in table 1. These methods will be briefly introduced now, but for a detailed description we refer to corresponding earlier publications.

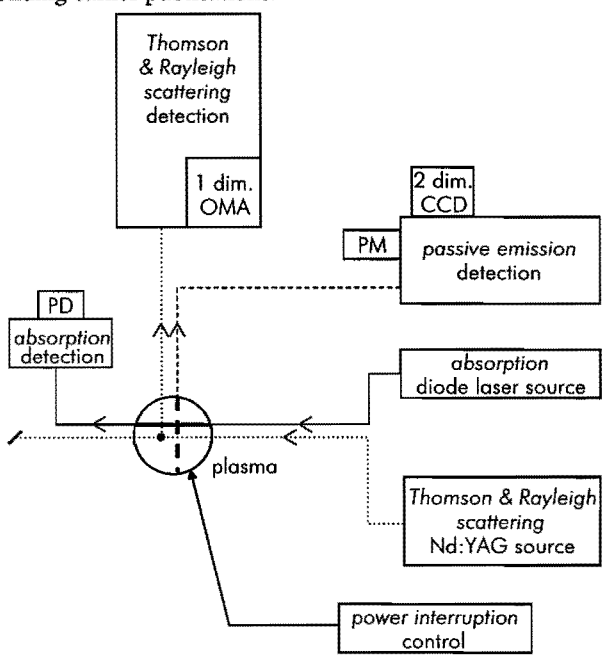

Figure 1. The experimental setup with three diagnostic branches: Thomson and Rayleigh scattering, diode laser absorption and optical emission spectroscopy. Note that the detection volume is fixed in space (except for diode laser diagnostics). 2 dim. CCD and PM refer to the two dimensional CCD array and photomultiplier as detectors for optical emission spectroscopy (respectively ALI and HB, and LIPI). OMA refers to the one dimensional photo diode array as detector for Thomson and Rayleigh scattering experiments. PD is a photo diode for detecting the DLA signal.

parameter	preferred	alternative
n_e	TS	ALI, HB
n_a	RS	
T_e	TS	ALI
T_h	RS	DLA, (TSPI, ALI + LIPI)
T_e^*	TSPI	ALI + LIPI

Table 1. Overview of the applied diagnostics and the measured parameters. TS: Thomson scattering, RS: Rayleigh scattering, TSPI: Thomson scattering during power interruption, DLA: diode laser absorption, HB: H_β-broadening, ALI: absolute line emission intensities, LIPI: line emission intensities during power interruption. Since the electron temperature during power interruption turns out not to be equal to the heavy particle temperature diagnostics for both T_e^* and T_h are given.

2.1 Thomson and Rayleigh scattering

Thomson and Rayleigh scattering is the scattering of incident light on respectively free and bound electrons. Since the scatter efficiency is extremely low (for Thomson scattering about 10^{-14}), the light source has to be powerful and the detector very sensitive. In the used setup a 10 Hz pulsed Nd:YAG laser at doubled frequency (532 nm) acts as the source, having an energy of 0.45 J per pulse. The scattered light is detected by an intensified one dimensional photo diode array, allowing quick measurements and giving spectra of the scattered signal with a resolution of 0.14 nm. Note that both Thomson and Rayleigh measurements are *local* measurements since the scattered signal is detected under 90 degree with the incident laser beam.

Thomson scattering (TS)

The Thomson scattered photons are broadened by the Doppler effect, so that the width of the wavelength profile gives the electron temperature. After calibration the total number of scattered photons determines the electron density. The measurements are fitted using an expression[7,8] that includes collective scattering, which is required due to the relatively high electron densities and low temperatures in the ICP. For a detailed description of the setup and calibration procedure we refer to [1].

By performing TS during power interruption (TSPI), we are able to measure the temperature of the electrons (T_e^*) directly (5 μs) after the removal of the energy input. This temperature T_e^* gives an indication of the steady state value of the heavy particle temperature (T_h). The method of measuring T_e^* has been published earlier [2].

Inaccuracies in the temperatures obtained by TS and TSPI are about 150 K. However, the reproducibility of the plasma conditions reduces the total accuracy towards about 500 K. The inaccuracy in the electron density is about 15%, including reproducibility of the plasma.

Rayleigh scattering (RS)

The same setup can be used for measuring Rayleigh scattering. This signal is in principle Doppler broadened, but since Rayleigh scattering originates from electrons bound to heavy particles the corresponding broadening is much smaller than that of the free electrons (Thomson) and can therefore not be resolved by this setup. Nevertheless, Rayleigh scattering can be used in atmospheric plasmas to measure T_h. This method has been performed earlier on ICPs by Huang[9,10] *et al.* The basis of the method is the ideal gas law in combination with constant atmospheric pressure.

The starting point is measuring the number of Rayleigh scattered photons on argon (I_{off}) at room temperature (T_r) when the plasma is off. If the plasma is switched on, the Rayleigh scattering intensity (I_{on}) will decrease since the temperature increase at constant pressure will be accompanied by a decrease in the number density. More specifically, the ratio of the temperatures with plasma on (T_h) and off (T_r) is equal to the ratio of the particle density with plasma off (n_r) and on (n_h) that is $T_h = T_r(n_r/n_h) = T_r(I_{off}/I_{on})$, as can be found using the ideal gas law $p = nk_BT$. Since the density is directly proportional to the total number of scattered photons, i.e. the detected signal and the scattered intensity at room temperature is known, the heavy particle temperature can be calculated.

There is one important disturbing phenomena in this procedure and that is the presence of stray light generated by improper reflections on several optical components. This stray light enters the detection system in the same way as Rayleigh scattering does and since both coincide within the apparatus profile, they cannot be distinguished from each other. Therefore, in practice, additional measurements on a different gas like He are performed to estimate the amount of stray light. It is obvious that a lot of attention is paid to reduce the stray light. Reducing the detection angle appears to be most effective, since, due to the nature of stray light, it decreases relatively more than the Rayleigh signal does. The RS method for the determination of T_h has an accuracy of about 8%.

2.2 Diode laser absorption (DLA)

A diode laser is used to measure the absorption profile of an argon line.[11] By selecting a diode laser with a wavelength corresponding to a transition, like the measured 4s $^3P_2$ – 4p $^3D_3$ (811.53 nm), the wavelength of the laser can be scanned around the line by varying the current through the laser. Pointing the laser beam through the plasma and detecting the intensity, the absorption coefficient can be obtained as a function of wavelength. Note that Abel-inversion is needed to obtain local values of the absorption coefficient. The measured absorption profile can be fitted with a Voigt function, containing a pressure broadened Lorentzian shape profile and a Doppler broadened Gaussian profile. The width of the latter profile can easily be used for determining the heavy particle temperature as a function of the radius of the plasma. The resulting temperature is accurate within 10%, except in the center of the plasma ($r < 3$ mm), where due to Abel-inversion the inaccuracies are higher. In principle, the Lorentzian part of the profile obtained by DLA can be used for the determination of n_e if other broadening mechanisms than Stark broadening can be neglected. However, in the open ICP van der Waals broadening turns out to be

important as well and using DLA for n_e determination becomes difficult. For further details concerning the absorption diagnostic and the van der Waals broadening effect we refer to [3].

2.3 Optical emission spectroscopy

Optical emission spectroscopy presents a class of techniques, for which the plasma is not probed by an external source. The setup consist of a set of lenses and mirrors that images the plasma on the entrance slit of the 1 m monochromator. This slit has a width of 100 μm for line intensity measurements (ALI and LIPI) and 10 μm for the H_β-measurements (HB). For the ALI and HB measurement a 2 dimensional CCD-array (SBIG, type ST6-UV) is used. The CCD-array, cooled at –28° C, allows to measure the emission intensity as a function of wavelength of the whole radius of the plasma (8.8 mm) at once, as is depicted in figure 2. The wavelength window is 5 nm broad whereas the resolution of 0.02 nm is determined by the size of one pixel (25 μm). This setup is calibrated absolutely using a tungsten ribbon lamp. For the LIPI experiments we use an other detector mounted on the same monochromator, namely a photomultiplier (Hamamatsu R376) in combination with a multichannel scaler to measure time-resolved emission information with a resolution of 2 μs. Note that the lateral data of the absolute line emission and H_β-broadening experiments has to be Abel-inverted in order to obtain radial information on the parameters.

Absolute line emission intensities (ALI)

The intensity measurements of several emission lines together with their transition probabilities yield absolute values for the number densities $\eta(p)$ of the corresponding states. The $\eta(p)$-values as a function of ionization potential show the atomic state distribution function (ASDF). If the population of these levels obey Saha's law,[4,12] the ASDF can be used to calculate T_e via the slope. Under the assumption that $n_e = n_i$ (n_i the ion density) n_e can be determined using the Saha equation,

$$\eta(p) = \frac{h^3}{2g_+(2\pi m_e k_B)^{3/2}} \frac{n_e^2}{T_e^{3/2}} e^{\left(\frac{I_p}{k_B T_e}\right)}. \qquad (1)$$

The constants k_B, m_e and h have their usual meaning, g_+ is the degeneracy of the ion ground state and I_p is the ionization potential of the state p. In the present experiment the 8d - 4p (506.0 nm), 7s - 4p (588.9 nm), 5d' - 4p (518.8 nm) and 7d' - 4p' (531.8 nm) transitions are measured which corresponding levels are verified to be in Saha-equilibrium.[13,14] However, the results have an inaccuracy of about 15% in T_e and n_e.

Line emission response to power interruption (LIPI)

The response of the line emission intensity to the power interruption of the generator (LIPI) can be used to determine the ratio $\gamma^* = T_e/T_e^*$, in which T_e^* is the temperature of the electrons just after the power interruption. Performing these measurements using a photomultiplier in combination with a multi channel scaler, the emission is registered as a function of time, showing a nearly instantaneous jump upwards at the moment of power

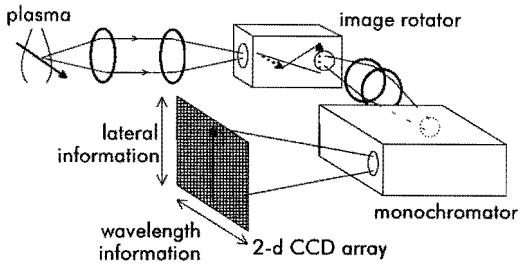

Figure 2. The detection of emission for the ALI and HB measurements. The plasma radius is rotated and imaged (1 : 1) on the entrance slit. The first set of lenses has a focal length of f = 50 cm (effective diameter of 4 cm), the second set before the monochromator f = 25 cm. In combination with the two dimensional CCD-array information of both wavelength and lateral profile is obtained.

interruption. This jump is induced by the sudden change in temperature of the electrons from T_e to T_e^*, while the electron density stays more or less constant during this cooling period of about 5 μs. Assuming Saha before (t = 0 s) and 5 μs after the elimination of the EM field, the size of the jump, that is the ratio of the intensity with power on ($\eta(p)$) and off ($\eta(p)^*$) will give the ratio $\gamma^* = T_e/T_e^*$, since[5]

$$\ln\left(\frac{\eta(p)^*}{\eta(p)}\right) = \frac{\gamma^* - 1}{k_B T_e} I_p + \frac{3}{2}\ln\gamma^*, \qquad (2)$$

which can be obtained taking the ratio of equation (1) for power off and the steady state (on). This method is introduced by Gurevich[15] *et al.* and is among others used by Fey[5] *et al.* Just as in the case of ALI measurements, the data has to Abel-inverted. For the measured plasma conditions the inaccuracy in T_e/T_e^* turns out to be better than 10%. Unless there are other mechanisms which heat the electrons during the off period, we may assume that $T_e^* = T_h$.

H_β-broadening (HB)

In an open ICP hydrogen lines are always present. These lines can be used to measure the electron density with a f = 1 m monochromator since they are more broadened than the width of the apparatus profile of this setup. For the H_β-line (486.13 nm), the Stark broadening mechanism dominates over the Doppler and other broadening processes. An example of an HB measurement is depicted in figure 3. With the same setup the emission from a pure argon closed ICP,[16] so likely with significantly less hydrogen, is measured which might indicate that the presence of a background emission on the right side causes the asymmetry of the profile. Using the Stark broadening theory of Griem,[17] the work of Vidal[18] *et al.* and Czernichowski[19] *et al.* the width of the H_β-line can be converted to electron density using[19]

$$\log(n_e) = 22.758 + 1.478\log\left(\Delta\lambda_{1/2}\right) - 0.144\left(\log\left(\Delta\lambda_{1/2}\right)\right)^2 - 0.1265\log(T_e), \qquad (3)$$

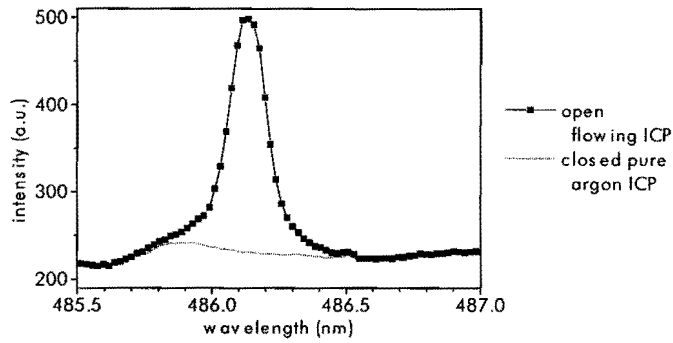

Figure 3. An example of the H_β profile representing an electron density of 1.28×10^{21} m^{-3} measured at $r = 6$ mm and $h = 7$ mm ALC. The dotted line is the emission as obtained from a pure argon filled closed ICP presumably without the presence of hydrogen, so probably indicating the origin of the asymmetry of the H_β-profile.

with $\Delta\lambda_{1/2}$ the FWHM wavelength of the hydrogen emission line. All the used units are in SI-units. Note that an estimation of T_e is necessary to obtain n_e, but that the influence of T_e on n_e determination is rather limited. Equation (3) is valid[19] for 3×10^{20} $m^{-3} < n_e < 3 \times 10^{22}$ m^{-3} and 5000 K $< T_e <$ 20 000 K. The total inaccuracy of this method is about 20% in the present work, and errors are mainly introduced by the rather broad apparatus profile and the Abel-inversion procedure which causes an increasing inaccuracy towards the center of the plasma. In the past the H_β-broadening method was used in our group[6] and by Caughlin[20] *et al.* to study the properties of an ICP.

3 Results and discussion

The measurements are carried out at 7 mm above the load coil (ALC), that is 2 mm above the end of the quartz torch. The advantage of measuring just above instead of through the torch is clear for all the diagnostics, but certainly important for Thomson and Rayleigh scattering. However, it should be realized that since the plasma operates in the open air, a small contamination of nitrogen and water vapor will be present especially near the edge of the plasma. A point of attention is the reproducibility of the ICP itself. The inaccuracy is limited in both power ($\Delta P = 0.1$ kW) and radial position ($\Delta r = 0.4$ mm). A change in power of 0.1 kW has a significant influence on the electron temperature (300 K) as measured by Thomson scattering experiments. The inaccuracy in the radial position limits the accuracy in the plasma parameters if gradients are large, e.g. for n_e at the edge of the plasma. To determine the quality of the various diagnostics we will discuss the determination of each parameter successively and finish with a discussion on the behavior of T_e during the power interruption.

3.1 Comparison of the n_e-values

In figure 4 the electron density profiles are depicted as obtained by Thomson scattering (TS), absolute line emission intensities (ALI) and H_β-broadening (HB) methods. The in-

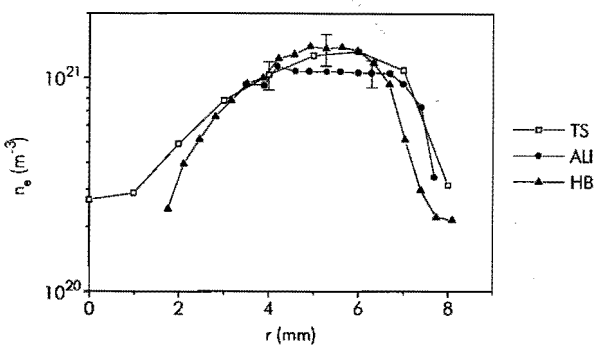

Figure 4. The electron density as a function of radial position measured by Thomson scattering, absolute line intensities and H_β-broadening. The measurements are performed at 7 mm ALC with an input power of 1.2 kW.

accuracies are shown as error bars. It is found that for $3 < r < 6$ mm the n_e-values of TS, ALI and HB reasonably agree with each other within the error bars, but that n_e as obtained by ALI in the active zone ($4 < r < 6$ mm) is systematically lower. This might be due to the Abel-inversion. In contrast with Thomson scattering ALI and HB measurements have to be Abel-inverted, so that the accuracy of these techniques decreases towards the center of the plasma. Therefore, n_e can hardly be determined with these techniques in the center of the plasma at 7 mm ALC and Thomson scattering is expected to be the most powerful since the Thomson scattering setup directly gives local values for n_e.

Of course, there are limitations in the accuracy for all the three diagnostics. Thomson scattering provides electron densities with an accuracy mainly determined by the calibration. This results in a systematic inaccuracy which is the same for all positions. Moreover, at the edge of the plasma ($r > 7.5$ mm), the Thomson scattered profile itself will be disturbed by the presence of air. The temperatures at the edge of the plasma are low enough to keep the molecules intact. These molecules are responsible for a Raman scattered signal. Both Thomson and Raman signals are weak since the temperatures and densities of the species are low and this makes it impossible to discern Raman scattering from Thomson scattering. As a result, the electron densities by TS are always overestimated at the edge of the plasma. A third inaccuracy in n_e obtained by TS is introduced by the instability of the setup. An in time changing laser beam alignment directly influences the n_e determination. In the present results this influence is estimated to be smaller than 10%.

The electron density as determined by ALI requires the assumption of $n_e = n_i$, where n_i represents the number density of argon ions. If there are also other ions present than Ar^+, this assumption will be invalid and leads to an underestimation of n_e by this technique. Furthermore, it should be mentioned that in these results only highly excited levels in the argon system are involved. Lower levels can deviate from local Saha equilibrium especially when n_e or T_e is low.

H_β-broadening is obtained by applying equation (3) for which the validity range is limited as stated before.[19] While at the top of the profile the n_e-values fits the TS-values, at the

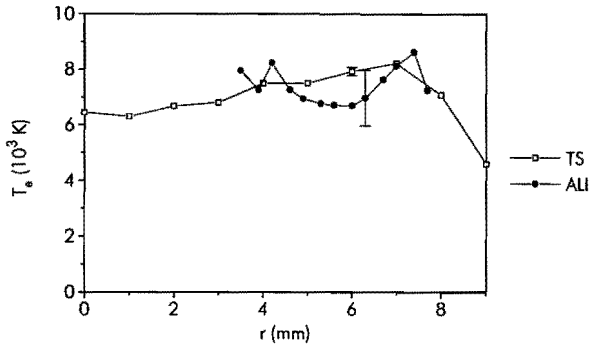

Figure 5. The electron temperature as a function of radial position measured by Thomson scattering and absolute line intensities. The measurements are performed at 7 mm ALC with an input power of 1.2 kW. Note that the complete radial structure is only obtained with Thomson scattering.

edges the HB electron density is apparently lower. This comparison shows that HB is reasonable in providing the n_e in the active zone, but that due to Abel-inversion and to the limited validity region a different n_e determination method is required at the edge and the central part.

We can state that for measuring the electron densities in an atmospheric argon plasma Thomson scattering is the most powerful tool, but at the same time it is expensive. The method of absolute line intensity measurements is an alternative if one is sure that the higher levels are populated according to Saha, but the method is labor-intensive.

3.2 Comparison of the T_e-values

The electron temperature values are shown in figure 5. Thomson scattering provides accurate values for T_e ($\Delta T_e < 150$ K), which are only affected by Raman scattering at the edge of the plasma ($r > 8$ mm). Another problem at the plasma edge is the presence of large gradients. These are not easily measurable since the detection volume (a radius of about 0.5 mm) of the diagnostic is rather large.

Compared to TS, T_e as obtained by ALI does not give a smooth radial profile. This can partially be due to the applied Abel-inversion routine. Since T_e is estimated by the slope of the Boltzmann plot (the logarithm of the density versus ionization potential), which equals $1/k_B T_e$, the temperature is very sensitive to a small variation in the slope especially if T_e is high. The slope is strongly influenced by taking levels into account which are not populated according to Saha. In order to be sure that levels are in pLSE only those levels are involved which are at a maximum distance of 0.6 eV from the continuum. These effects make the method less accurate. Nevertheless, we can state that T_e values measured with ALI reasonably agree with those obtained by TS.

3.3 Comparison of the T_h-values

As shown in figure 6, the heavy particle temperature measured using DLA and RS show a good agreement. Rayleigh scattering shows the most accurate profile of which the accuracy is limited by the influence of possible stray light. However, after minimizing, the amount of

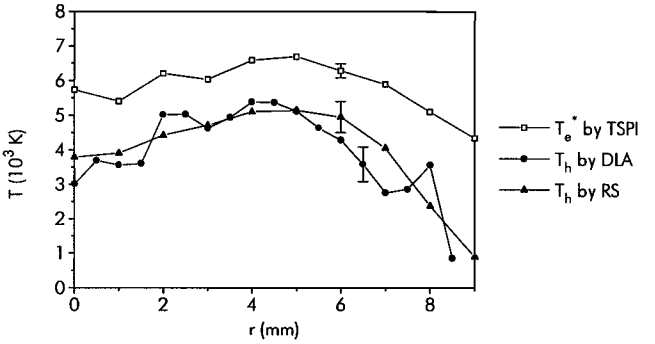

Figure 6. The heavy particle temperature as a function of radial position measured by Rayleigh scattering, diode laser absorption and Thomson scattering during power interruption. The measurements are performed at 7 mm ALC with an input power of 1.2 kW.

stray light turns out to be negligible as is verified by measuring Rayleigh scattering on helium gas, having a 61 times smaller cross-section than argon. The uncertainty in this measurement together with the stability in alignment of the system determines the final accuracy of the Rayleigh scattering method to about 8%.

The method of DLA has also proved to be a powerful tool for obtaining T_h. However, the scatter of DLA T_h is large compared to the temperatures measured by RS. This scatter originates from inaccuracies in the measured absorption profiles which are enlarged by the Abel-inversion process.

The third method of obtaining T_h is TS during power interruption (TSPI) using the assumption that immediately after the power is interrupted T_e drops down to T_h. This technique gives too high values for T_h (see figure 6), which cannot be due to the inaccuracies in the methods. Therefore, remarkably, we have to conclude that during the power interruption period the temperature of the electrons is not equal to the temperature of the heavy particles, but stays depending on the radial position 1000 to 2000 K higher. Note that the gradient in T_e^*, the value of T_e just after the cooling period, is small compared to the gradient in T_e and T_h.

3.4 Behavior of T_e during the power interruption

In the last section it is found by TSPI that the electron temperature during power interruption (T_e^*) is not equal to T_h. The technique of line emission intensities during power interruption (LIPI) shows the same behavior. The ratios T_e/T_e^* obtained by the TSPI and LIPI are depicted in figure 7, error bars are included. The agreement of these two methods is within the experimental error. However, the ratio T_e/T_e^* proves to be certainly not equal to the ratio T_e/T_h as obtained by TS and RS (see figure 7). Therefore, we may state that after switching of the generator there are other sources of energy which keep the electrons at a higher temperature than the bulk of the plasma, the heavy particles.

The difference between the ratio T_e/T_e^* and T_e/T_h is striking and we can conclude that TSPI and LIPI can only be used for the determination of an upper limit for T_h.

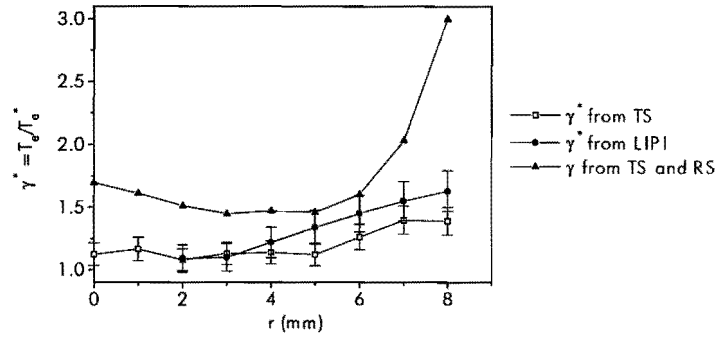

Figure 7. The T_e/T_e^* ratio as a function of radial position measured by Thomson scattering and line emission intensities, both during the power interruption. The measurements are performed at 7 mm ALC with an input power of 1.2 kW.

Unfortunately, the combination of the temperatures T_e by ALI with the ratio T_e/T_e^* by LIPI in order to estimate T_e^* have too large inaccuracies for retrieving an acceptable accuracy (< 25%) in T_e^*. For an estimation of the temperature of the electrons while the power is interrupted Thomson scattering is the most accurate tool.
In figure 8 an overview is given of the temperatures of the different species in a stationary plasma and for the electrons at 5 μs after the power is switched off. The results in this figure are all obtained using the Thomson and Rayleigh scattering diagnostics.

3.5 Heavy particle densities and ionization degree

Rayleigh scattering can also be used for measuring the heavy particle density n_h as it is linear with the scattered intensity. The results are depicted in figure 9. Of course, the radial profile is the inverted heavy particle temperature profile. Combining this information with the measured electron density we are able to calculate the ionization degree as a function of radial position. This is shown in figure 10. At 7 mm ALC the ionization degree is roughly

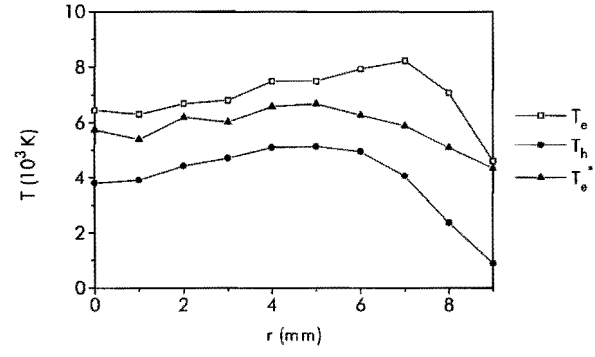

Figure 8. Temperatures in the ICP as a function of radial position measured by Thomson and Rayleigh scattering, steady state electron and heavy particle temperatures and the electron temperature during power interruption. Note that T_e stays higher than T_h during this period. The measurements are performed at 7 mm ALC with an input power of 1.2 kW.

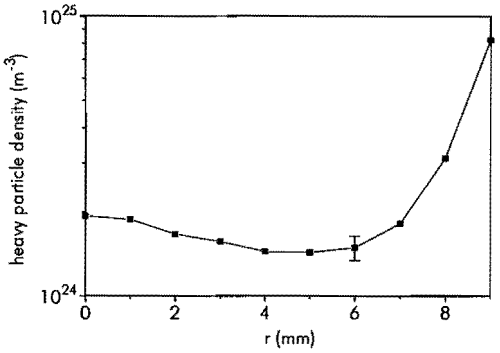

Figure 9. The heavy particle density as a function of radial position. The measurements are performed at 7 mm ALC with an input power of 1.2 kW.

0.1% at the maximum in the hottest area at this height of the plasma.

4 Conclusions

The results of Thomson and Rayleigh scattering, diode laser absorption, H_β-broadening and absolute line intensity measurements are all in agreement within the experimental accuracy with respect to the electron density, electron temperature and heavy particle temperature. The scattering techniques turn out to be the most powerful in retrieving the shape of the radial profile since they measure locally. Nevertheless, the emission and absorption technique are quite useful due to their easy requirements with respect to the setup. Besides, the extensive mutual comparison of the results of the different techniques proves that the power interruption method can be applied for measuring the temperature of the electrons during power interruption. However, this temperature differs from the temperature of the heavy particles. This implies that the electrons remain at higher temperatures than the heavy particles when the power is interrupted.

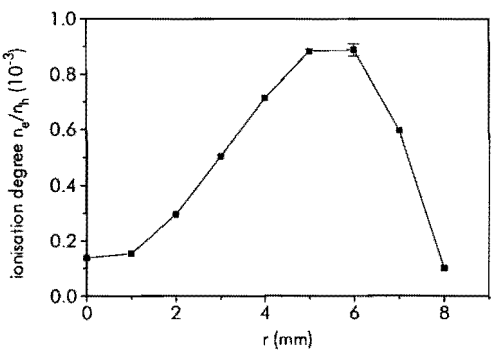

Figure 10. The ionization degree of the ICP as a function of radial position, obtained by a combination of the Rayleigh and Thomson scattering measurements.

[1] J.M. de Regt, R.A.H. Engeln, F.P.J. de Groote, J.A.M. van der Mullen and D.C. Schram, "Thomson scattering experiments on a 100 MHz inductively coupled plasma calibrated by Raman scattering", Review of Scientific Instruments **66** (3228), 1995. (Chapter 3)
[2] J.M. de Regt, J.A.M. van der Mullen and D.C. Schram, "The response of the electron density and temperature to the power interruption measured by Thomson scattering in an inductively coupled plasma", Physical Review E **52** (2982),1995. (Chapter 4)
[3] J.M. de Regt, R.D. Tas and J.A.M. van der Mullen, "Characterization of a 100 MHz inductively coupled argon plasma by diode laser absorption", Journal of Physics D: Applied Physics, submitted for publication, 1995. (Chapter 5)
[4] J.A.M. van der Mullen, S. Nowak, A.C.A.P. van Lammeren, D.C. Schram and B. van der Sijde, "Non equilibrium characterization and spectroscopic analysis of an inductively coupled argon plasma", Spectrochimica Acta **43B** (317), 1988.
[5] F.H.A.G. Fey, W.W. Stoffels, J.A.M. van der Mullen, B. van der Sijde and D.C. Schram, "Instantaneous and delayed responses of line intensities to interruption of the RF power in an argon inductively coupled plasma", Spectrochimica Acta **47B** (885), 1991.
[6] S. Nowak, J.A.M. van der Mullen and D.C. Schram, "Electron density and temperature determination in an ICP using a non-equilibrium concept", Spectrochimica Acta **43B** (1235), 1988.
[7] D.E. Evans and J. Katzenstein, "Laser light scattering in laboratory plasmas", Rep. Prog. Phys **32** (207), 1969.
[8] M. Huang and G.M. Hieftje, "A new procedure for determination of electron temperatures and electron concentrations by Thomson scattering from analytical plasmas, Spectrochimica Acta **44B** (291), 1989.
[9] M. Huang and G.M. Hieftje, "Simultaneous measurement of spatially resolved electron temperatures, electron number densities and gas temperatures by laser light scattering from the ICP", Spectrochimica Acta **44B** (739), 1989.
[10] M. Huang, D.S. Hanselman, Pengyuan Yang and G.M. Hieftje, "Isocontour maps of electron temperature, electron number density and gas kinetic temperature in the Ar inductively coupled plasma obtained by laser-light Thomson and Rayleigh scattering", Spectrochimica Acta **47B** (765), 1992.
[11] D.S. Baer and R.K. Hanson, "Tunable diode laser absorption diagnostics for atmospheric pressure plasmas", J. Quant Spectrosc. Radiat. Transfer **47** (455), 1991.
[12] J.A.M. van der Mullen, "On the atomic state distribution function in inductively coupled plasmas - II. The stage of local thermal equilibrium and its validity region", Spectrochimica Acta **45B** (1), 1990.
[13] J.M. de Regt, R.D. Tas J.A.M. van der Mullen and D.C. Schram, "Determination of transition probabilities for argon using Thomson scattering experiments on an inductively coupled plasma", to be published, 1995. (Chapter 6)
[14] J.A.M. van der Mullen, D.A. Benoy, F.H.A.G. Fey, and B. van der Sijde, "Saha equation for two-temperature plasmas: Theories, experimental evidence, and interpretation", Physical Review E **50** (3925), 1994.
[15] D.B. Gurevich and I.V. Podmoshenskii, "The relationship between the excitation temperature and the gas temperature in the positive column of an arc discharge", Opt. Spectrosc. **15** (319), 1963.
[16] J.M. de Regt, R.D. Tas, J.A.M. van der Mullen and D.C. Schram, "A closed inductively coupled plasma for lighting purposes mapped by spectroscopical techniques", to be published, 1995. (Chapter 10)
[17] H.R. Griem, "Spectral line broadening by plasmas", Academic Press, Inc., 1974.
[18] C.R. Vidal, J. Cooper and E.W. Smith, "Hydrogen Stark-broadening tables", Astrophysical Journal Supplement Series **25** No. 214 (37), 1973.
[19] A. Czernichowski and J. Chapelle, "Experimental study of Stark broadening of the argon I 430.01 nm line", Acta Physica Polonica **A63** (67), 1983.
[20] B.L. Caughlin and M.W. Blades, "An evaluation of ion-atom emission intensity ratios and local thermodynamic equilibrium in an argon inductively coupled plasma", Spectrochimica Acta **39B** (1583), 1984.

Chapter 8

Air entrainment*

* J.M. de Regt, F.P.J. de Groote, J.A.M. van der Mullen and D.C. Schram, "Air entrainment in an inductively coupled plasma measured by Raman and Rayleigh scattering", submitted for publication to Spectrochimica Acta B.

The entrainment of air into the inductively coupled argon plasma is studied. The combination of vibrational Raman scattering and Rayleigh scattering enables measuring absolute particle densities of air and argon. The measurements show a large entrainment of air into the plasma. At an axial position of 2 mm above the end of the quartz torch it is found that at 90% of the plasma radius 55% of the particles originate from air and by exponential extrapolation towards 70% of the radius about 1% entrainment of air is predicted to be present. Furthermore, a comparison with a cold argon flow shows that due to the higher viscosity the entrainment in the plasma is lower than in the cold argon flow.

1 Introduction

The atmospheric inductively coupled plasma (ICP) is well-known from its application for spectrochemical analysis. Contaminated liquids are introduced into the central argon flow. The line emission from the plasma can be used to determine the excited elements. The plasma operates at atmospheric pressure since it ends into the open air. Therefore, this emission is conveniently taken from the ICP above the end of the torch. However, at this height the plasma will be influenced by the entrainment of air. Knowledge on this behavior at the edges of the plasma helps to understand the fundamentals and can be possibly used to improve the applicability of the ICP.

In order to study the effect of air entrainment in the argon plasma, absolute densities of air and argon are measured as a function of radial position. Similar experimental studies are performed by Murphy[1] on free-burning thermal arcs using optical emission experiments. We will use vibrational Raman scattering to determine the nitrogen density and Rayleigh scattering to obtain the argon density in the plasma. Since 78% of air consist of nitrogen, the density of air can easily be calculated from the N_2 measurements. The atmospheric conditions of the plasma enables to use the ideal gas law to calculate the heavy particle temperature[2,3] (T_h) and successively the partial pressures of N_2 (p_{N_2}) or air (p_{air}) and Ar (p_{Ar}). The comparison under the same conditions without plasma ignited shows that the viscosity is much higher under plasma conditions. In section 2 the used methods of Raman and Rayleigh scattering for the determination of the densities and partial pressures will be presented. The experimental setup is described in section 3 whereas the results are discussed in section 4.

2 Method

In order to obtain the absolute densities of argon (n_{Ar}) and nitrogen (n_{N_2}) Rayleigh scattering (RS) and Raman scattering (RnS) are applied. For both techniques calibrations are performed on respectively pure Ar and N_2 at room temperature (T_r) under atmospheric pressure conditions. Using the ideal gas law $p = nk_BT_r$ the densities are calculated and the number of scattered photons can directly be related to densities. A brief description of the two scattering processes will be discussed below.

2.1 Rayleigh scattering

Rayleigh scattering (RS) is the scattering of light on electrons bound to atoms and molecules. In principle, the scattered radiation is Doppler broadened, but our setup does not resolve this so that only the integrated number of scattered photons is counted. This RS signal is proportional to the density of particles. Therefore, after calibration with a room temperature argon flow, the absolute density of argon n_{Ar} can be determined in a pure Ar plasma. Since at the edge of the plasma Rayleigh scattering originates from Ar as well as from N_2 and O_2, the main components of air (others are neglected), we have to unravel the contributions of the two gases air and argon from each other. To simplify the calculations we can assume that the cross section of Rayleigh scattering on O_2 is equal to that of N_2 which results in a error of only about 3% since the Rayleigh scattering contribution of O_2 is small due to its low partial presence in air. Furthermore, we suppose that the relative presence of the components of N_2 and O_2 as present in air does not change under plasma conditions.

The procedure of unraveling uses Raman scattering (RnS), which is only created by molecules (in our case N_2 and O_2) and not by atoms (Ar). The measurement of the N_2 density is chosen because N_2 is the most present molecule in air and has a relative large cross section. These N_2 densities n_{N_2} are converted into a corresponding Rayleigh scattering signal of air and successively subtracted from the total Rayleigh scattering intensity and so n_{Ar} can be obtained. Note that the ratio of cross sections σ for RS has to taken into account ($\sigma_{N_2}/\sigma_{Ar} = 1.12$) since the Rayleigh scattering calibration is performed on argon.

A disturbing phenomena could be the presence of stray light. Stray light originates from light scattering on optical components and the edge of the torch. However, scattering on a gas with a different cross section like Helium can be used to estimate the level of stray light. For the used setup, the level of stray light turns out to be negligible.

2.2 Vibrational Raman scattering

Vibrational Raman scattering originates from excitation or deexcitation of a vibrational excited molecule. Depending on the transition, Raman scattering will undergo wavelength shifts which are typical for a certain molecule. We use the vibrational transition from $v = 0$ to $v = 1$ in the nitrogen molecule creating a frequency shift[4] of $\Delta G_{1/2} = 2331$ cm^{-1}. When excited with 532 nm, the wavelength of a frequency doubled Nd:YAG laser, the Raman emission can be found at 607 nm. Apart from frequency shifts induced by vibrational excitation there are rotational transitions as well. However, these separate rotational

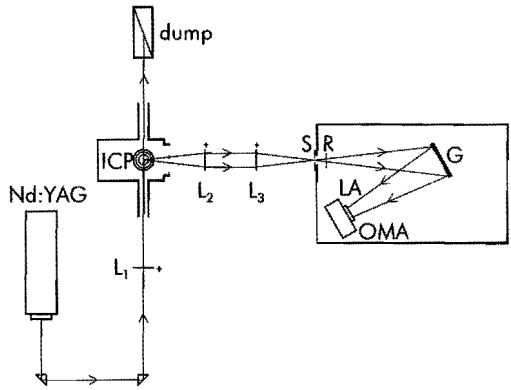

Figure 1. The scattering setup, viewed from the top. With L_1, L_2 and L_3 focusing and detection lenses, S the entrance slit of the monochromator, M mica retarder, G a 2000 lines/mm grating, LA light intensifier and OMA the one-dimensional photo-diode array.

transitions could not be resolved by the used setup due to a poor apparatus profile for this wavelength region so that the vibrational shift consists of the integrated effect of all possible rotational transitions.

The distribution over the different vibrational states depends on the temperature. This implies that Raman scattering from the $v = 0$ to 1 transition decreases in intensity for higher temperatures not only due to lower particle densities, but also because of the shift of the distribution over vibrational states towards higher states. The population ratio $n^{v=1}/n^{v=0}$ for a certain temperature of the $v = 1$ and $v = 0$ state is given by[4]

$$\frac{n^{v=1}}{n^{v=0}} = e^{-\frac{\Delta G_{1/2} hc}{k_B T_h}}, \qquad (1)$$

with h, k_B and c having their usual meaning. Therefore, RnS measurements on the $v = 0$ to 1 transition give the $n^{v=0}$ density of nitrogen, where for higher temperatures this is an underestimation of the total n_{N_2}, e.g. at 2000 K the underestimation will be about 20%. Here is assumed that the occupation of states higher than $v = 1$ can be neglected. This is reasonable since due to quadratic dependency the occupation of the $v = 2$ state is expected to be 4% of the ground state population under these temperature conditions. Since, as we will find, the temperature of 2000 K is reached at $r = 8$ mm, we may neglect the states higher than $v = 1$. In this way n_{N_2} can be calculated and even be corrected for the occupation in the $v = 1$ state if the temperature is available. RS and RnS together with the fact that the pressure condition is atmospheric enables the calculation of n_{N_2}, n_{Ar} and T_h as a function of radius. The minimum density of nitrogen which could be measured with the used setup proves to be about 10^{23} m^{-3}. Note that n_{N_2} is related to the density of air (n_{air}) by $n_{air} = 1.28\ n_{N_2}$ since N_2 in the plasma represents the main component of air (78%).

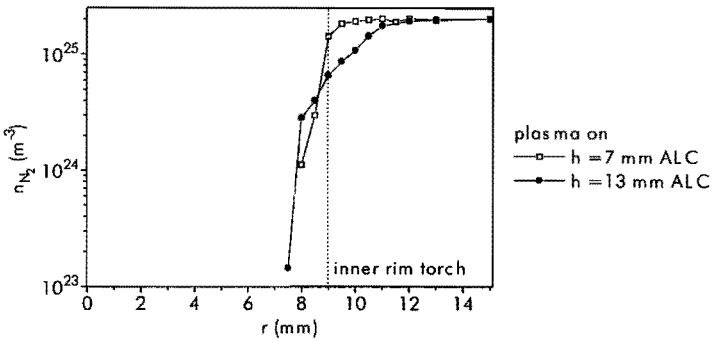

Figure 2. The nitrogen densities as a function of radial position with plasma on. The measuring heights are 7 and 13 mm ALC. The inner rim of the plasma torch is indicated in the figure. Note that the densities in this plot are not corrected for variations in the v = 0 state population density as a result of temperature changes. This leads in this plot to a maximum underestimation of 20%.

2.3 Partial pressures

The absolute densities of species present in the plasma and its surroundings give information on the presence of particles but does not indicate the relative presence of the components and the entrainment of air into the plasma. The use of the partial pressures enables to estimate the amount of entrainment, but to calculate these pressures the temperature is required. Since we have atmospheric pressure conditions and the absolute densities of the species as a function of radius available, the radial dependent temperature can be calculated using the ideal gas law. The measured n_{N_2} will be converted to the partial *air* pressure by taking the fraction of nitrogen in air into account.

3 Experimental/Diagnostics

The measurements are performed at 7 mm and 13 mm above the load coil (ALC) as a function of the radius till 15 mm from the plasma center. Note that the quartz torch ends at about 5 mm ALC.

In figure 1 the used setup is depicted where a 10 Hz pulsed Nd:YAG laser at doubled frequency (532 nm) acts as the source with an energy of 0.45 J per pulse. The scattered light is detected by a monochromator equipped with a gated intensified one-dimensional photo-diode array. This gating allows measuring the scattered signals while the amount of plasma light is minimized. The Rayleigh signal is attenuated by a ND3.0 gray filter. The average measurement is obtained from scattered light of 1000 laser shots. For more details concerning the setup we refer to [5].

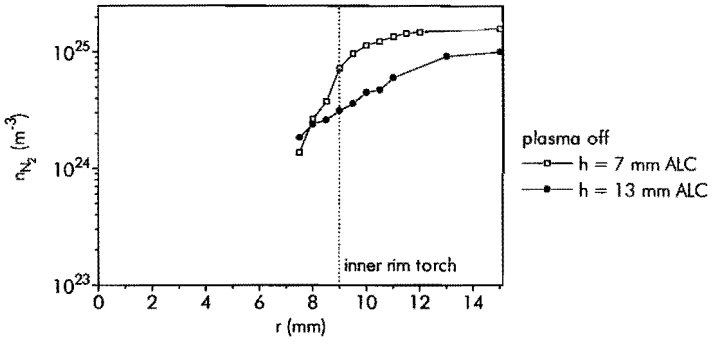

Figure 3. The nitrogen densities as a function of radial position with plasma off, so with only an argon flow through the torch. The measuring heights are 7 and 13 mm ALC.

4 Results and discussion

Figure 2 presents the densities of nitrogen at 7 and 13 mm ALC with plasma on as obtained by RnS. It should be noted that the nitrogen densities in this plot are not corrected for the effect of depopulation of the $v = 0$ state as a result of increasing temperatures. In this plot it leads to a maximum underestimation of 20% at the radial position where the highest temperatures can be expected (at about $r = 5$ mm). Due to low densities it was not possible to measure densities at 7 mm ALC for $r < 8$ mm and at 13 mm ALC for $r < 7.5$ mm. There are two reasons for the decrease in n_{N_2} towards the center. First, the higher temperature lowers the particle density (at constant pressure) and second, the nitrogen molecules are replaced by argon atoms. Therefore, these two effects make this figure less useful for studying the importance of air entrainment. Nevertheless, the comparison of these heights show that at 13 mm ALC the plasma flow is broader since just outside the torch at 13 mm ALC n_{N_2} is lower due to the presence of argon or due to higher temperatures.

Since for the argon flow without plasma the temperature is constant over the radius a decrease in n_{N_2} can directly be attributed to an increase in n_{Ar}. This situation is shown in figure 3 at 7 and 13 mm ALC. Obvious is the fact that at a higher position the argon flow is much broader than at lower positions. The result is difficult to compare with the plasma on condition of figure 2 since it is not corrected for the effect of temperature on the densities.

Therefore, a better insight can be obtained determining the absolute densities of both air and Ar by the method discussed in section 2, using the RS experiments under plasma-on conditions. The results are depicted in figure 4 for the axial position of 7 mm ALC which are now corrected for the depopulation of the $v = 0$ state at higher temperatures. At about $r = 8$ mm the densities of air and Ar are nearly equal, which indicates that a strong entrainment of air into the plasma is present. An exponential extrapolation of n_{air} towards inner regions leads to the conclusion that even at $r = 6$ mm the n_{air} could in the order of 10^{22} m^{-3},

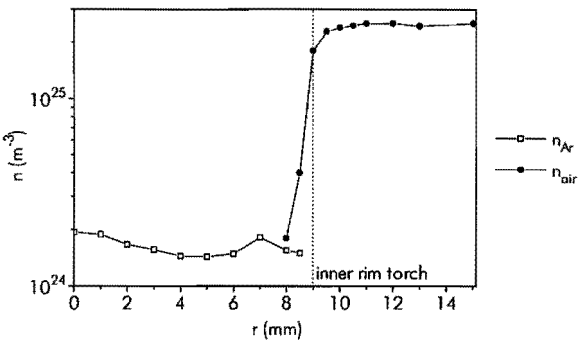

Figure 4. The densities of argon and air by respectively RS and RnS, measured at 7 mm ALC with plasma on. The air (obtained via nitrogen) density is corrected for variations in v = 0 state population changes due to temperature changes.

still about 1% of the heavy particle density. This high density will influence the plasma properties.

The heavy particle temperature T_h at 7 mm ALC is depicted in figure 5 as a function of radius. At the edge of the plasma the temperature decreases fast towards the room temperature.

This T_h is used to calculate partial pressures of argon and air. These are depicted in figure 6 and show the relative contribution of air and argon as a function of radius. Striking is that at 8 mm from the center about half of the gas mixture consists of air. In figure 6 the situation of the argon flow without plasma is shown as well. The partial pressure p_{Ar} is obtained from RnS measurements in combination with the known atmospheric pressure conditions. The difference between plasma on and off is large. While the plasma is on, air entrainment is significantly less than with a room temperature argon flow. The explanation is that the viscosity of the plasma is much higher than the viscosity for the cold argon flow. This reduces the possibility of air entrainment into the plasma.

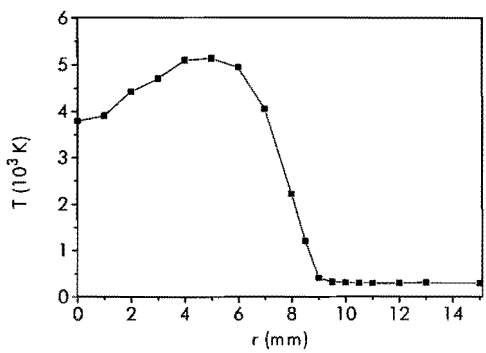

Figure 5. The temperature at 7 mm ALC in and around the plasma obtained by using total particle densities with the atmospheric pressure condition.

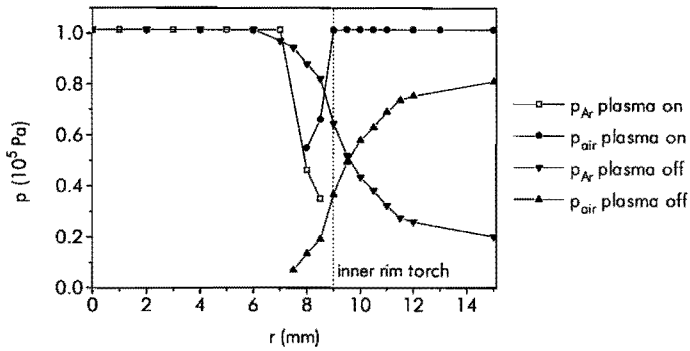

Figure 6. The partial pressures of argon and air with plasma on and off at 7 mm ALC.

5 Conclusions

Rayleigh scattering in combination with vibrational Raman scattering is used to study air entrainment into the atmospheric flowing inductively coupled plasma. The results show a significant entrainment of air into the plasma just above the torch. At 2 mm above the end of the torch and at 8 mm from the center 55% of the particles originates from the entrainment of air. By exponential extrapolation of the results towards 6 mm from center still 1% of the heavy particles can be expected to be entrained from air. A comparison with measurements carried out on an argon flow without plasma shows that the viscosity of the plasma is higher than of the argon flow.

[1] A.B. Murphy, "Modified Fowler-Milne method for the spectroscopic measurement of temperature and composition of multielement thermal plasmas", Review of Scientific Instruments **65** (3423), 1994.
[2] M. Huang and G.M. Hieftje, "Simultaneous measurement of spatially resolved electron temperatures, electron number densities and gas kinetic temperatures by laser light scattering from the ICP", Spectrochimica Acta **44B** (739), 1989.
[3] J.M. de Regt, F.P.J. de Groote, J.A.M. van der Mullen and D.C. Schram, "Comparison of active and passive spectroscopic methods to investigate atmospheric plasmas", to be published 1995. (Chapter 7)
[4] G. Herzberg, "Spectra of Diatomic Molecules", D. van Nostrand Company Inc. 1950, 2nd ed. 1965.
[5] J.M. de Regt, R.A.H. Engeln, F.P.J. de Groote, J.A.M. van der Mullen and D.C. Schram, "Thomson scattering experiments on a 100 MHz inductively coupled plasma calibrated by Raman scattering", Review of Scientific Instruments **66** (3228), 1995. (Chapter 2)

Chapter 9

Recombination and diffusion processes*

* J.M. de Regt, J. Jonkers and J.A.M. van der Mullen, "Recombination and diffusion processes during power interruption in an inductively coupled argon plasma", submitted for publication to Phys. Rev. E.

The electron density and temperature behavior during the power interruption of an inductively coupled plasma is simulated by a one-dimensional model with ambipolar diffusion and three particle recombination. The simulation of the electron density time dependence fits the measurements in the center of the plasma; the measured increase in electron density can be explained by the three particle recombination and diffusion processes. However, for the measured fast decay in electron density at the outer half of the plasma radius a third process is responsible: charge exchange of atomic ions with molecules subsequently followed by dissociative recombination of the nitrogen molecular ion. By the entrainment of air, nitrogen is sufficiently present at the outer side of the plasma. A complementary mechanism contributing to the fast electron density decay might be the formation of Ar_2^+ molecules followed by dissociative recombination. Furthermore, it is shown that the energy obtained by three particle recombination can heat the electrons to temperatures above the heavy particle temperature during the power interruption. At the same time, heat conduction is presumably responsible for the leveling out of the electron temperature gradients as is concluded from the measured flat radial electron temperature profile.

1 Introduction

Inductively coupled plasmas (ICPs) are interesting from fundamental point of view as well as from their widely technological applicabilities. Nowadays, ICPs are used for spectrochemical analysis, material treatment and might be promising efficient light sources[1] in the future. Fundamental research on ICPs is needed to improve their performance. Therefore, the study of the fundamental plasma parameters, such as densities and temperatures, is of interest. A variety of methods is applied to obtain information on the behavior of the plasma particles.

One of the techniques used in the past is the combination of emission measurements with the power interruption of the generator, first introduced by Gurevich[2] *et al.* for arcs and, amongst others, applied by Bydder[3] *et al.* and Fey[4] *et al.* for the ICP. This technique promises to be useful for estimating the ratio between electron temperature (T_e) and heavy particle temperature (T_h). The basis of this technique is the assumption that after the power is instantaneously switched off, T_e, normally higher than T_h, will immediately (that is within a few microseconds) drop to T_h. This assumption implies that after the power is switched off no sources of heating are available to keep the electrons at a higher temperature than that of the heavy particles.

However, a recent study[5] using two independent methods shows that the T_e in an ICP does not drop to T_h. By the use of Thomson and Rayleigh scattering, diode laser absorption and absolute line emission intensity measurements, T_e is found to cool indeed instantaneously, but remain at a significantly higher temperature than the temperature of the bulk T_h. This behavior is shown in figure 1, where the stationary temperature of electrons and heavy particles are depicted together with the temperature of electrons just after (5 μs) the removal of the power (T_e^*), all as functions of radial position, for an input power of 1.2 kW and at about 7 mm above the load coil (ALC).

The aim of this paper is to clarify the mechanism in the atmospheric argon ICP that could heat the electrons during the power interruption period. At the same time, we will look at the reason of the increasing electron density (n_e) in the plasma center during the power interruption period as measured earlier.[6] The first approach will be the simulation of the density behavior after the power removal. With this simulation we estimate the influence of recombination and diffusion processes in order to explain the observed temporal behavior of the electron density profile. Also the energy transfered to the electrons during power interruption will be calculated and will be compared to the energy required to hold the temperature of the electrons above the temperature of the heavy particles. However, as we will see, the two processes of three particle recombination and ambipolar diffusion turn out to be insufficient for explaining the temporal behavior of n_e at the edge of the plasma. In order to clarify the behavior at the edge, two additional electron loss processes are discussed.

2 Experiment

The measurements presented in this paper are obtained from a flowing inductively coupled plasma in argon which operates at atmospheric pressure conditions. This plasma[7,8] is situated in an open quartz torch with an inner diameter of 18 mm. The total argon gas-consumption is about 13 l/min. A 100 MHz generator delivers the power of 1.2 kW to the induction coil, resulting in a typical electron density (n_e) of about 10^{21} m^{-3} and a neutral density of about 10^{24} m^{-3} at 7 mm above the load coil (ALC), the height where the measurements are performed. This height is about 2 mm above the end of the quartz torch.

2.1 Thomson scattering

For the determination of the electron temperature T_e and density n_e a Thomson scattering setup is used. The main components are a frequency-doubled Nd:YAG laser and a monochromator with an intensified photo diode array. The laser and generator of the

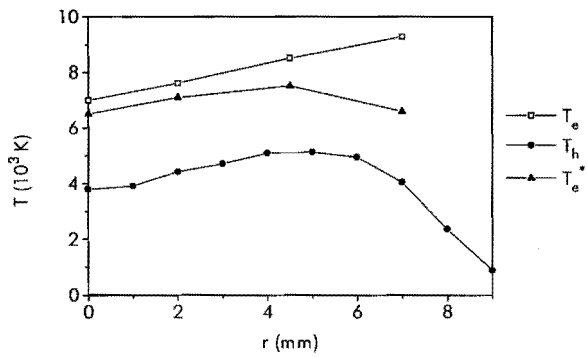

Figure 1. The temperatures of the electrons for stationary conditions (T_e) and during the power interruption (T_e^*) together with the heavy particle temperature (T_h) as a function of radius at 7 mm ALC; the input power is 1.2 kW. The electron temperatures are obtained by Thomson scattering experiments and the heavy particle temperatures by Rayleigh scattering.

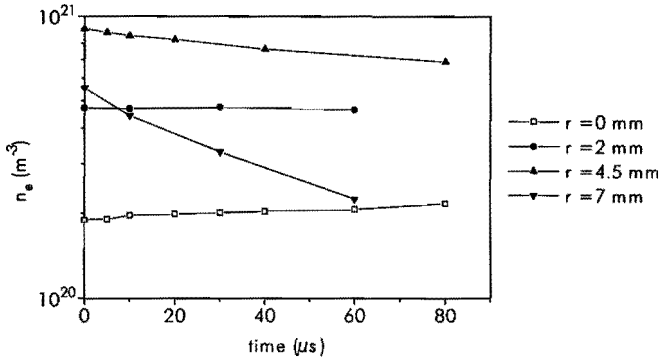

Figure 2. The time-dependent response of the electron density to the power interruption for 4 different radial positions.

power supply are triggered in such a way that the time between switching off the generator and firing the laser can be adjusted between 0 and 80 μs. For more details concerning the Thomson scattering setup, the reader is referred to earlier publications.[6,8] Each experimental value of n_e and T_e is obtained by about 1000 repetitive power interruptions in combination with laser pulses.

In figure 2 the response of n_e to the power interruption is depicted for 4 radial positions. The inaccuracies (typically 15%) are mainly due to the absolute calibration of n_e. The relative inaccuracy between the measured points is only a few percent. Note that, while at the outer edge of the plasma n_e decays after the power switch off, it slightly increases in the center of the plasma ($r < 2$ mm), as can also be seen in figure 3.

The behavior of T_e in response to the power interruption is shown in figure 4 for the same radial positions. The instantaneous drop of T_e to a lower level can easily be recognized, the subsequent decrease of the temperature is much slower or not measurable. The uncertainty of one measurement is about 150 K. However, the temperature depends strongly on the input power and a slight change in power changes the temperature significantly. Therefore, since the generator is not perfectly stable, but varies slowly in time, the relative accu-

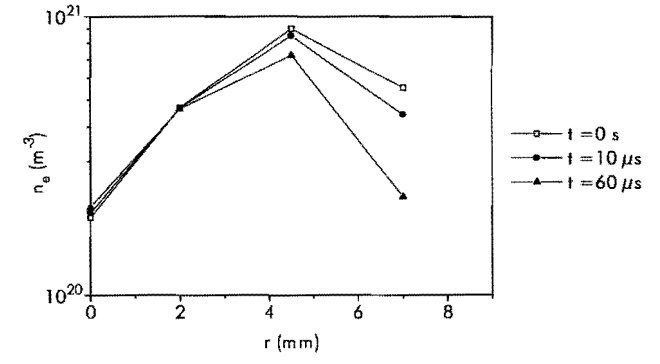

Figure 3. The temporal behavior of n_e as a function of radial position. Note the n_e increase in the center and the fast decrease at the edge of the plasma.

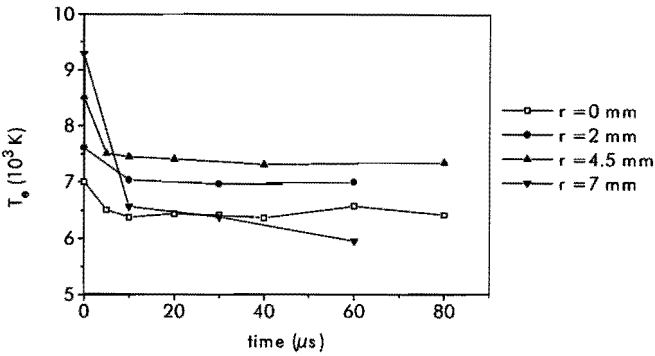

Figure 4. The time-dependent response of the electron temperature on the power interruption for 4 different radial positions.

racy between the measured positions is about 500 K.
To study the decay of n_e and T_e, we introduce the exponential decay frequencies ν_{n_e} and ν_{T_e},

$$n_e(r,t) = n_e(r,0)e^{-\nu_{n_e}(r)t}, \tag{1}$$

$$T_e(r,t) = T_e(r,0)e^{-\nu_{T_e}(r)t}. \tag{2}$$

Here the initial values $n_e(r,0)$ and $T_e(r,0)$ are the values just after the power switch off and after the induced fast temperature decay. However, to be sure that the EM field is removed we use for $T_e(r,0)$ the values obtained by an extrapolation towards $t = 0$ of the experimental T_e-values measured during the power interruption. Due to the presence of the temperature fall, $T_e(r,0)$ is significantly lower than the steady state T_e-value.
A negative value of the decay frequencies represents an increasing n_e or T_e. The measurements as presented in figure 2 and figure 4 can be fitted with these equations in order to

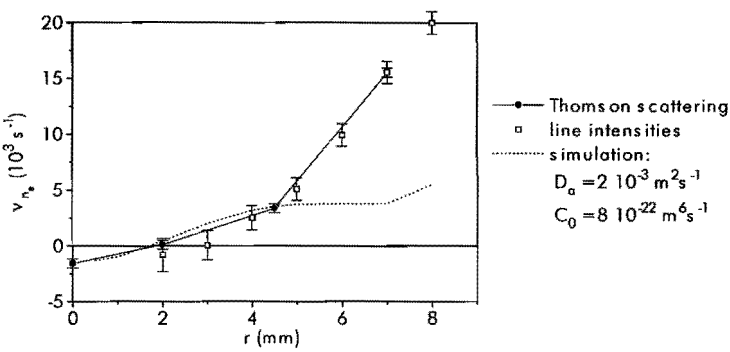

Figure 5. The decay frequency ν_{n_e} in n_e as a function of radial position during the power interruption measured by Thomson scattering (circles with error margin, connected with straight line) and line emission intensity experiments (squares with error margin). Note the increase of n_e in the center of the plasma. The dotted line shows the simulation for the decay frequency of electrons (see section 3).

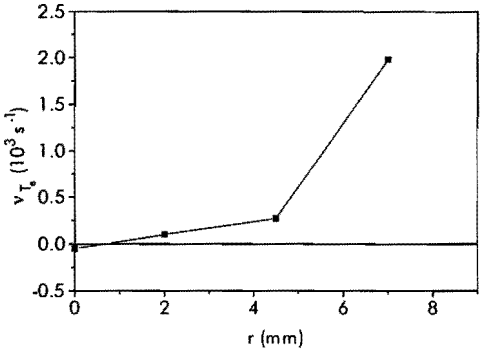

Figure 6. The decay frequency of T_e during power interruption. Note the significant lower frequencies compared to the decay frequencies of n_e.

estimate the decay frequencies of n_e and T_e. The results are depicted in figure 5 and figure 6. The behavior of ν_{n_e} shows an increasing n_e for $r < 2$ mm and a decreasing n_e for $r > 2$ mm. A decrease of n_e is to be expected from the removal of the power, the increase in the center can be understand if the inward diffusion towards the central region after the power interruption exceeds the local recombination processes. The magnitude of ν_{T_e} is small compared to that of ν_{n_e}. In the center T_e seems to increase slowly after $t = 5$ μs. Moving to larger r positions, T_e first decreases slowly, but close at the edge the temperature decreases much faster. In general we may state that T_e during power interruption is roughly constant for time scales smaller than 1 ms, except at the edge where the decay in T_e becomes significant.

2.2 Line emission intensities

Since line emission intensities can be assumed to have an n_e^2-dependency,[4,7] emission measurements can be used to determine ν_{n_e} as well. An example of such a measurement at 588.9 nm is presented in figure 7, where the full line is the fitted time dependence of the intensity. The part with the exponential decay during power interruption is the part of interest for the present investigations. Since the line emission intensities are line-of-sight measurements, all the data is Abel-inverted in order to obtain local information. Unfortunately, it is impossible to obtain accurate information in the center with this procedure. The fitted decays of five emission lines (420.1 nm, 588.9 nm, 591.2 nm, 696.5 nm and 750.5 nm) are averaged and plotted with squares in figure 5. The agreement with the ν_{n_e}-value obtained by Thomson scattering is excellent. It is expected that Thomson scattering provides more accurate values towards the center whereas line emission intensity measurements can be used more close to the edge of the plasma. At the edge of the plasma ($r > 7$ mm) the Thomson scattered signal is disturbed by Raman scattering due to the presence of (mainly nitrogen) molecules resulting in an overestimation of n_e.[5]

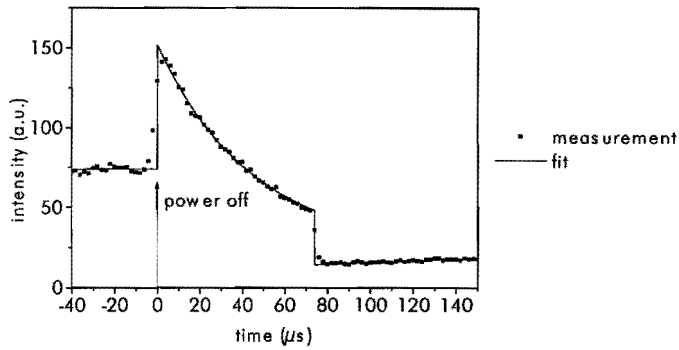

Figure 7. An example of line emission intensity measurement at λ = 588.9 nm during the interruption of the power for r = 6 mm. The jump upwards at the moment of the removal of the power is due to the sudden jump downwards of T_e, creating a relative overpopulation (compared to the stationary plasma) of the excited states in argon causing an increase in emission intensity.

3 Simulation of n_e during power interruption

Now that we have determined experimentally the behavior of n_e and T_e during the power interruption as a function of time, a simulation for the temporal behavior of n_e will be introduced. Input parameters are the, with a polynomial fitted, initial values of n_e and T_e (as defined in section 2.1) and the decay frequency of the electron temperature ν_{T_e}. The output is the temporal behavior of $n_e(t)$ which can be easily transferred into the decay frequency of electrons ν_{n_e} by applying formula (1). For this simulation we consider in a first approximation that in the electron particle balance only ambipolar diffusion and three particle recombination will be present, i.e. other possible electron loss processes are neglected. The electron production processes can be neglected since there is no energy supply to the plasma during power interruption. Furthermore, we assume that the plasma volume under study stays constant in time. This is reasonable since the n_e and T_e gradients in the axial direction (*1/e* gradient length $\approx 2 \times 10^{-2}$ m), that is the direction of the argon flow, are small compared to the considered gradients in the radial direction (*1/e* gradient length $\approx 10^{-3}$ m). Moreover, the velocity of the plasma (10 ms^{-1}) together with the axial gradient length leads to a time scale ($\approx 2 \times 10^{-3}$ s) which is long compared to the characteristic time-scales of our study (10^{-4} s). Hence only radial diffusion needs to be considered. For this situation, the time dependent behavior of n_e can be described by the following differential equation,

$$\frac{\partial n_e}{\partial t} = \nabla \cdot (D_a \nabla n_e) - K_{rec,3} n_e^3. \qquad (3)$$

The first term on the r.h.s. represents the transport of electrons due to ambipolar diffusion with ambipolar diffusion coefficient D_a whereas the second term refers to three particle recombination of the argon ion with rate coefficient $K_{rec,3}$. The mechanism of two particle recombination can be ignored.[9]

Since the temperature variations along the radius influence the ambipolar diffusion coefficient D_a as given by Devoto[10] only weakly, we can take D_a constant for all radial positions with a time independent value of 2×10^{-3} m^2s^{-1} making a maximum estimated error of 40% in D_a. The first term on the r.h.s. of equation (3) transforms with these assumptions into:

$$\nabla \cdot (D_a \nabla n_e) \approx D_a \nabla^2 n_e = D_a \left(\frac{1}{r} \frac{\partial n_e}{\partial r} + \frac{\partial^2 n_e}{\partial r^2} \right) = D_a \frac{n_e}{\Lambda^2}, \tag{4}$$

with Λ is the radially dependent gradient length. As stated before, we will not take the time dependence of the diffusion contribution into account. This allows to write a time independent gradient length by

$$\Lambda = \left(\frac{1}{n_e} \left(\frac{1}{r} \frac{\partial n_e}{\partial r} + \frac{\partial^2 n_e}{\partial r^2} \right) \right)^{-1/2}, \tag{5}$$

where for n_e the initial $n_e(r,0)$ value can be taken.
For the estimation of the three particle recombination processes, a temperature dependence is used, since the influence of T_e on $K_{rec,3}$ is large:[11]

$$K_{rec,3}(t) = C_0 \left(T_e(t) \right)^{-\frac{9}{2}} = C_0 \left(T_e(0) e^{-\nu_{T_e} t} \right)^{-\frac{9}{2}}. \tag{6}$$

The measured initial $T_e(0)$ and ν_{T_e} can be used in this formula, whereas the factor C_0 will be adjusted by fitting the simulation to the measurements. Note that in the three last equations the radial dependence is implicitly present by the radial dependence of $n_e(0)$, $T_e(0)$ and ν_{T_e}.
The solution of equation (3) together with equations (4) and (6) can be obtained by a substitution of $f = n_e^{-2}$ and will predict the time dependent behavior for n_e:

$$n_e(t) = \left(\frac{e^{-2\frac{D_a}{\Lambda^2}t}}{n_e^2(0)} - \frac{2C_0 \left(T_e(0) \right)^{-\frac{9}{2}}}{\frac{9}{2}\nu_{T_e} + 2\frac{D_a}{\Lambda^2}} \cdot \left(e^{-2\frac{D_a}{\Lambda^2}t} - e^{\frac{9}{2}\nu_{T_e} t} \right) \right)^{-\frac{1}{2}}. \tag{7}$$

Using the initial values for n_e and T_e and using the measured ν_{T_e}, the results of this equation for the estimation of ν_{n_e} at the different radial positions is depicted in figure 5, for $C_0 = (8 \pm 2)\ 10^{-22}$ m^6s^{-1}. The agreement with the measurements is striking for $r < 5$ mm, even the increase of n_e in the center is predicted. This agreement indicates that in this part ($r < 5$ mm) of the plasma ambipolar diffusion together with three particle recombination can describe the electron particle behavior. Note that the good agreement yields for this particular value of C_0, which value is also found by Benoy[12] *et al.* for similar plasma conditions. For $r > 5$ mm we see that the decay in n_e as predicted by the simulation is significantly lower than the measured values. Moreover, the difference between experiment and model increases for larger r positions up to 10^4 s^{-1} at $r = 7$ mm. Apparently, a third electron loss process is required in order to explain the electron decay behavior present at the edge of the plasma.

4 Discussion

4.1 Electron density

The simulation as presented in the last section proved that three particle recombination and ambipolar diffusion are insufficient to predict the large electron loss at the edge of the plasma. Two candidates for additional electron loss will be discussed below.

- Molecular recombination via the molecular argon ion Ar_2^+

One way of loosing electrons is the formation of the molecular ion Ar_2^+, which subsequently decays by dissociative recombination into two argon atoms. This electron decay channel has two steps:

$$Ar^+ + 2Ar \rightarrow Ar_2^+ + Ar, \tag{8}$$
$$Ar_2^+ + e^- \rightarrow Ar^* + Ar + h\nu. \tag{9}$$

Here Ar^+ is single ionized argon, Ar_2^+ denotes the molecular argon ion, Ar^* an argon atom in an excited state and $h\nu$ an emitted photon. The first step with a rate coefficient[13] of about 2×10^{-43} m^6s^{-1} is the limiting factor. This results in a decay frequency $\nu_{Ar_2^+}$ of

$$\nu_{Ar_2^+} = 2 \times 10^{-43} n_{Ar}^2, \tag{10}$$

with n_{Ar} the neutral argon particle density. At the edge of the plasma this rate will be about 10^6 s^{-1}. Note that in fact both processes are accompanied by their reverse processes. This balances the number densities of the species on both sides and apparently limits the effective rate of the processes down to the measured values of 10^4 s^{-1}.

- Molecular recombination of N_2^+

The presence of nitrogen can offer another electron decay channel. Since the plasma operates under atmospheric pressure conditions in air, nitrogen can penetrate into the plasma and could influence the electron loss by the following process:

$$Ar^+ + N_2 \rightarrow Ar + N_2^+, \tag{11}$$
$$N_2^+ + e^- \rightarrow N^* + N + h\nu, \tag{12}$$

with N^* an nitrogen atom in an excited state. In the same way as with the Ar_2^+ process, these processes are in fact partially balanced which limits the effective rate of the decay. Again the first step with a rate coefficient[14] of 4×10^{-16} m^3s^{-1} is about 100 times slower than the second step. This leads to an estimation of the rate $\nu_{N_2^+}$ of this process, being

$$\nu_{N_2^+} = 4 \times 10^{-16} n_{N_2}, \tag{13}$$

with n_{N_2} the N_2 density. Measurements[15] point towards a 1% presence of N_2 at r = 6 mm, so a density of about 10^{23} m^{-3}. A rough estimation of $\nu_{N_2^+}$ at the edge of the plasma leads to a frequency of about 8×10^6 s^{-1}, the same order of magnitude as $\nu_{Ar_2^+}$.

Since the estimated rates of both processes turns out to be equal, none of these two processes can be stated to be dominant and further research is required to establish this. However, both processes might be present and are capable to explain the difference in electron decay rate of the measurements and the simulation which can not be explained by three particle recombination and ambipolar diffusion solely.

4.2 Electron temperature

As shown in figure 1, a difference between T_e^* and T_h is present during the power interruption which can only be explained by the presence of an electron heat mechanism. The power Q required for keeping a temperature difference $\Delta T = T_e^* - T_h$ can be estimated by[15]

$$Q_{loss} = 3\frac{m_e}{m_a}(\nu_{ei} + \nu_{ea})n_e k_B \Delta T, \tag{14}$$

with m_e and m_a the electron and argon atom mass, k_B the Boltzmann constant and ν_{ei} and ν_{ea} the average electron-ion and electron-atom collision frequencies for momentum transfer.

Three particle recombination could be responsible for the effect of heating since each recombination process provides an energy gain ΔE to the electrons between about 1 and 15 eV, depending on the transition,

$$Q_{gain} = K_{rec,3} n_e^3 \Delta E. \tag{15}$$

In order to estimate the temperature difference ΔT, equations (14) and (15) are combined and applied to the ICP conditions using the collision frequencies

$$\nu_{ei} = 3.61\times10^{-5}\frac{n_e}{T_e^{3/2}}, \tag{16}$$

$$\nu_{ea} = 6.2\times10^{3} n_{Ar}\sqrt{T_e}\times \left(\frac{5\times10^{-20}}{\left(1+1.7\times10^{-3}T_e\right)^2} - 3\times10^{-21} + 2.8\times10^{-24}T_e - 4.1\times10^{-34}T_e^3\right), \tag{17}$$

as is given by Mitchner and Kruger[16] and by Rees[17] *et al.*, respectively (in SI-units). Using equation (16) and (17) in equation (14) and equaling Q_{loss} and Q_{gain}, a spatially dependent ΔT is obtained as depicted in figure 8. In these calculations the recombination rate C_0 is used as obtained by the simulation of the electron density behavior in section 3.

Whereas ΔE is chosen to be 5 eV, comparing ΔT obtained with the experimental values, it is found that the *order of magnitude* is roughly in agreement. However, the *shape of the radial profile* is certainly not in agreement. The measurements show a rather flat T_e^* profile as depicted in figure 1, whereas the calculated temperature of T_e^*, obtained by combining T_h with the calculated ΔT ($T_e^* = T_h + \Delta T$), is more peaked at the top of the density profile.

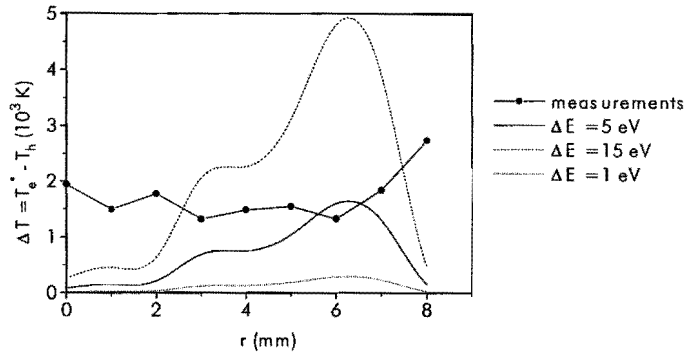

Figure 8. The measured and calculated temperature difference of T_e^* and T_h during power interruption. For the calculations we used three different energy gains of the recombination process (1, 5 and 15 eV)

This is not surprising since here the largest production of energy will be present due to the largest number of recombination processes. The disagreement in shape of the radial profile can be explained by the presence of relatively fast heat conduction which is not taken into account in the present calculations. This heat conduction could levels out the gradients in the T_e^* profile, clarifying that the measured T_e^* profile is rather smooth.

5 Conclusions

After the power interruption the electron density in an ICP will decay, except in the center where the density slightly increases as a function of time. A one-dimensional simulation shows that the increasing electron density in the center can be explained by an inward flux generated by ambipolar diffusion which exceeds the electron losses due to three particle recombination processes. Fitting the simulation to the measurements enables to determine the temperature independent factor in the rate coefficient of the three particle recombination process which turns out to be $(8 \pm 2)\ 10^{-22}\ m^6s^{-1}$. However, at the outer half of the plasma radius the decay in electron density is much faster than what can be expected from diffusion and three particle recombination solely. The presence of nitrogen in this plasma part by the entrainment of air is presumably responsible for this fast decay in electron density by successively charge transfer and molecular recombination processes. A second possibility is the formation of Ar_2^+ molecules followed by dissociative recombination. Furthermore, the higher temperature of the electrons compared to the heavy particles during power interruption can be explained by an energy gain from three particle recombination processes. Moreover, heat conduction is held responsible for the low radial gradients in the radial profile of the electron temperature during this period.

[1] J.M. de Regt, R.D. Tas, J.A.M. van der Mullen and D.C. Schram, "A closed inductively coupled plasma for lighting purposes mapped by spectroscopical techniques", to be published, 1995. (Chapter 10)
[2] D.B. Gurevich and I.V. Podmoshenskii, "The relationship between the excitation temperature and the gas temperature in the positive column of an arc discharge", Opt. Spectrosc. **15** (319), 1963.
[3] E.L. Bydder and G.P. Miller, "A relaxation method for determining state of equilibrium and temperature ratio T_e/T_g in an argon ICPT", Spectrochimica Acta **43B** (819), 1988.
[4] F.H.A.G. Fey, W.W. Stoffels, J.A.M. van der Mullen, B. van der Sijde and D.C. Schram, "Instantaneous and delayed responses of line intensities to interruption of the RF power in an argon inductively coupled plasma", Spectrochimica Acta **46B** (885), 1991.
[5] J.M. de Regt, F.P.J. de Groote, J.A.M. van der Mullen and D.C. Schram, "Comparison of active and passive spectroscopic methods to investigate atmospheric plasmas", submitted to Spectrochimica Acta B, 1995. (Chapter 7)
[6] J.M. de Regt, J.A.M. van der Mullen and D.C. Schram, "The response of the density and temperature to the power interruption measured by Thomson scattering in an inductively coupled plasma", Phys. Rev. E **52** (2982), 1995. (Chapter 4)
[7] J.M. de Regt, J. van Dijk, J.A.M. van der Mullen and D.C. Schram, "Components of continuum radiation in an inductively coupled plasma", J. Phys. D: Applied Physics **28** (40), 1995. (Chapter 2)
[8] J.M. de Regt, R.A.H. Engeln, F.P.J. de Groote, J.A.M. van der Mullen and D.C. Schram, "Thomson scattering experiments on a 100 MHz inductively coupled plasma calibrated by Raman scattering", Rev. Sci. Instrum. **66** (3228), 1995. (Chapter 3)
[9] S. Nowak, J.A.M. van der Mullen, A.C.A.P. van Lammeren and D.C. Schram, "On the influence of water on the electron density in an argon inductively coupled plasma", Spectrochimica Acta **44B** (411), 1989.
[10] R.S. Devoto, Phys. Fluids **10** (354), 1967.
[11] J.A.M. van der Mullen, "Excitation equilibria in plasmas; a classification", Phys. Rep. **191** (109), 1990.
[12] D.A. Benoy, J.A.M. van der Mullen, M.C.M. van de Sanden, B. van der Sijde, and D.C. Schram, "Application of a hybrid collisional radiative model to recombining argon plasmas", J. Quant. Spectrosc. Radiat. Transfer **49** (129), 1993.
[13] A.K. Bhattacharya, "Mass spectrometric study of argon afterglow plasmas", Journ. Appl. Phys. **41** (1707), 1970.
[14] D. Smith and N.G. Adams, Physical Review A **23** (2327), 1981.
[15] J.M. de Regt, F.P.J. de Groote, J.A.M. van der Mullen and D.C. Schram, "Entrainment of air in an inductively coupled plasma measured by Raman and Rayleigh scattering", submitted to Spectrochimica Acta B, 1995. (Chapter 8)
[16] M. Mitchner and C.H. Kruger, "Partially Ionized Gases", Wiley & Sons, New York, 1973.
[17] J.A. Rees, H.B. Milloy, R.W. Crompton and A.G. Robertson, Austr. Journ. of Phys. **30** (61), 1977.

Chapter 10

Closed ICP for lighting*

* J.M. de Regt, R.D. Tas, J.A.M. van der Mullen and D.C. Schram, "A closed Inductively Coupled Plasma for lighting purposes mapped by spectroscopical techniques", submitted for publication to J. Phys. D: Appl. Phys.

A closed 13.6 MHz inductively coupled argon plasma with a volume of 2 cm³, is investigated by active and passive diagnostics. The study considers the influence of varying argon filling pressures between 10 and 100 mbar and different input powers between 50 and 125 W. The combination of the applied techniques of absolute line emission intensities, Thomson scattering and diode laser absorption measurements reveal the typical behavior in temperatures and electron density of the plasma. One of the observed characteristics is that by increasing the filling pressure the ring-shaped radial distribution of the electron density becomes more pronounced, while the electron temperature decreases over the whole radial profile. Furthermore, the influence of input power on the electron temperature and density depends strongly on the filling pressure. It is to be expected that insight in plasma processes and parameters for an argon filling will lead to a better understanding of future light sources as well.

1 Introduction

The use of electricity for lighting is a considerable part of the total energy consumption. Therefore, the development of light sources with a high efficacy is an important approach in reducing the energy consumption. One of the future light sources might be an inductively coupled high pressure plasma[1,2] (ICP). With this paper we report on a fundamental research carried out on a high pressure inductively coupled argon plasma in order to improve the understanding of this type of light source. Argon gas is used for the present study to get more insight in the characteristics of closed ICPs. This study is later to be extended to gas and vapour compound fillings more appropriate for light generation.

Several types of measurements are performed under different plasma conditions. The applied techniques are optical emission spectroscopy, Thomson scattering and diode laser absorption. These techniques[3] have recently been compared to each other for a study on an open and flowing ICP which is more suited for active spectroscopic techniques like Thomson scattering and diode laser absorption. Insight obtained by the comparison for the open ICP gives a strong basis for the optical emission spectroscopy on the closed ICP which is completely enclosed in a quartz vessel.

In this article we present a mapping of the plasma by measuring the electron density (n_e) and temperature (T_e) and the heavy particle temperature (T_h). The behavior of these parameters is obtained for different input powers and filling pressures. In the next section a description of this particular plasma setup is given. Section 3 is devoted to a discussion on the applied experimental diagnostics. The results and the discussion on properties of the closed ICP are presented in section 4.

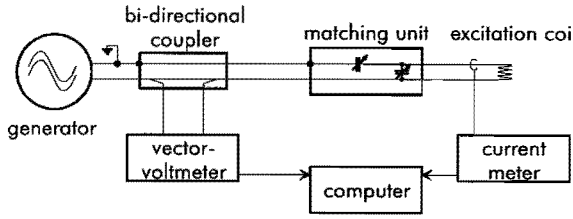

Figure 1. The experimental setup of the electronic devices controlling and feeding the primary coil.

2 Plasma setup

The plasma is created in a closed quartz vessel by means of the generation of inductive currents. The primary coil consisting of three windings is fed by a generator of 13.56 MHz. The matching network with two capacitors, between the generator and the coil, is adjusted for each power setting and for every filling pressure of the vessel, as depicted in figure 1. A computer controlled Vector-voltmeter (Rohde & Schwarz ZPV) and RF power meter (HP 438A with a HP 8481H power sensor) provide information to optimize the matching network and to calculate the effective input power. This is the generator power minus the power losses in the matching network and coil. The effective powers are varied from 50 to 125 W. Effective powers above the 125 W are avoided since the resulting high wall-temperatures would damage the quartz vessel.

The dimensions of the cylindrical vessel are an inner radius of 9 mm and an inner height of 8 mm. To enable spatially resolved measurements, the cylindrical vessel is provided with optical windows on the top and the bottom. A cross-section of the plasma is depicted in figure 2. The filling pressures are 10, 50 and 100 mbar of high purity argon. During operation the pressures are about a factor of ten higher due to the temperature increase.

3 Diagnostics

The ICP is studied using the following methods: 1) absolute line emission intensities (ALI), 2) line emission intensities during power interruption (LIPI), 3) Thomson scattering (TS) and 4) diode laser absorption (DLA). Not all these techniques are applicable under every plasma condition. The largest range of application is offered by ALI which measures the atomic state distribution function (ASDF). The other techniques will be used to support the ASDF method (there where possible).

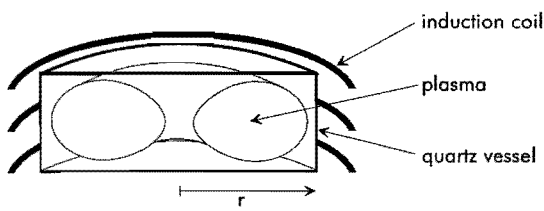

Figure 2. Cross section of the inductively coupled light source: the closed ICP.

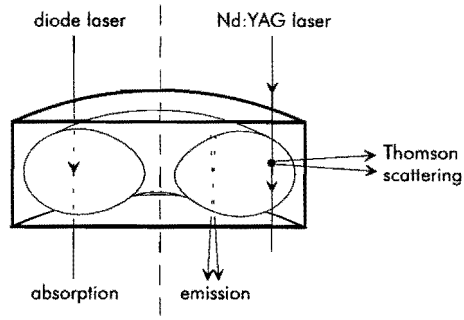

Figure 3. The closed ICP during the line emission experiments, the Thomson scattering and the diode laser absorption diagnostics.

3.1 Absolute line emission intensity measurements

The ALI measurements are performed using a 1 m monochromator in combination with a two-dimensional CCD-array.[3] This setup enables to measure emission lines with the adjacent continuum radiation simultaneously for all radial positions. It is calibrated by a ribbon band lamp. As depicted in figure 3, the measurements parallel to the axis of the discharge give the line-of-sight information. In the data handling is it assumed that the emission profile is flat along the line of sight over 6 mm and that appreciable gradients are only present close to the windows. As a consequence, the same applies to the final parameters n_e, T_e and T_h.

The intensity measurements of several emission lines together with their transition probabilities yield absolute values for the corresponding level densities $n(p)$. For levels in partial local Saha equilibrium (pLSE) ruled by the Saha balance of ionization and recombination, the density is given by the Saha[3,4] value ($n_e = n_i$):

$$\eta^S(p) = \frac{n^S(p)}{g(p)} = \frac{1}{2g_+} n_e^2 \frac{h^3}{(2\pi m_e k_B T_e)^{3/2}} e^{\frac{I_p}{k_B T_e}}. \qquad (1)$$

Here $g(p)$ and g_+ are the degeneracies of level p and the ion ground state and I_p is the ionization potential of level p, whereas the other symbols have their usual meaning. Thus the pLSE part of the ASDF can be used to calculate T_e from the slope in a Saha-Boltzmann plot (log $\eta(p)$ versus I_p plot) and n_e from the density η_∞ at the intersection at $I_p = 0$ assuming that $n_e = n_i$.

The presence of pLSE can be expected for highly excited states since approaching the ionization limit the effect of outward transport of radiation and charged particles can be neglected with respect to the increasing rate of ionization and recombination processes.

In figure 4 two Saha-Boltzmann plots are shown for two positions in the plasma of the 100 mbar argon filling vessel with 100 W input power. One of the positions presents the high density and temperature situation (r = 6 mm), the other shows the low density and temperature case (r = 0 mm). Note that both T_e and n_e are sensitive to variations in this slope, easily introduced by taking lower levels into account which are definitely not populated according to Saha. To establish which levels are populated according to Saha, the

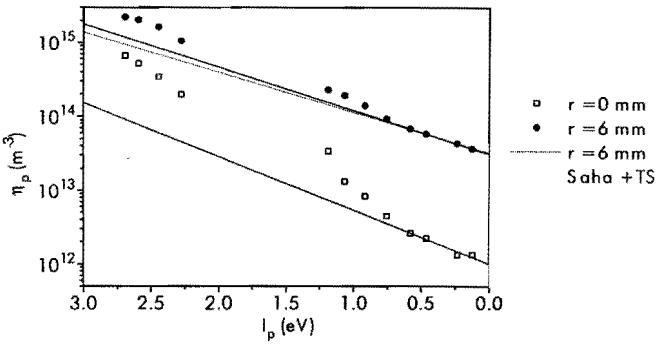

Figure 4. Saha-Boltzmann plot for two cases: a high and low density plasma condition. The measurements are obtained from a 100 mbar argon filling operated at 100 W effective input power. The straight lines are fits using the four highest levels in the system, the slope of the dashed line is obtained by TS. Note the agreement of this line with the ALI measurements.

following procedures can be used.

1) In a Saha-Boltzmann plot the levels in pLSE should be on a straight line and any deviation from this line can point towards a non-pLSE situation. Since the densities of the measured states are obtained using the corresponding transition probability, large uncertainties in these values would obscure the precise level densities and so the state of pLSE. Fortunately, recent efforts[5] led to better known transitions probabilities of 20% for transitions high in the electronic system. However, applying this procedure solely does not give a firm base in finding the precise pLSE part of the system and other means are needed to mark the transition from non-pLSE to pLSE more sharply.

2) An independent measurement can be provided via Thomson scattering giving the T_e-value and thus defining the pLSE slope. This approach is shown in figure 4 for the high density and temperature case (r = 6 mm) with T_e from TS and η_∞ from ALI. The plot demonstrates that under these plasma conditions only the four highest considered levels (with I_p < 0.8 eV) are indeed populated according to Saha; lower levels turn out to be overpopulated.

3) However, not under all conditions TS can be applied so that an additional method is needed to establish the state of pLSE more firmly. The method we use takes advantages of the knowledge of deviations from Saha as expressed by the factor

$$b(p) = \frac{\eta(p)}{\eta^S(p)}, \tag{2}$$

which for an ionizing collisional dominated plasma can be approximated by[6]

$$b(p) = b_0 p^{-6} + 1, \tag{3}$$

where p is the effective principal quantum number $p = \sqrt{Ry / I_p}$ (Ry = 13.6 eV) and b_0 is a boundary value. This expression can be rewritten using equation (2) and (3) as

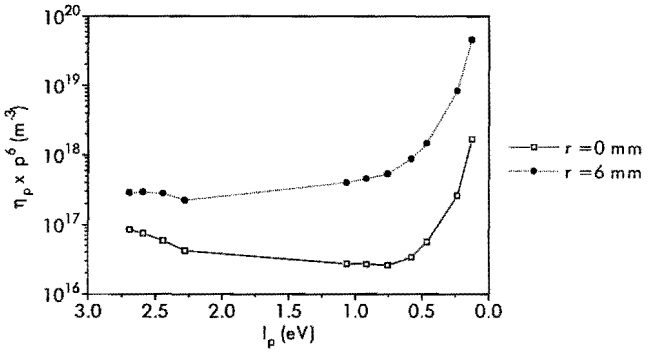

Figure 5. Example of using the criterion as given in equation (4) for finding the lower boundary of partial Local Saha Equilibrium. The conditions are similar to the ones of figure 4.

$$\eta(p)p^6 = b_0\eta^S(p) + \eta^S(p)p^6. \tag{4}$$

The behavior of $\eta(p)p^6$ as a function of p establishes the presence of pLSE. Low in the electronic system, thus for low p or high I_p values $\eta(p) >> \eta^S(p)$, and the second term at the r.h.s. of equation (4) can be neglected. Here, the approximative relation

$$\eta(p)p^6 \approx b_0\eta^S(p) \propto b_0 e^{I_p/k_B T_e} \tag{5}$$

holds, which represents a decreasing quantity as a function of p. For higher excited states where pLSE will be present, the behavior of the $\eta(p)p^6$ function is determined by the second term of the r.h.s. of equation (4) which is a strong increasing function of p. The ionization potential I_p for which the contribution of this second term becomes important will be used as the lower limit of the pLSE region. To illustrate this procedure $\eta(p)p^6$ is plotted as a function of I_p in figure 5 for the same conditions as in figure 4. The behavior is as expected: for higher I_p values $\eta(p)p^6$ is decreasing and closer to the continuum, at about 0.8 eV, we see that the weak decline transforms into a strong increase. This leads to the conclusion that for $0.8 < I_p < 0$ eV the levels are in pLSE at $r = 6$ mm, so that the four highest considered levels can be safely used for estimating n_e and T_e under these conditions. Even for the lower density case at $r = 0$ mm ($n_e \approx 10^{20}$ m^{-3}) we see that for the lowest of the four considered levels at $I_p = 0.58$ eV the presence of state of pLSE is also a reasonable assumption.

Concluding we may state that the four levels 8d (506.0 nm), 7s (588.9 nm), 5d' (518.8 nm) and 7d' (531.8 nm) can be assumed to belong to the pLSE ASDF. It is found that the error in n_e and T_e using the ASDF method is about 15%.

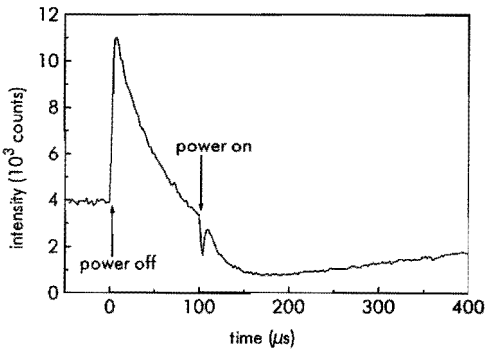

Figure 6. The response of the 588.9 nm argon line to the power interruption for the closed ICP with a 100 mbar filling and operated at 100 W. Note that the level of power increases slowly when the power is switched on, a property of the generator.

3.2 Line emission intensities during power interruption

The method of line emission intensities can be extended with the power interruption technique.[7,8] For these power interruption experiments we use a photomultiplier in combination with a multi channel scaler[3] in order to obtain time resolved information of the line intensities. The instantaneous removal of the EM field will induce a jump in intensity shown in figure 6, which is caused by a sudden cooling of the electron gas $\{e\}$, that is a change of T_e towards a lower value T_e^*. Since the measured intensities are proportional to the level density $n(p)$ (the transitions are optically open), the ratio before and just after cooling is described by the ratio of the Saha equation (1) for T_e and the Saha equation for T_e^*, giving

$$\ln\left(\frac{\eta^S(p)^*}{\eta^S(p)}\right)=\frac{\gamma^*-1}{k_B T_e}I_p+\frac{3}{2}\ln\gamma^*, \qquad (6)$$

with $\gamma^* = T_e/T_e^*$. For this expression we assume that the observed levels before and immediately after cooling are in pLSE and that during the cooling period (typically 5 μs) n_e does not change. Extrapolation of the cooling jumps of highly excited states towards $I_p = 0$ (figure 7) and using equation (6) gives γ^*. Note that the restrictions concerning the state of pLSE for ALI also apply for this power interruption method.

It should be realized that after the removal of the power the internal energy of excited atoms and ions will be partially converted into kinetic energy of the electron gas. So that recombination and deexcitation processes will create a heating source of $\{e\}$ with as a result that (T_e^*) will stay larger than heavy particle temperature T_h.

Therefore, the method of power interruption for determining the heavy particle temperature should be applied with care. In combination with the T_e-value obtained by ALI, only an upper limit of T_h can be obtained.

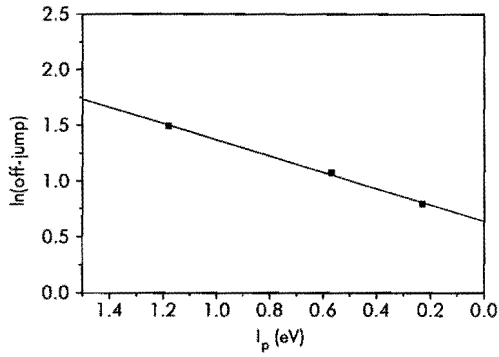

Figure 7. The jump in intensity proportional to the jump in level density depicted for 3 levels as a function ionization potential, the plasma conditions are equal to those of figure 6. Note that the level at I_p = 1.2 eV is not in the pLSE region as established in section 3.1.

3.3 Thomson scattering

Thomson scattering is used to determine T_e, which can be deduced from the Doppler broadened spectrum. The total scattered number of photons can be used to calculate n_e after calibration, but this is not done in the present work. The beam of the 10 Hz pulsed Nd:YAG laser enters and leaves the plasma through the flat windows (see figure 3). The scattered light is detected under 90 degree with the laser beam. Observations were done in between the windings of the coil by a monochromator equipped with a one-dimensional intensified photo diode array.[9]

Applying the TS on a plasma of small dimensions surrounded by quartz walls at high wall temperatures induces high levels of stray light which dominate the TS-signal. This effect can be reduced by a factor of 2 using a polarization filter in the detection branch, taking advantage of the fact that the Thomson scattered signal is polarized whereas stray light is not. A second manner to decrease the stray light level is lowering the detection solid angle, which can be achieved by using two extra diaphragms in the detection branch. However, these efforts do not lower the stray light sufficiently. Therefore, measurements are performed with plasma on and plasma off and with blocking the central channels of the array. This in order to prevent the detector from blooming caused by the intense Rayleigh scattering and stray light. The difference in intensity of these two measurements is attributed to Thomson scattering.

Using a polarization filter, a narrow solid angle and the on-off method, it is possible to obtain an electron temperature for the highest n_e-value condition. The highest n_e is obtained for the 100 mbar filling at high power (100 W) and at the radial position of the density maximum $r \approx 6$ mm. A single measurement takes about 30 minutes. For the fit an estimation for n_e is required in order to determine the importance of collective scattering. This n_e (8.2×10^{20} m^{-3}) is taken from ALI measurements. It should be noted that for the assessment of the collective behavior a rough n_e-value is sufficient since variations in n_e of 25% do not effect T_e more than with 1%. The result is shown in figure 8 with a fit of a

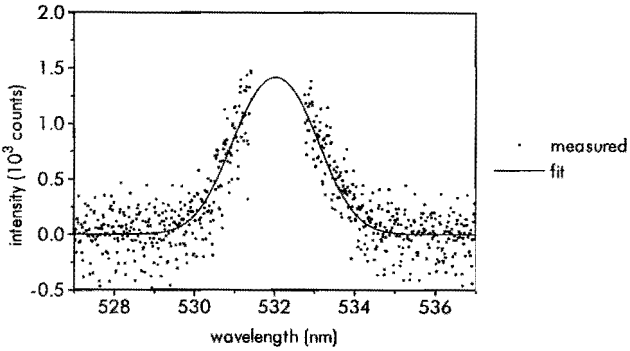

Figure 8. The Thomson scattering wavelength profile measured at r = 6 mm on the 100 mbar 100 W closed ICP. The measurement is fitted with a gauss corrected for collective scattering giving a corresponding electron temperature of 9300 ± 600 K.

Gaussian profile corrected for collective scattering, leading to a T_e-value of 9300 ± 600 K. Other positions and lower powers turn out to have too low electron densities and temperatures to obtain accurate T_e-values. Nevertheless, TS provides a reference value of T_e, which can be used to calibrate the ASDF method.

3.4 Diode laser absorption

Finally we discuss the diode laser absorption technique. This technique can be used to measure 4s-level densities, heavy particle temperatures and electron densities. A current and temperature controlled diode laser system with a wavelength corresponding to the 4s $^3P_2$ - 4p $^3D_3$ transition in argon (811.531 nm) is applied to measure the absorption profile. By changing the current through the laser, the wavelength changes slightly with 0.3 pm per step. The absorption profile is broadened by a Gaussian shaped Doppler effect and a Lorentzian shaped Stark effect. The two components can be obtained by fitting the profile with a Voigt profile and can be used to calculate the T_h (Doppler) and n_e (Stark).
However, a recent study[10] proved that the method of determining n_e by DLA in atmospheric plasmas is difficult because of the strong presence of van der Waals broadening which equals, or even exceeds the contribution of Stark broadening. Note that both profiles have a Lorentzian shape which implies that they can not be distinguished from each other. Therefore, good values for n_e by diode laser absorption can only be obtained for conditions with negligible van der Waals broadening, e.g. low filling pressures at 10 mbar. There is an additional experimental difficulty. Due to the heating of the vessel windows, the distance between the windows varies in time. This causes a changing interference of the diode laser beam, affecting the stability of the measured absorption signal. For the higher filling pressures the windows are hotter, so more pliable. Because of this complication we have limited our experiments to the low filling pressure of 10 mbar.

The applicability of the described techniques for the different plasma conditions is shown in table 1.

filling pressure	n_e	T_e	T_h	T_e^*
10 mbar	ALI, DLA	ALI	DLA	LIPI + ALI
50 mbar	ALI	ALI	-	LIPI + ALI
100 mbar	ALI	ALI, TS	-	LIPI + ALI

Table 1. The applicability of the available diagnostics for the different plasma conditions; ALI absolute line emission intensities, LIPI line emission intensities during power interruption, TS Thomson scattering and DLA diode laser absorption.

4 Results and discussion

In the discussion of the measurements on the closed ICP we will discern two aspects, the influence of the filling pressure and the influence of the input power on n_e, T_e and T_h. At the same time the different applied techniques are discussed. Most of the information is obtained from ALI measurements. The other techniques are used to give support.

4.1 The influence of filling pressure

Figure 9 shows the behavior of the radial n_e profile in response to an increasing filling pressure at a constant power of 100 W. Most of the information is obtained by ALI whereas an additional set of DLA measurements on the 10 mbar filling is given as well. A comparison of the two diagnostics shows a systematic difference of about 15% which can be due to inaccuracies of the measurements. However, this might also indicate that Van der Waals broadening is still present in the 10 mbar filling vessel. Since in these measurements all the Lorentzian broadening is attributed to the Stark effects, this will result in a slightly overestimated n_e by DLA as depicted in figure 9.

Both methods reveal that the radial n_e profile is flat for the 10 mbar filling pressure which is in contrast with the 100 mbar case and can not be explained by the difference in energy coupling region. The skin depth $\delta = \sqrt{2/\mu_0\sigma\omega}$, with ω the frequency of the EM field, depends on the electrical conductivity[11] σ which increases with the electron temperature. Therefore, σ decreases under increasing filling pressure from $\sigma = 4.3 \times 10^3\ \Omega^{-1}m^{-1}$ (10 mbar,

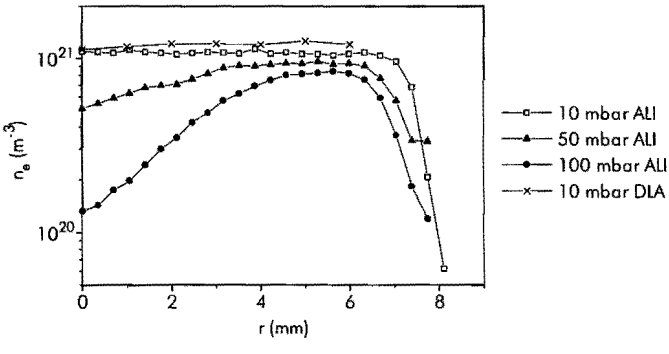

Figure 9. The influence of filling pressure on the electron density as a function of radius as obtained by ALI and DLA experiments for an input power of 100 W.

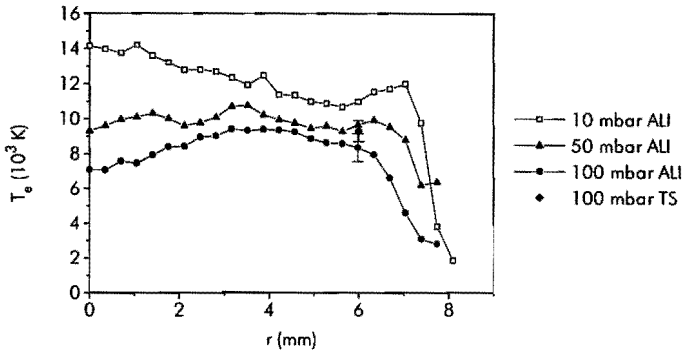

Figure 10. The influence of filling pressure on the electron temperature as a function of radius as obtained by ALI and TS experiments for an input power of 100 W.

12 000 K) towards $\sigma = 1.5 \times 10^3\ \Omega^{-1}m^{-1}$ (100 mbar, 9000 K) and thus the skin depth increases for increasing filling pressure from 2.1 mm (10 mbar) towards 3.5 mm (100 mbar). The fact that the n_e profile is flatter in the 10 mbar case instead of more peaked can be explained by the influence of diffusion. At a lower background pressure the diffusion coefficient is larger so that potential n_e differences as created by a more located energy coupling region (small δ) are leveled out more easily. Therefore, at the low filling pressure of 10 mbar the plasma is more like a homogeneous glow, while at high filling pressure the plasma has a torodial shape since the higher neutral density apparently obstructs the diffusion of electrons towards the central region and so the effect of limited skin depth becomes more dominant. Remember that the actual pressure during operation is typically 10 to 20 times the filling pressure.

The pressure dependence of T_e is different. In figure 10 we see that there is not much difference in shape of the radial T_e profiles for the different pressures. So, in contrast to n_e, the shape of the radial T_e profile is for all the filling pressures more or less flat. The pressure dependence of T_e can only be found in the magnitude of T_e. For increasing filling pressure

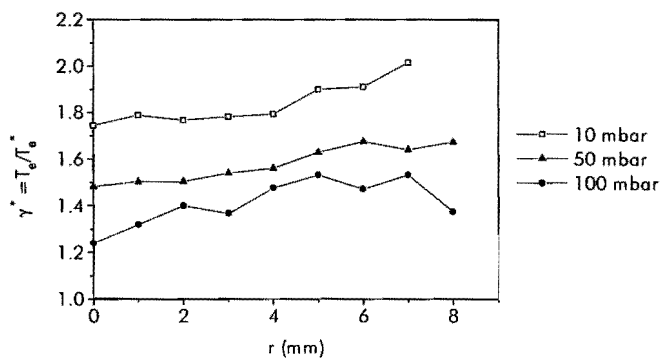

Figure 11. As a function of radius the ratio T_e/T_e^* obtained by LIPI experiments for three different filling pressures operated at 100 W input power.

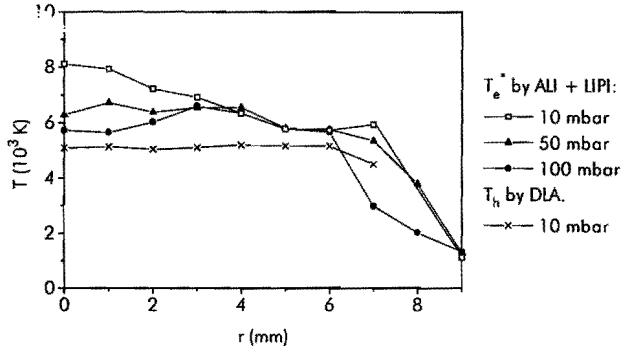

Figure 12. Heavy particle temperatures as a function of radius obtained by DLA and ALI in combination with LIPI. The input power is 100 W for all filling pressures. The temperatures at r = 9 mm are measured using an IR-pyrometer with an accuracy of 100 K.

we find a decreasing T_e-value, which can be explained by a better coupling of the electrons with the heavy particles at high pressures. This better energy transfer reduces the temperature difference between the electrons and heavy particles by lowering T_e towards T_h.
The better energy coupling is also illustrated by the power interruption experiment. LIPI gives γ^*, the ratio of the stationary electron temperature T_e and the electron temperature during the power interruption T_e^* (cf. equation (6)). The γ^* values are depicted in figure 11 as a function of radius for the three filling pressures. As previously mentioned, T_e^* might be different from T_h. Therefore, this method of measuring the ratio T_e/T_e^* is only a first estimate for T_e/T_h and the deviation of T_e^* from T_h could be as high as 40%. Nevertheless, the tendency that T_e/T_h decreases as a function of filling pressure as found in figure 11 is real and to be expected.
Using ALI together with LIPI, the radial T_h profile can be obtained, see figure 12. The difference between the results of these emission measurements (ALI and LIPI) and T_h obtained by diode laser absorption shows that for the 10 mbar vessel the γ^* obtained by LIPI indeed gives on overestimation of T_h. Nevertheless, it is still instructive to use the LIPI method for estimating upper limits of the heavy particle temperature and it is expected that a decreasing T_h for increasing filling pressures as found in figure 12 is indeed realistic.
Using an IR-pyrometer the wall temperature of the vessels is measured and depicted in figure 12. The value is accurate within 100 K.

4.2 The influence of power

The influence of power on the radial n_e and T_e distributions has been studied for the filling pressures of 10, 50 and 100 mbar. We will only present the results of the 10 and 100 mbar vessels since the behavior of the 50 mbar vessel as a function of power turns out to be in between the two extremities of 10 and 100 mbar.
Figure 13 gives the radial n_e profiles for the 100 mbar case as a function of power. These are obtained by ALI. The general behavior is as expected, an increasing density in response

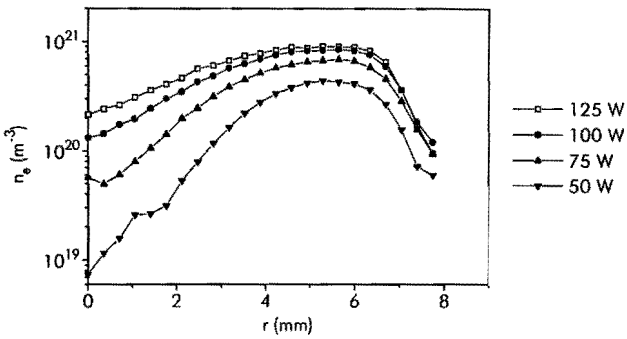

Figure 13. The electron density as a function of radius and input power measured by ALI experiments on the 100 mbar argon filling.

to an increasing input power P. However, apart from the magnitude also the radial distribution of the electrons changes. At low P-values the profile is hollow whereas for higher input powers the plasma tends to level out the differences in density between the center and the active zone.

A similar behavior is found in T_e, as is shown in figure 14. Here, for low powers the temperature in the center at $r = 0$ mm is about 3000 K increasing for higher powers up to 8000 K, while the maximum temperature, at about $r = 6$ mm, does hardly change. At this maximum power of 125 W, the T_e-profile is almost flat. Apparently, the increasing power is mainly used for ionization, the production of electrons, and less for heating the electrons. The T_e-value as obtained by Thomson scattering is also depicted in figure 14 and shows that for this particular plasma position and condition the method of ALI is in agreement with TS.

In general, it should be mentioned that with respect to the T_e- and n_e-values this 100 mbar filling pressure with argon is very much alike the open flowing argon ICP.[9] This is not surprising, since the operation pressure is comparable to that of the atmospheric flowing

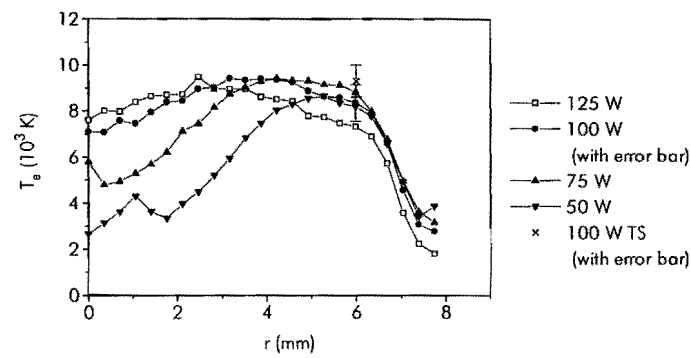

Figure 14. The electron temperature as a function of radius and input power measured by ALI and TS experiments on the 100 mbar argon filling.

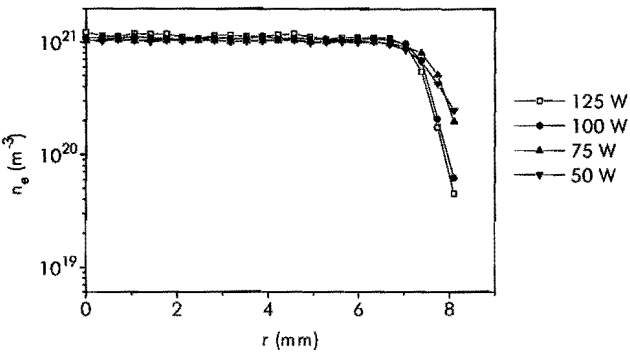

Figure 15. The radial electron density profile as a function of input power measured by ALI on the 10 mbar filling.

ICP. However, there are also large differences. The main energy loss process in the open flowing ICP is the transport of hot gas out of the plasma whereas the energy losses of the closed ICP configuration are dominated by heat conduction losses. This is also reflected in the fact that much higher effective input powers are typical for the open ICP (± 0.6 kW) than for the closed ICP (± 0.1 kW) to sustain a plasma of similar n_e and T_e-values.
The influence of power for the 10 mbar filling vessel is considerably different from that for the 100 mbar case. Figure 15 shows that increasing the power does hardly lead to higher electron densities and does certainly not affect the radial shape as we found in the 100 mbar vessel. Also the shape of the T_e *profile* is not sensitive to power, but the *magnitude* of T_e decreases under increasing power conditions (see figure 16). Again a striking difference with the 100 mbar vessel where the averaged T_e increases for higher powers. The obtained heavy particle temperatures with DLA are depicted in figure 17, where it is found that T_h increases with power, as expected. Note that no measurements are available for $r > 7$ mm. This is due to refraction of the laser beam on the edges of the vessel.
The fact that for increasing input power 1) n_e stays more or less constant, 2) T_e decreases

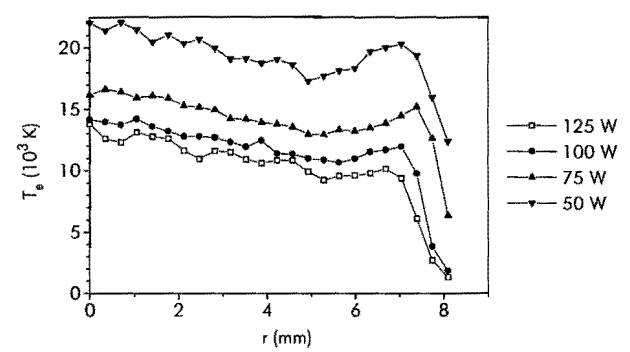

Figure 16. The electron temperature as a function of radius and input power measured by line emission measurements on the 10 mbar filling.

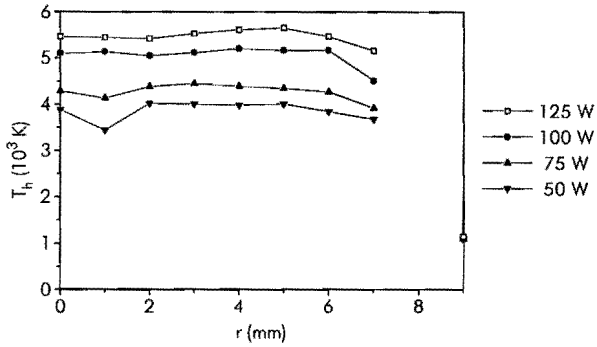

Figure 17. Heavy particle temperature for several input powers as a function of radius for the 10 mbar argon filling. T_h is obtained by DLA. The temperature at r = 9 mm is measured using an IR-pyrometer having an accuracy of 100 K.

and 3) T_h increases shows that the increasing power is completely used to heat the heavy particles, which will lead to an increasing pressure in the closed vessel. This higher actual pressure allows the plasma to be sustained at a lower T_e. It is also found that in this 10 mbar case the increase of power hardly leads to a higher emissivity of the plasma.

5 Conclusions

For the investigation of a closed inductively coupled argon plasma with pressures close to atmospheric conditions absolute line emission measurements are powerful in measuring the electron temperature and density. At lower filling pressures the diode laser absorption technique becomes also profitable, providing the heavy particle temperature. Deploying Thomson scattering has shown to be an option only for high electron density and temperature situations where the Thomson signal is significantly present compared to the stray light signal. The behavior of the closed ICP with a filling pressure of 100 mbar shows that the hollow structure of the electron temperature disappears for increasing input powers, whereas the 10 mbar vessel gives for any investigated power a flat radial electron temperature profile. This flat electron temperature plateau decreases for increasing powers due to an increase in heavy particle temperature and actual pressure. The electron density in the 100 mbar vessel increases with input power as expected, but is independent on the power in the 10 mbar vessel. For decreasing filling pressure, the radial electron density profile becomes rather flat instead of strongly peaked at the edge, while the top values stay in the same order of magnitude. On the other hand, the influence on the shape of the electron temperature profile is weak, but the magnitude of the electron temperature increases if the filling pressure is reduced.

[1] M.E. Duffy, J.T. Dakin, G.E. Guffy and M.M. Secen, "Diagnostics and Model of an Inductive HID Hg Discharge", 6th Intern. Symp. on the Science and Technology of Light Sources, Budapest, 1992.
[2] D. Hollister, M. Neiger and S. Berman, "Operation of low wattage electrodeless HID lamps", 5th Intern. Symp. on the Science and Technology of Light Sources, York, 1989.
[3] J.M. de Regt, F.P.J. de Groote, J.A.M. van der Mullen and D.C. Schram, "Comparison of active and passive spectroscopic methods to investigate atmospheric plasmas", to be published, 1995. (Chapter 7)
[4] J.A.M. van der Mullen, S. Nowak, A.C.A.P. van Lammeren, D.C. Schram and B. van der Sijde, "Non equilibrium characterization and spectroscopic analysis of an inductively coupled argon plasma", Spectrochimica Acta **43B** (317), 1988.
[5] J.M. de Regt, R.D. Tas, J.A.M. van der Mullen and D.C. Schram, "Determination of transition probabilities for argon using Thomson scattering experiments on an inductively coupled plasma", to be published. (Chapter 6)
[6] J.A.M. van der Mullen, "Excitation equilibria in plasmas; a classification", Physics Reports **191** (109), 1990.
[7] E.L. Bydder and G.P. Miller, "Excitation and kinetic equilibria in an argon inductively coupled plasma torch-I. Coolant flow only", Spectrochim. Acta **44B** (165), 1988.
[8] F.H.A.G. Fey, W.W. Stoffels, J.A.M. van der Mullen, B. van der Sijde and D.C. Schram, "Instantaneous and delayed responses of line intensities to interruption of the RF power in an argon inductively coupled plasma", Spectrochimica Acta **47B** (885), 1991.
[9] J.M. de Regt, R.A.H. Engeln, F.P.J. de Groote, J.A.M. van der Mullen and D.C. Schram, "Thomson scattering experiments on a 100 MHz inductively coupled plasma calibrated by Raman scattering", Rev. Sci. Instrum. **66** (3228), 1995. (Chapter 3)
[10] J.M. de Regt, R.D. Tas and J.A.M. van der Mullen, "Characterization of a 100 MHz inductively coupled argon plasma by diode laser absorption", Journal of Physics D: Applied Physics, submitted for publication, 1995. (Chapter 5)
[11] R. Rhodes and D. Keefer, "Numerical modeling of a radio frequency plasma in argon", AIAA Journal **27** (1779), 1989.

Chapter 11

General conclusions

The present work reports on the application of various accurate techniques in order to investigate atmospheric inductively coupled plasmas. An extensive comparison of these techniques proved to benefit the optimization of these diagnostics and, at the same time, proved to provide a strong basis for the characterization of this kind of plasmas. This results in a consistent picture of the dynamics of the (sub)atmospheric argon plasmas created by inductively coupling. Conclusions in more detail are listed below.

- The power interruption technique can successfully be applied in order to determine the different mechanisms which are responsible for continuum radiation. In the investigated open ICP electron-ion as well as electron-atom interactions contribute significantly to the continuum radiation at moderate powers. However, for higher powers the electron-ion interactions become dominant.
  (Chapter 2)

- The rotational Raman scattering spectrum of nitrogen can be used to calibrate the Thomson scattering setup. This Raman calibration method has the advantages of being fast and stray light independent.
  (Chapter 3)

- Diode laser absorption spectroscopy provides information on heavy particle temperatures and 4s-level densities. However, electron density determination is more difficult due to the presence of an additional pressure broadening effect: Van der Waals broadening. By Van der Waals broadening the Lorentz part of the argon line profiles increases in width towards the edge of the plasma.
  (Chapter 5)

- Thomson scattering in combination with absolute line emission intensity measurements can be used to determine the transition probabilities of transitions high in the excitation space of argon with accuracies better than 20%.
  (Chapter 6)

- Both Thomson scattering and absolute line emission intensities can be used to determine the electron density and temperature profiles in the plasma. Concerning the electron density Thomson scattering proves to be also accurate in the plasma center, since Thomson scattering measures locally. The line intensity measurements have to be Abel-inverted and are therefore inaccurate in the center because of the hollow density and temperature profile. On the other hand, at the edge of the plasma, Thomson scattering overestimates the electron density due to the presence of another scattering process: Raman scattering on nitrogen and oxygen, present in the plasma by the entrainment of air.
  (Chapter 7 & 8)

- During power interruption, the electron density is found to increase in the plasma center, which can be explained by inward diffusion which exceeds the local three particle recombination processes. The presence of nitrogen at the edge of the plasma might be responsible for the anomalously large decay in electron density in this region by the mechanism of charge exchange subsequently followed by molecular recombination via the nitrogen molecular ion. A second explanation of the large decay at the edge can be the formation of molecular argon ions in combination with recombination.
  (Chapter 3, 4, 8 & 9)

- During power interruption, the electron temperature stays at higher values than the heavy particle temperature. Energy from three particle recombination can heat the electrons to temperatures of about 1500 K above the heavy particle temperature. At the same time, heat conduction levels out the gradients in the electron temperature.
  (Chapter 3, 4, 7 & 9)

- An atmospheric closed ICP can be investigated using the methods of diode laser absorption, Thomson scattering and absolute line emission intensities. It is observed that by increasing the filling pressure the ring-shaped radial distribution of the electron density becomes more pronounced, while the electron temperature decreases over the whole radial profile. Furthermore, the influence of input power on the electron temperature and density depends strongly on the filling pressure.
  (Chapter 10)

We may state that this study has given more insight into the shape of the plasma, especially the shape of the radial electron density profile, and that a qualitative explanation for the origin of these profiles is within reach. However, in particular at the edge of the plasma, the numerical models are not yet able to describe quantatively the basic plasma parameters and therefore more information on elementary processes is needed. This is important since the behavior at the edge is strongly connected with the confinement of the plasma in a quartz torch or closed vessel without affecting the wall. This latter is required for high purities and long lifetimes. Furthermore, the investigations in the behavior at the edge, the boundary between plasma and cold gas, may also provide insight in mechanisms which are important to understand the energy housekeeping and the aspects contributing to the plasma stability and to understand the evaporation processes of material introduced along the central axis of the ICP.

Summary

Inductively coupled plasmas (ICPs) are widely used for spectrochemical analysis and might be used in the future as light sources. Increasing the knowledge on the fundamental behavior of the ICP could improve their applicability. For this objective, information on the plasma parameters is indispensable. This research project deals with the study of this type of plasma and can be divided in three objectives. First the development of several diagnostics which are optimized for investigations of the open flowing inductively coupled plasma and second, the research for the fundamental properties of this plasma. The third aspect is the investigation of a closed ICP configuration, a feasible light source with high efficacy. In the present study, research is performed on pure argon plasmas.

The developed and implemented active diagnostics are Thomson and Rayleigh scattering and diode laser absorption spectroscopy.

The advanced Thomson and Rayleigh scattering setup provides local values of the plasma parameters, like the electron density and temperature, and the heavy particle temperature. For the absolute calibration of the setup a new procedure is introduced: Raman scattering on nitrogen. The heavy particle temperature is measured in two manners using Rayleigh scattering and using diode laser absorption. The diode laser absorption diagnostic can be used, in principle, to measure electron densities, heavy particle temperatures, and level densities of excited states. The latter is used to study non-LTE effects. In high pressure circumstances, diode laser absorption shows the presence of Van der Waals broadening, making the argon line profiles broader towards the edge of the plasma.

Supplementary, passive optical emission experiments are carried out. H_β-broadening showed to be useful to determine the electron density and absolute line emission experiments to determine the electron temperature and density. Both methods are performed using the new developed and convenient technique with a 2-dimensional CCD-array in the focal plane of a spectrograph. This new setup allows an accurate determination of transition probabilities of 15 highly excited states, increasing the accuracy of the line emission experiments.

The method of time resolved emission registration during the power interruption is verified by Thomson scattering experiments and is deployed for determining the electron temperature during power interruption. These measurements show that while the power is interrupted the electrons stay at significantly higher temperatures than the heavy particles. These higher temperatures can be explained by three particle recombination being the energy source for the electrons. Besides this, the determination of continuum radiation during power interruption shows that under standard conditions of the plasma electron-atom interactions are just as important as electron-ion collisions.

The more detailed study of Thomson scattering during power interruption shows that after the power switch off the electron density in the center of the plasma increases. A time dependent simulation proves that diffusion is responsible for this increase. At the same time, the electron density decreases faster at the edge of the plasma than that what is calculated with the simulation. The presence of molecular nitrogen or molecular argon ions

could be responsible for this effect by offering molecular recombination channels. Raman scattering measurements show that relative high densities of nitrogen are present at the edge of the plasma by the entrainment of air.
The closed ICP[1] is investigated using the techniques mentioned above applied for several filling pressures and input powers. This provides radial dependent information on temperatures and densities. The radial dependence of the electron temperature on the input power is strong for the high pressure filling but weak for the low pressure filling. The input power has a large effect on the electron density for the 100 mbar filling, but has hardly any effect on the electron densities for the 10 mbar filling. This research on the closed ICP is a step forward in the understanding of this kind of plasmas and in improving the applicability of it.

Hans de Regt, December 1995.

[1] The research on the closed ICP configuration has been done in cooperation with Philips Forschungslaboratorien Aachen (Germany) and Philips Lighting Eindhoven (The Netherlands).

Samenvatting

Inductief gekoppelde plasma's (ICP's) worden wereldwijd toegepast voor spectrochemische analyse en worden mogelijk in de toekomst inzetbaar als lichtbronnen. Uitbreiding van de kennis over de fundamentele eigenschappen van ICP's kan de toepasbaarheid verbeteren en vergroten. Hiervoor is informatie over de plasmaparameters onmisbaar. Dit onderzoeksproject is een studie naar dit type plasma's en beoogt daarbij drie doelen. Als eerste de ontwikkeling van verschillende diagnostieken welke zijn geoptimaliseerd voor onderzoek aan het open, stromend ICP en als tweede de studie naar de fundamentele eigenschappen van dit plasma. Het derde aspect is het onderzoek naar een gesloten ICP-configuratie welke wellicht in de toekomst uitgroeit tot een energie-zuinige lichtbron. In dit werk zijn argonplasma's onderzocht.

De ontwikkelde en geïmplementeerde actieve diagnostieken zijn Thomson- en Rayleighverstrooiing en laserdiode absorptie-spectroscopie. Deze geavanceerde Thomson- en Rayleighdiagnostiek levert lokale waarden voor de elektonendichtheid en -temperatuur en de zware-deeltjestemperatuur. Voor het kalibreren van deze opstelling is een nieuwe methode geïntroduceerd, namelijk Ramanverstrooiing aan stikstof. De zware-deeltjestemperatuur is gemeten op twee manieren, gebruikmakende van Rayleighverstrooiing en van laserdiode absorptie. De laserdiode absorptiediagnostiek kan ook worden ingezet voor de bepaling van niveau-dichtheden welke noodzakelijk zijn voor een studie naar evenwichtsafwijkingen. Daarnaast toont deze diagnostiek aan dat Van-der-Waals-verbreding een belangrijk mechanisme is in atmosferische argonplasma's.

Naast deze actieve zijn ook een aantal passieve technieken gebruikt, zoals H_β-verbreding voor de bepaling van de elektronendichtheid en absolute lijnintensiteiten voor de bepaling van elektronendichtheid en -temperatuur. Beide technieken maken gebruik van een nieuw ontwikkelde en handige techniek die gebaseerd is op een twee-dimensionaal CCD-array geplaatst in het focus van een spectrograaf. Deze nieuwe opstelling heeft ook een nauwkeurige bepaling van 15 overgangswaarschijnlijkheden van hoog geëxciteerde argonniveaus mogelijk gemaakt. Hierdoor is de techniek van absolute lijnintensiteiten aanzienlijk nauwkeuriger geworden.

De methode van tijdopgeloste lijnemissiemeting gedurende de vermogensinterruptie is gecontroleerd met Thomsonverstrooiing experimenten en is gebruikt voor de bepaling van de temperatuur van de elektronen tijdens de vermogensinterruptie. Deze metingen laten zien dat gedurende deze periode de temperatuur van de elektronen hoger is dan de temperatuur van de zware deeltjes. Dit temperatuurverschil kan worden verklaard met drie-deeltjesrecombinatie hetgeen energie levert aan de elektronen. Daarnaast is met het meten van continuümstraling gedurende de vermogensinterruptie bepaald dat onder standaardcondities van het plasma elektron-atoominteracties ongeveer even belangrijk zijn als elektron-ionbotsingen.

De meer gedetailleerde studie van Thomsonverstrooiing tijdens vermogensinterruptie laat zien dat nadat het vermogen is uitgeschakeld de elektronendichtheid in het centrum van het plasma stijgt. Een tijdafhankelijke simulatie toont aan dat diffusie hiervoor verant-

woordelijk moet zijn. Tevens is gevonden dat de elektronendichtheid aan de rand van het plasma sneller daalt dan wat de simulatie laat zien. De aanwezigheid van moleculaire stikstof of moleculaire argonionen is mogelijk de oorzaak van dit snelle verval doordat zij extra, moleculaire, recombinatiekanalen biedt. Raman-verstrooiingsmetingen laten dan ook relatief hoge stikstofdichtheden zien aan de rand van het plasma door het meezuigen van de omringende lucht.
Het gesloten ICP[i] is onderzocht met behulp van bovengenoemde technieken voor verschillende vuldrukken en vermogens. Dit heeft radiaal afhankelijke informatie over temperaturen en dichtheden opgeleverd. De radiale afhankelijkheid van de elektronentemperatuur als functie van het vermogen is sterk voor de hoge vuldruk maar zwak voor de lage. Het vermogen heeft een groot effect op de elektronendichtheid in de 100 mbar vulling, maar heeft juist nauwelijks invloed op de elektronendichtheden in de 10 mbar vulling. Daarmee is het onderzoek aan het gesloten ICP een stap voorwaarts om dit soort plasma's beter te begrijpen en daarmee de toepassing ervan te verbeteren.

Hans de Regt, december 1995.

[i] Het onderzoek aan de gesloten ICP-configuratie is uitgevoerd in samenwerking met Philips Forschungslaboratorien Aachen (Duitsland) en Philips Lighting Eindhoven.

Abbreviations

a	atom
ADC	analogue digital converter
ALC	above load coil
ALI	absolute line emission intensities
ASDF	atomic state distribution function
DLA	diode laser absorption
e	electron
fb	free-bound
ff	free-free
FWHM	full width at half maximum
h	heavy particle
HB	H_β broadening
i	ion
ICP	inductively coupled plasma
LA	light intensifier
LIPI	line emission intensities during power interruption
LTE	local thermodynamic equilibrium
MCS	multi channel scaler
ND	neutral density
OMA	optical multichannel array
PD	photo diode
PI	power interruption
pLSE	partial local Saha equilibrium
PM(T)	photomultiplier (tube)
RnS	Raman scattering
RS	Rayleigh scattering
TS	Thomson scattering
TSPI	Thomson scattering during power interruption
VDD	variable delay device

T_x (T_x^*)	temperature of particle x (during power interruption)
n_x	density of particle x
γ (γ^*)	ratio of T_e/T_h (T_e/T_e^*) (not in chapter 5)
γ	broadening coefficient (only in chapter 5)
ν_x	decay frequency during power interruption of the density of particle x
α	degree of ionization
Λ	gradient length
ε	emission coefficient
χ	contribution to continuum radiation by ff-ea interactions over the total

Stellingen

behorende bij het proefschrift

Fundamentals of inductively coupled argon plasmas

a spectroscopic study

door

J.M. de Regt

28 februari 1996

I

Het drie-deeltjes-recombinatieproces zorgt in een afterglow situatie voor significante verhitting van het elektrongas.
(dit proefschrift)

II

Om meer inzicht te krijgen in de eigenschappen van plasmalampen moeten ook plasma's bestudeerd worden die weinig licht geven.
(dit proefschrift)

III

Voor een realistische numerieke simulatie van atmosferische plasma's is het erin opnemen van moleculaire processen aan de rand van het plasma noodzakelijk.
(dit proefschrift)

IV

Het feit dat tijdens vermogensinterruptie van het ICP de elektronentemperatuur niet gelijk wordt aan de temperatuur van de zware deeltjes, maakt een heroverweging van eerdere publikaties betreffende dit onderwerp noodzakelijk.
(F.H.A.G. Fey *et al.*, Spectrochim. Acta **46B** (885), 1991)

V

De aanname dat bij atmosferische argon-ICP's alleen Starkverbreding bijdraagt aan de Lorentzverbreding van het 4s-niveau en dat daarmee de breedte van het Lorentzprofiel afneemt naar de rand van het plasma is onjuist.
(D.S. Baer en R.K. Hanson, J. Quant. Radiat. Transfer **47** (455), 1991)

VI

De toepassing van verschillende meettechnieken voor het bepalen van eenzelfde parameter leidt zowel tot optimalisatie van deze technieken als tot een breder fysisch inzicht.

VII

De mogelijkheden die laserdiode-absorptie en Ramanverstrooiing als plasmadiagnostiek bieden worden tot op heden onvoldoende benut.

VIII

Om te komen tot minder milieubelastend goederentransport, moet het gebruik van de trein voor lange-afstandstransport worden gestimuleerd door het goederenvervoer over de weg zwaarder te belasten.

IX

De grote impact die meerschermen diapresentaties hebben, wordt hoofdzakelijk veroorzaakt door de stilstaande beelden waaruit deze presentaties zijn opgebouwd, hetgeen confronterender is dan de bewegende beelden bij film en televisie.

X

Het veelvuldig gebruik van het woord "absoluut" als antwoord op een vraag duidt op een gebrek aan relativeringsvermogen.

XI

Gezien de grote problemen die burengerucht oplevert, zouden ankerloze spouwmuren en gescheiden gestorte vloeren moeten behoren tot de algemene bouwvoorschriften voor woningen.

XII

Een grotere drinkwaterconsumptie zou een aanzienlijke verbetering voor de volksgezondheid betekenen.

XIII

De enige lamp van de toekomst is de zon.

XIV

Verdrinkend Nederland verdroogt.

Hans de Regt was born on December 24th, 1967, in Oudenbosch (NL) where he finished his secondary school education (Athenaeum) at the Thomas More College in 1986.

Attracted by science, he then studied Applied Physics at Eindhoven University of Technology. During his study he worked for three months on the subject of X-ray diffractometry at the Koninklijke/Shell Laboratories in Amsterdam. In December 1991 he received his Master's Degree after completing a graduation project on expanding plasma jets.

Since February 1992 he has been working for the fundamental research foundation FOM and the technology foundation STW within the research group called 'Equilibrium and Transport in Plasmas', also at Eindhoven University's Faculty of Applied Physics. The results of a research project into the fundamentals of inductively coupled plasmas, partially carried out in co-operation with Philips Forschungslaboratorien Aachen (Germany), are the subject of this Ph.D. thesis.

Since 1984 he has been a scientific assistant at the public astronomical observatory 'Simon Stevin' in Hoeven. He has also served as a regional secretary and member of a national environmental study group for the youth wing of a political party. In his spare time, he likes to play the piano and work on black-and-white photography.

ISBN 90-386-0237-5